

The role of the metalloprotease ADAM17 in metastasis

Dissertation

zur Erlangung des Doktorgrades
der Mathematisch-Naturwissenschaftlichen Fakultät
der Christian-Albrechts-Universität
zu Kiel

**vorgelegt von
Julia Bolik
Kiel 2019**

Erster Gutachter: Prof. Dr. Stefan Rose-John

Zweiter Gutachter: Prof. Dr. Eric Beitz

Tag der mündlichen Prüfung: 04.07.2019

gez. Prof. Dr. Frank Kempken, Dekan

Eidesstattliche Erklärung

Ich erkläre hiermit, dass die nachfolgende Abhandlung eigenständig und unter Einhaltung der Regeln der guten wissenschaftlichen Praxis der Deutschen Forschungsgemeinschaft verfasst wurde. Nur die angegebenen Quellen und Hilfen wurden verwendet. Zitate, wörtlich oder sinngemäß, wurden als solche gekennzeichnet.

Die Arbeit wurde weder ganz, noch zum Teil im Rahmen eines Prüfungsverfahrens vorgelegt und ist weder veröffentlicht, noch zur Veröffentlichung eingereicht worden.

Ich versichere, dass ich bis zum heutigen Tag weder an dieser, noch an einer anderen Hochschule ein Promotionsverfahren endgültig nicht bestanden habe oder mir ein akademischer Titel aberkannt wurde.

Kiel, Mai 2019

Julia Bolik

Abstract

Metastasis is the major cause of death in cancer patients. Especially, patients undergoing primary tumor resection are at a high risk of developing metastases. This is partly due to inflammatory stimuli priming the metastatic niche. The pro-inflammatory cytokine tumor necrosis factor α (TNF α) has been shown to promote lung metastases formation in a mouse model. Soluble TNF α is released by the protease a disintegrin and metalloprotease (ADAM) 17 in a process called ectodomain shedding. Albeit ADAM17 has been shown to be overexpressed in primary tumors, its role in metastasis and in particular for tumor cell extravasation and seeding remains elusive.

Here we used mouse lines with genetic deficiency of ADAM17 in different tissues and injected either LLC or B16F1 cells intravenously to mimic hematogenic tumor cell metastasis. We demonstrate that endothelial ADAM17 is essential for tumor cell extravasation, seeding and metastases formation. We show that ADAM17 promotes extravasation through enabling death receptor-induced endothelial cell necroptosis. In this context, ADAM17 is essential for TNF α and TNF receptor signaling. We furthermore revealed that tumor cell-secreted CC-chemokine ligand 2 (CCL2) induces ADAM17 activity via protein kinase C (PKC) β .

In conclusion, we identified a central role for endothelial ADAM17 during metastases formation, therefore representing a novel, promising target for advanced cancer therapy.

Zusammenfassung

Die Bildung von Metastasen ist die Haupttodesursache bei Krebspatienten. Besonders Patienten, die sich einer primären Tumorresektion unterziehen, haben ein hohes Risiko, Metastasen zu entwickeln. Dies ist zum Teil auf Entzündungsreaktionen zurückzuführen, die die metastatische Nische bereiten. Es wurde festgestellt, dass das proinflammatorische Zytokin TNF α die Bildung von Lungenmetastasen im Mausmodell begünstigt. Lösliches TNF α wird durch die Protease *a disintegrin and metalloprotease* ADAM17 freigesetzt. Dieser Prozess wird *ectodomain-shedding* genannt. Obwohl gezeigt wurde, dass ADAM17 in Primärtumoren überexprimiert ist, wurde seine Rolle in der Extravasierung von Tumorzellen und in der Ausbildung von Metastasen noch nicht erforscht.

In dieser Arbeit verwendeten wir Mauslinien mit einem ADAM17 *knock-out* in verschiedenen Geweben und injizierten entweder LLC- oder B16F1-Zellen intravenös, um hämatogene Metastasierung nachzuahmen. Wir zeigen, dass ADAM17 in Endothelzellen für die Extravasierung und die Bildung von Metastasen essentiell ist. Dabei begünstigt ADAM17 die Tumorzellextravasierung, indem es die durch Todesrezeptoren induzierte Nekroptose von Endothelzellen ermöglicht. In diesem Zusammenhang ist ADAM17 für den TNF α Signalweg unerlässlich. Wir haben außerdem gezeigt, dass der durch Tumorzellen sekretierte CC-Chemokin-Ligand 2 (CCL2) die ADAM17-Aktivität durch Proteinkinase C (PKC) β induziert.

Zusammenfassend haben wir eine zentrale Rolle für ADAM17 in Endothelzellen während der Metastasierung identifiziert und zeigen somit ein neues, vielversprechendes Ziel für die Krebstherapie auf.

Index

| | | |
|----------|--|-----------|
| 1 | INTRODUCTION | 1 |
| 1.1 | A disintegrin and metalloproteases (ADAMs) | 1 |
| 1.1.1 | Domain structure of ADAMs | 2 |
| 1.1.2 | Biological function of ADAMs | 3 |
| 1.1.3 | A disintegrin and metalloprotease 17 | 5 |
| 1.1.4 | Regulators of ADAM17 | 7 |
| 1.2 | Tumor metastasis | 9 |
| 1.2.1 | Primary tumor | 9 |
| 1.2.2 | Tumor microenvironment | 10 |
| 1.2.3 | Metastasis | 11 |
| 1.3 | Death receptor-induced necroptosis | 15 |
| 1.3.1 | Pro-survival signaling by TNF-R | 15 |
| 1.3.2 | Induction of cell death by TNF-R | 18 |
| 1.3.3 | Death receptor 6 signaling | 20 |
| 1.4 | Aim | 21 |
| 2 | MATERIAL & METHODS | 22 |
| 2.1 | Material | 22 |
| 2.1.1 | Chemicals and recombinant proteins | 22 |
| 2.1.2 | Primer | 24 |
| 2.1.3 | siRNA | 25 |
| 2.1.4 | Antibodies | 26 |
| 2.1.5 | Cell lines | 28 |
| 2.1.6 | Mice | 29 |
| 2.2 | Methods | 30 |
| 2.2.1 | Animal experimentation | 30 |
| 2.2.1.1 | Housing | 30 |
| 2.2.1.2 | Breeding | 30 |
| 2.2.1.3 | Genotyping | 30 |
| 2.2.1.4 | Experimental metastasis model | 33 |

| | | |
|----------|---|-----------|
| 2.2.1.5 | Organ harvesting and blood sampling | 33 |
| 2.2.1.6 | Immunohistochemistry | 34 |
| 2.2.1.7 | Immunofluorescence | 34 |
| 2.2.1.8 | β -galactosidase staining | 34 |
| 2.2.1.9 | RNA isolation..... | 35 |
| 2.2.1.10 | cDNA synthesis | 35 |
| 2.2.1.11 | Quantitative real-time PCR | 35 |
| 2.2.2 | Cell culture..... | 36 |
| 2.2.2.1 | Culture conditions | 36 |
| 2.2.2.2 | Passaging..... | 36 |
| 2.2.2.3 | Freezing and thawing..... | 36 |
| 2.2.2.4 | Cell count | 36 |
| 2.2.2.5 | Transient transfection of cells..... | 36 |
| 2.2.2.6 | Cell transfection with siRNA..... | 37 |
| 2.2.2.7 | Cell staining with CFSE..... | 37 |
| 2.2.2.8 | Transmigration assay..... | 37 |
| 2.2.2.9 | Co-culture and necroptosis experiments | 37 |
| 2.2.2.10 | Cell death analysis | 38 |
| 2.2.2.11 | APP/jagged-1 assay..... | 38 |
| 2.2.2.12 | TNF-R1 stimulation..... | 38 |
| 2.2.2.13 | Isolation of TNF-R1 complex I and complex II | 38 |
| 2.2.3 | Proteinbiochemistry | 40 |
| 2.2.3.1 | Protein lysates | 40 |
| 2.2.3.2 | Determination of protein concentration..... | 40 |
| 2.2.3.3 | SDS-PAGE | 40 |
| 2.2.3.4 | Immunoblot | 41 |
| 2.2.3.5 | Stripping of immunoblot..... | 42 |
| 2.2.3.6 | Enzyme-linked immunosorbent assay | 42 |
| 2.2.3.7 | Activity assay..... | 43 |
| 2.2.4 | Statistics..... | 43 |
| 3 | RESULTS | 44 |
| 3.1 | ADAM17 mediates tumor cell extravasation..... | 44 |
| 3.2 | Endothelial permeability upon tumor cell contact is regulated by ADAM17 | 46 |
| 3.3 | PKC β is a potent activator of ADAM17 in metastasis..... | 48 |
| 3.4 | Tumor cells induce ADAM17-mediated cell death in endothelial cells..... | 51 |

| | | |
|----------|--|------------|
| 3.5 | ADAM17 is essential for death receptor-induced necroptosis..... | 57 |
| 3.6 | Myeloid ADAM17 has no impact on metastasis of tumor cells to the lung..... | 69 |
| 3.7 | Activated Notch1 signaling leads to tumor cell stemness and proliferation..... | 72 |
| 3.8 | Specific inhibition of ADAM17 prevents tumor cell metastasis | 74 |
| 4 | DISCUSSION | 78 |
| 4.1 | ADAM17 activity in the microenvironment for tumor cell extravasation..... | 78 |
| 4.2 | Regulation of cell death by ADAM17 | 81 |
| 4.3 | Function of ADAM17 during tumor cell seeding..... | 85 |
| 4.3.1 | ADAM17 on immune cells in tumor growth | 85 |
| 4.3.2 | Tumor cell proliferation mediated by ADAM17 | 86 |
| 4.4 | ADAM17 as clinical target in cancer therapy | 87 |
| 4.5 | Conclusion | 89 |
| 5 | REFERENCES | 90 |
| 6 | APPENDIX | 106 |
| 6.1 | Abbreviations..... | 106 |
| 6.2 | List of Figures..... | 110 |
| 6.3 | List of Tables | 111 |
| 6.4 | Curriculum Vitae..... | 112 |
| 6.5 | Acknowledgments..... | 114 |

1 Introduction

1.1 A disintegrin and metalloproteases (ADAMs)

Proteolysis is an irreversible posttranslational process of protein regulation, which is mediated by proteases. Based on their catalytic residues proteases can be divided in seven groups.

Among those, the metalloproteases are further grouped according to their complexed metal ion.

The zinc protease superfamily is in need of a zinc ion to catalyze the proteolytic cleavage of substrates. A disintegrin and metalloproteases (ADAMs) are grouped with a disintegrin and metalloproteases with thrombospondin motifs (ADAMTS) and class III snake venoms (SVMP) as metzincins (Figure 1.1).

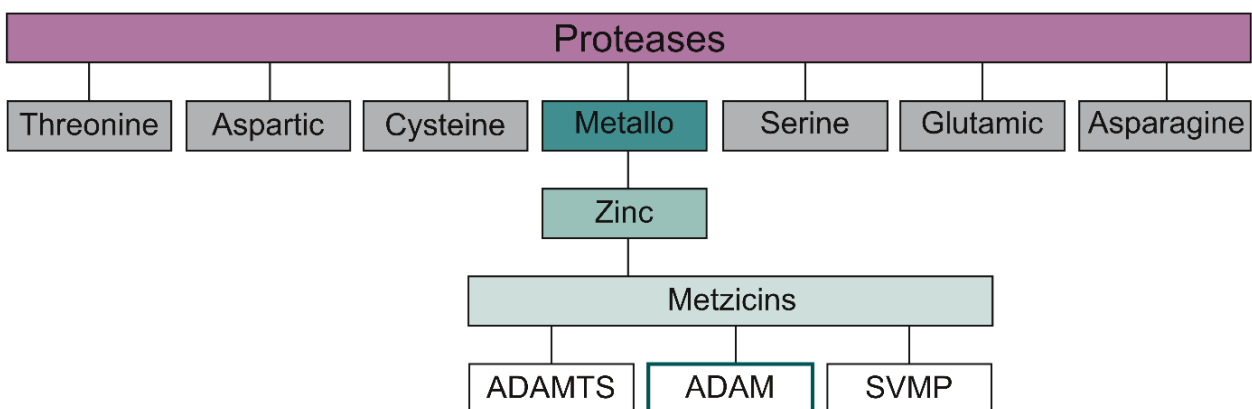


Figure 1.1: Classification of proteases according to their catalytic residues. ADAM proteases are members of the zinc protease superfamily and grouped with ADAMs with thrombospondin motif (ADAMTSs) and Snake venom metalloproteases (SVMPs) as metzincins.

ADAMs are the most abundant among these with 34 members described in many species [1]. ADAMs are either soluble or type I transmembrane proteins, that are capable of a limited form of proteolysis called ectodomain shedding, whereby other transmembrane proteins are cleaved near their transmembrane domain, leaving a soluble ectodomain and a C-terminal fragment (CTF). ADAMs are characterized by their unique domain structure and are involved in many important cell biological processes, like membrane fusion, cytokine and growth factor cleavage, cell migration, differentiation as well as cell fate determination [2].

1.1.1 Domain structure of ADAMs

ADAM proteases are synthesized as zymogens in the endoplasmic reticulum, displaying a characteristic domain structure (Figure 1.2A).

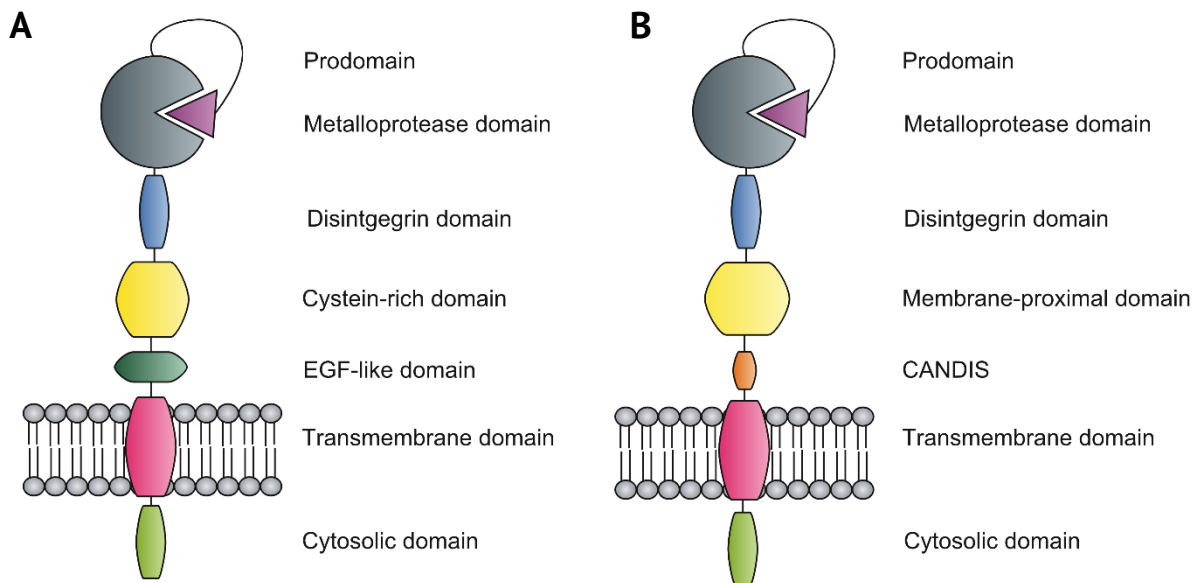


Figure 1.2: Domain structure of ADAM proteases. A: Schematic domain structure of a typical transmembrane ADAM family protease. **B:** Schematic domain structure of ADAM17. Different to other family members, ADAM17 displays a membrane-proximal domain (MPD) and a conserved ADAM seventeen dynamic interaction sequence (CANDIS).

The N-terminal prodomain is thought to have chaperone as well as inhibitory functions by interfering with the Zn^{2+} -ion in the catalytic center. It is generally cleaved off in the Golgi apparatus on the secretory pathway by protein convertases like furin [3]. For ADAM8 and ADAM28 however, autocatalytic prodomain cleavage was demonstrated [4, 5]. Interestingly, very recently Wong et al. succeeded in recombinantly producing the prodomain of ADAM17 and showed its specific inhibition of ADAM17 enzyme activity *in vitro* and *in vivo* (Chapter 1.1.4) [6]. In experiments with recombinant domains, the disintegrin domain of ADAMs was found to mediate interactions with integrins [7]. However, the binding seems to be selective, since e.g. ADAM17 was shown to exclusively bind $\alpha_5\beta_1$ -integrin, supporting adhesion and cell-cell interactions [8]. The function of the cysteine-rich and epidermal growth factor (EGF)-like domain remains inconclusive to date. However, there is strong evidence that this domain facilitates substrate binding, since an interaction of the cysteine-rich domain of ADAM12 with syndecans was found [9]. Structurally, ADAM17 as well as ADAM10 seem to differ from the other family members by lacking the cysteine-rich and EGF-like domain. Instead a membrane-proximal domain (MPD) was postulated (Figure 1.2) [10]. Similar to the cysteine-rich and EGF-like domain, the MPD is thought to facilitate substrate binding and thereby regulates shedding. The structure

of ADAM17 additionally revealed a so-called conserved ADAM seventeen dynamic interaction sequence (CANDIS) region, which is able to interact with the cell membrane [11].

The cytoplasmic tails of transmembrane ADAMs vary in their sequence and length, but contain phosphorylation sites for several kinases, which led to the assumption that the cytoplasmic domain of ADAMs is essentially involved in the regulation of protease activity and downstream signaling (Chapter 1.1.4).

1.1.2 Biological function of ADAMs

In mammals ADAMs are expressed in a wide range of tissues. Given their numerous substrates, they have diverse functions in development, physiology and in disease. In *homo sapiens* 22 ADAMs were identified of which 10 are considered proteolytically inactive and are thought to facilitate protein folding and protein-protein interactions [12]. Three of the residual catalytic active ADAMs are expressed in testis and two exclusively in hematopoietic cells [2], whereas the rest is ubiquitously present in all other tissues. Here, only a brief insight in ADAM-mediated pathways and processes can be given, since substrates of those active ADAMs are very diverse and the role of many family members has not been solved yet.

Substrates of ADAMs include cytokines, receptors and cell-adhesion molecules (Figure 1.3). Additionally, there is evidence that ADAMs are able to degrade extracellular matrix components. It was shown, that ADAM10 cleaves type IV collagen *in vitro* and ADAM13 and ADAM9 might be capable of degrading fibronectin [13-15].

Not only do ADAMs regulate the availability of signaling molecules by releasing them from the cell surface, but also essentially influence receptor signaling by shedding their ectodomains and thereby inhibit or terminate ligand signaling. Signal transduction based on substrate shedding by ADAMs can occur autocrine, paracrine and juxtacrine. Cleaved cytokines or growth factors can bind to their corresponding receptors on the same, neighboring or a distant cell (Figure 1.3). A special form of paracrine receptor signaling mediated by ADAM proteases is termed trans-signaling. This process is best characterized for interleukin-6 receptor (IL-6R) and ADAM17. The binding of interleukin 6 (IL-6) to membrane-bound IL-6R leads to the dimerization of glycoprotein 130 (gp130) molecules and the signal transduction, which is referred to as classic IL-6 signaling. However, whereas IL-6R expression is restricted to certain cell populations, gp130 is expressed on almost every cell type. IL-6 binding and subsequent shedding of the receptor by ADAM17 releases an IL-6/IL-6R complex, which is able to bind to gp130 on a neighboring or distant cell. This process is called IL-6 trans-signaling [16] (Figure 1.3). There is evidence that

this signaling concept also holds true for IL-11R and gp130 [17]. This mechanism plays a crucial role in infection, inflammation and tumorigenesis [18].

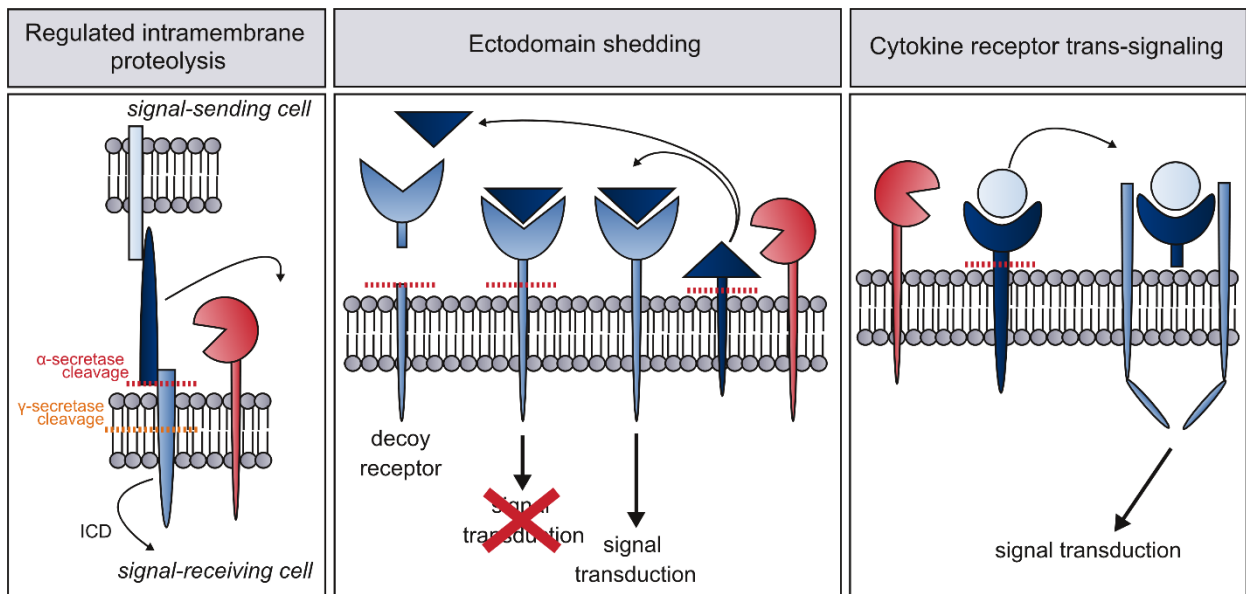


Figure 1.3: ADAM-mediated shedding events. Regulated intramembrane proteolysis (RIP) involves cleavage by an α -secretase (like ADAMs) of the receptor right after ligand binding, releasing the extracellular domain of the receptor. Subsequently an intramembrane protease, like the γ -secretase complex, liberates the intracellular domain (ICD), which induces gene expression by entering the nucleus and acting as transcription factor. Ectodomain shedding by ADAMs not only includes cytokines and growth factors, but also their receptors, whereby ADAMs regulate signal transduction. Moreover, soluble receptor ectodomains can function as decoy receptors for their soluble ligand. At least for the cytokine receptors IL-11R and IL-6R trans-signaling was shown, which is mediated by ADAMs. ADAMs cleave the receptors ectodomain, which binds the soluble ligand. The receptor/ligand-complex is then able to bind to its signal transducer.

The intensively studied Notch receptor signaling is the most prominent example for the role of ADAMs in contact-dependent cellular signaling. Membrane-bound Notch ligands on sending cells bind to the receptor of neighboring cells and induce proteolytic cleavage of Notch. Endocytosis of the receptor-bound ligand leads to conformational change of Notch and exposure of its α -secretase cleavage site [19]. The α -secretase cleavage step by ADAM10 (and ADAM17) generates a CTF, which is subsequently processed by the intramembrane protease-complex γ -secretase. The intracellular domain (ICD) is released, enters the nucleus and acts as transcription factor [20]. Therefore, ADAM10 plays an essential role in many developmental processes and it is hardly surprising that ADAM10^{-/-} mice are embryonic lethal, mimicking Notch^{-/-} mice [21]. The two subsequent cleavage events of α - and intramembrane secretase together are termed regulated intramembrane proteolysis (RIP) (Figure 1.3). Besides Notch receptor, amyloid precursor protein (APP) is processed via RIP. ADAM10 facilitates the α -secretase cleavage, which results in the production of a soluble APP α fragment [22]. The remaining CTF is further cleaved

by γ -secretase. This so-called non-amyloidogenic pathway is highly neuroprotective, whereas the generation of soluble APP β by a β -secretase leads to the production of an A β peptide, which forms plaques in the brain. This amyloidogenic pathway is thought to be the major cause of Alzheimer's disease [23]. These examples show the diversity of processes regulated by ADAM proteases. To date there are still new substrates to discover, as well as ADAM-mediated mechanisms to investigate. Especially signaling pathways regulated by ADAM17 gained attention over the last years as it was associated with several diseases and malignancies.

1.1.3 A disintegrin and metalloprotease 17

ADAM17 was first described 1997 and found to process the pro-inflammatory, membrane-bound cytokine tumor necrosis factor (TNF) α . TNF α is expressed as trimeric type II transmembrane protein, which is cleaved off from the cell surface by ADAM17. Therefore, ADAM17 was initially termed TNF α -converting enzyme (TACE) [24]. ADAM17 is ubiquitously expressed with high levels in small intestine, lung, liver and the adult heart [25].

To date, there are more than 80 diverse substrates of ADAM17 known [26]. ADAM17-mediated substrate shedding was linked to development, regeneration, immunity, inflammation and tumorigenesis [27]. Due to intense research on ADAM17, only a selection can be discussed here. It was shown that ADAM17 expression is upregulated upon inflammatory responses, hence it is considered as important target in TNF α -dependent diseases [28, 29]. Additionally, ADAM17 is the major sheddase for both TNF receptor (TNF-R) 1 and TNF-R2 [30, 31], i.e. ADAM17 regulates both, ligand availability and signal transduction of TNF α (Chapter 1.3). ADAM17 does not only contribute to inflammatory processes by shedding of TNF α . It was found, that the protease is involved in the migration of lymphocytes and neutrophils by regulating the cell surface density of L-selectin, which is needed for cell adhesion [32].

EGF receptor (EGF-R) ligands, like transforming growth factor (TGF) α , amphiregulin and heparin binding (HB)-EGF are also ADAM17 substrates. HB-EGF was shown to play a pivotal role in neuronal survival and proliferation as well as in the repair of DNA-damage in the liver [33, 34], highlighting the diversity of mechanisms ADAM17 is involved in.

The importance of ADAM17 is underlined by the fact, that ADAM17^{-/-} mice are not viable. They die between embryonic day 17.5 and few days after birth. ADAM17-deficient mice mainly showed eye, skin and hair defects, which were attributed to impaired epithelial cell maturation [30]. A similar phenotype was observed in EGF-R^{-/-} and TGF α ^{-/-} mice [35-37]. Moreover, impaired HB-EGF shedding in those ADAM17^{-/-} mice lead to late embryonic cardiomegaly, thickened

semilunar and atrioventricular valves [38]. More recently, Chalaris and colleagues succeeded in generating a hypomorphic ADAM17 mouse, called ADAM17^{ex/ex}. They used the so-called exon induced translational stop strategy. They introduced an additional exon 11 (exon 11a) flanked by non-canonical donor and acceptor splicing sites into the *Adam17* gene. 95 % of the produced mRNA contains exon 11a, which was designed with an in-frame stop codon (Figure 1.4).

This results in a premature translational stop and thereby to strongly reduced ADAM17 protein levels in all tissues and cell types.

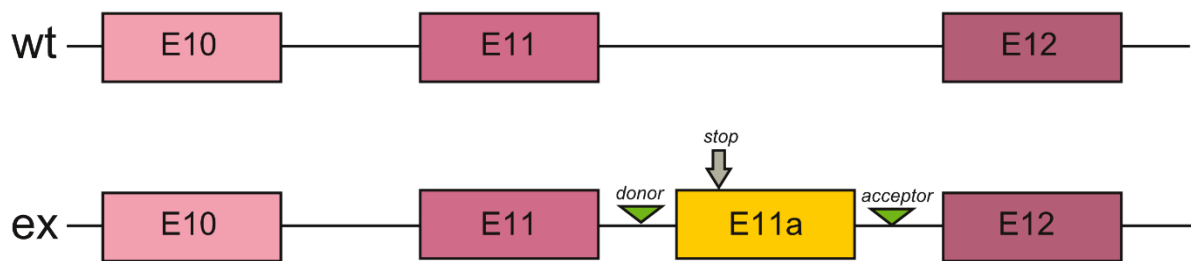


Figure 1.4: Generation strategy for hypomorphic ADAM17^{ex/ex} mice. The modified allele contains an artificial exon 11 (E11a), flanked by non-canonical donor and acceptor splicing sites (green arrow heads). Grey arrow indicates the in-frame translational stop codon. 95 % of the mature mRNA contains the artificial exon 11a. The in-frame stop codon in exon 11a leads to a premature translational stop (modified after [39]).

ADAM17^{ex/ex} mice are viable, but share most phenotypic features with ADAM17^{-/-} and EGF-R^{-/-} mice, like skin defects, blindness and wavy hair [39].

These mice opened up a unique possibility to study ADAM17-mediated processes *in vivo*. Since their generation they were subjected to different mouse models of human disease. ADAM17^{ex/ex} mice are more susceptible to dextran sulfate sodium-induced colitis, they show decreased kidney fibrosis in a model of ischemia reperfusion injury and they display enhanced levels of atherosclerosis [39-41]. Recently, it was additionally shown that tumor formation in ADAM17^{ex/ex} mice in a genetic model of colorectal cancer is drastically reduced, which was attributed to impaired IL-6 trans-signaling and therefore decreased β -catenin-dependent tumorigenesis [42]. Along with increased expression levels of ADAM17 on tumor cells (TCs) in many cancer types, i.e. breast, kidney and prostate [43], this study identifies the protease as promising target for cancer therapy. In order to regulate ADAM17-activity specifically in cancer, inflammation and other pathologies, it is of great interest to find pharmacological inhibitors and investigate upstream effectors of the protease.

1.1.4 Regulators of ADAM17

Under physiological conditions ADAM17 is highly regulated. Whereas constitutive substrate shedding was shown for ADAM10, ADAM17-mediated shedding is thought to depend on activation of the protease [44].

As mentioned earlier (Chapter 1.1.1), the cytoplasmic tail of ADAM17 contains several phosphorylation sites. Indeed, it was shown that the protease can be phosphorylated by several kinases, e.g. protein kinase C (PKC) [45], the mitogen-activated protein kinase (MAPK) p38 [46], c-Jun N-terminal kinases (JNK) [47] and extracellular signal-regulated kinase (ERK) [48]. In *in vitro* experiments ADAM17 shedding is often induced by stimulating cells with the non-physiological stimulator of PKC phorbol-12-myristat-13-acetat. More physiological inducers of ADAM17 activity are histamine, thrombin and lysophosphatidic acid, which are ligands for G-protein coupled receptors (GPCRs) [49-51]. GPCRs are seven-transmembrane proteins that are intracellularly coupled to heterotrimeric G proteins. A signal is mainly transduced by the G_{α} subunit. There are four classes of α subunits (G_s , G_i , $G_{q/11}$, $G_{12/13}$), which induce different signaling pathways by dissociation from the receptor after ligand binding. The $G_{q/11}$ -subunit activates phospholipase C, which subsequently catalyzes the cleavage of phosphatidylinositol 4,5-bisphosphate to inositol 1,4,5-triphosphat und diacylglycerol. While 1,4,5-triphosphat induces Ca^{2+} release from the ER, diacylglycerol activates PKC which in turn can phosphorylate several other proteins. The G_s - and G_i -subunits induce signaling via cyclic adenosine monophosphate and the $G_{12/13}$ -subunit was reported to activate the small guanosine triphosphate hydrolase rho. Inoue et al. showed that GPCRs coupled to $G_{q/11}\alpha$ and $G_{12/13}$ are able to activate ADAM17. $G_{q/11}$ activate PKC, which in turn can phosphorylate ADAM17. The authors speculate that the activation of ADAM17 by $G_{12/13}$ is facilitated by rho-associated, coiled-coil-containing protein kinase [52].

Furthermore, increased catalytic activity of ADAM17 was found in response to infection, which was pinned down to toll-like receptor 4 stimulation by lipopolysaccharide (LPS) [53].

Cell surface availability of ADAM17 is regulated by iRhom1 and iRhom2. Those are members of the rhomboid superfamily of multi-transmembrane proteases, which lost their catalytic activity during their evolution. Whereas expression of iRhom2 is restricted to hematopoietic cells, iRhom1 is more widely expressed [54]. An interaction of both iRhoms with ADAM17 was demonstrated. They both engage ADAM17 in the ER, promoting its maturation and trafficking to the cell membrane *in vitro* [55]. However, there are reports that iRhom1 and 2 only influence

the shedding of specific substrates [56]. Maney and colleagues reported that mutations in the cytoplasmic tails of iRhom1 and 2 enhanced ADAM17-mediated shedding of TNF-R1 [57]. Similar regulatory functions are attributed to tetraspanins, which are four-transmembrane proteins. They were shown to form both homo- and hetero-oligomers and can associate with several other proteins like ADAM proteases. Tetraspanin 15, for example, was reported to regulate cell surface expression and trafficking of ADAM10 [58]. ADAM17 was found to co-localize with cluster of differentiation (CD) 9 on the cell surface, which leads to negative regulation of substrate shedding [59].

Regulation of ADAM17 was also proposed for protein disulfide isomerase [60]. The authors show, that downregulation of protein disulfide isomerase enhanced ADAM17 activity. Albeit, the exact underlying mechanism remains unclear.

Recently, Sommer et al. proposed a new activation mechanism for ADAM17. They found that exposure of phosphatidylserine (PS) on the outer leaflet of the plasma membrane leads to substrate shedding by ADAM17. The MPD of the protease can bind to PS which directs ADAM17 to its substrates [61].

Natural inhibitors of matrix metalloproteases (MMPs) and some selected ADAM proteases are the tissue inhibitor of metalloproteases (TIMPs). TIMP3, which binds to the extracellular matrix, was reported to interact with an ADAM17 homodimer [46, 62]. It binds with its N-terminal inhibitory domain to the active site of the metalloprotease domain of ADAM17, thereby regulating ADAM17 activity [12].

Another inhibitor of ADAM17 activity is its own prodomain, which usually is cleaved off in the Golgi apparatus by furin (Chapter 1.1.1). Recently, Wong et al. succeeded in producing the ADAM17 prodomain (ADAM17-PD) recombinantly [6]. ADAM17-PD blocks the catalytic site of mature ADAM17 on the cell surface, thereby inhibiting its activity. The authors demonstrated selective inhibition of ADAM17 *in vitro* as well as in mouse models of inflammatory bowel disease, septic shock and rheumatoid arthritis. There have been several approaches in inhibiting ADAM17 and its shedding, so far. Unfortunately, most synthetic small molecule inhibitors lack specificity. They often show inhibition of a broad range of metalloproteases. However, INCB7839, a low-nanomolar hydroxamate-based dual inhibitor of ADAM17 and ADAM10 is in clinical trial for treatment of large B cell non-Hodgkin lymphoma [26]. Higher specificity was achieved by developing an inhibitory antibody against ADAM17, which showed promising results in genetic mouse models of pancreatic cancer [63].

An advanced and selective inhibition of ADAM17 substrates is targeted with the so-called ligand

trap strategy. Modified ectodomains of receptors are used to bind their soluble ligands. Most prominent examples are Aflibercept and Etanercept. Aflibercept consists of the ligand binding domains of vascular endothelial growth factor receptor (VEGF-R) 1 and VEGF-R2 fused together with the immunoglobulin (Ig) G1 Fc region. It binds soluble vascular endothelial growth factor (VEGF)-A and is, among others, used for the treatment of retinopathies and colorectal cancer [64, 65]. Etanercept consists of two extracellular domains of human TNF-R2 fused together with the IgG1 Fc region. It binds soluble TNF α and is predominantly used in rheumatoid arthritis [66, 67].

1.2 Tumor metastasis

According to the world health organization, 9.6 million people died from cancer in 2018 worldwide [68]. Over 90 % of the mortality of cancer is attributed to the development and incurability of metastatic disease [69]. Metastasis is the process, by which TCs of a primary tumor spread to other tissues of the body. Especially in early stages, metastases are hard to diagnose, surgical resection is often incomplete and in many cases they are resistant to chemotherapy, as well as radiation. Therefore, extensive research is carried out on the prevention and treatment of metastasis.

1.2.1 Primary tumor

Tumorigenesis is a complicated multistep process. However, there is agreement, that external as well as endogenous factors induce mutations in certain cells that drive the progression towards highly aggressive TCs. Although a primary tumor is made up of heterogeneous TC populations, TCs share six characteristic features [70]. (I) They can provide themselves with growth factors, e.g. by positive feedback loops and autocrine stimulation, like it was reported for platelet-derived growth factor and TGF α [70]. Moreover, TCs often overexpress receptor tyrosine kinases and are therefore hyper-responsive to growth signals.

(II) TCs are insensitive to growth inhibiting signals. They achieve that e.g. by decreasing the expression of TGF β receptor [71].

Furthermore, (III) TCs show unlimited proliferative potential and (IV) can escape apoptosis. Additionally, (V) they release angiogenic factors to initiate vascularization of the tumor. Lastly, (VI) TCs are capable of invasion and metastasis. However, a tumor is not composed of TCs only, but is embedded in an environment of non-transformed host cells, collectively known as the tumor microenvironment [72].

1.2.2 Tumor microenvironment

TCs interact with a variety of non-malignant cells, namely immune cells, endothelial cells (ECs), lymphatic cells, fibroblasts and pericytes [73]. They can comprise 50 % of the mass of a primary tumor and regulate its growth and progression. Interestingly, the tumor microenvironment, especially its composition, has high prognostic value and consists of genetically stable cells, representing promising therapeutic targets [74, 75].

TCs secrete a great number of factors to recruit and mobilize host cells even from distant tissues, like the bone marrow. Here, tumor-associated macrophages play a critical role. Tumor-associated macrophages are known to promote tumor initiation and progression, e.g. through the release of IL-6 and EGF, respectively [76, 77]. Moreover, they were shown to critically contribute to angiogenesis [78].

The vascularization of the primary tumor is a prerequisite for its growth and is also partly facilitated by cells of the tumor microenvironment. Not only malignant cells secrete angiogenic factors, but also inflammatory cells release soluble signaling molecules, such as VEGF, fibroblast growth factor and platelet-derived growth factor that stimulate ECs. Additionally, hypoxic conditions within the tumor and its environment represent a trigger for neovascularization [79, 80].

The dominant cell type of the tumor microenvironment is mesenchymal or fibroblastic origin, collectively referred to as cancer associated fibroblasts (CAF). They were reported to drive tumor progression by modulating a variety of processes. Among many others, CAFs secrete IL-6, by which they influence vascularization and inflammation. Furthermore, they release MMPs and thereby change extracellular matrix composition [81].

Besides paracrine signaling between TCs and cells of the tumor microenvironment, the release of microvesicles and exosomes was reported as intercellular signaling mechanism [82]. They carry nucleic acid, proteins as well as lipids, which upon fusion can influence the behavior of distant cells [75]. To date, exosome release and their impact on tumor growth and progression is still incompletely understood. However, in several studies it was demonstrated, that TC-derived microvesicles educate the tumor microenvironment as well as distant tissue to prime the so-called pre-metastatic niche. Several circulating factors, derived from TCs or cells of the tumor microenvironment, were identified to increase the receptivity of a secondary organ to TCs. As an example, TC-derived CC-chemokine ligand 2 (CCL2) and versican were found to alter the lung microenvironment by recruitment and activation of myeloid cells [83, 84]. Beside preparing the

secondary organ for TC arrival, the tumor microenvironment is also crucial for the tumor invasiveness itself.

1.2.3 Metastasis

When a primary tumor breaks the basal membrane of its host tissue it is considered invasive. This invasiveness can stay local, but may spread to more distant organs through the vasculature (hematogenic metastasis) or the lymphatic system (lymphatic metastasis). The seeding of TCs to secondary organs is called metastasis. This complex process is divided in several distinct steps (Figure 1.5).

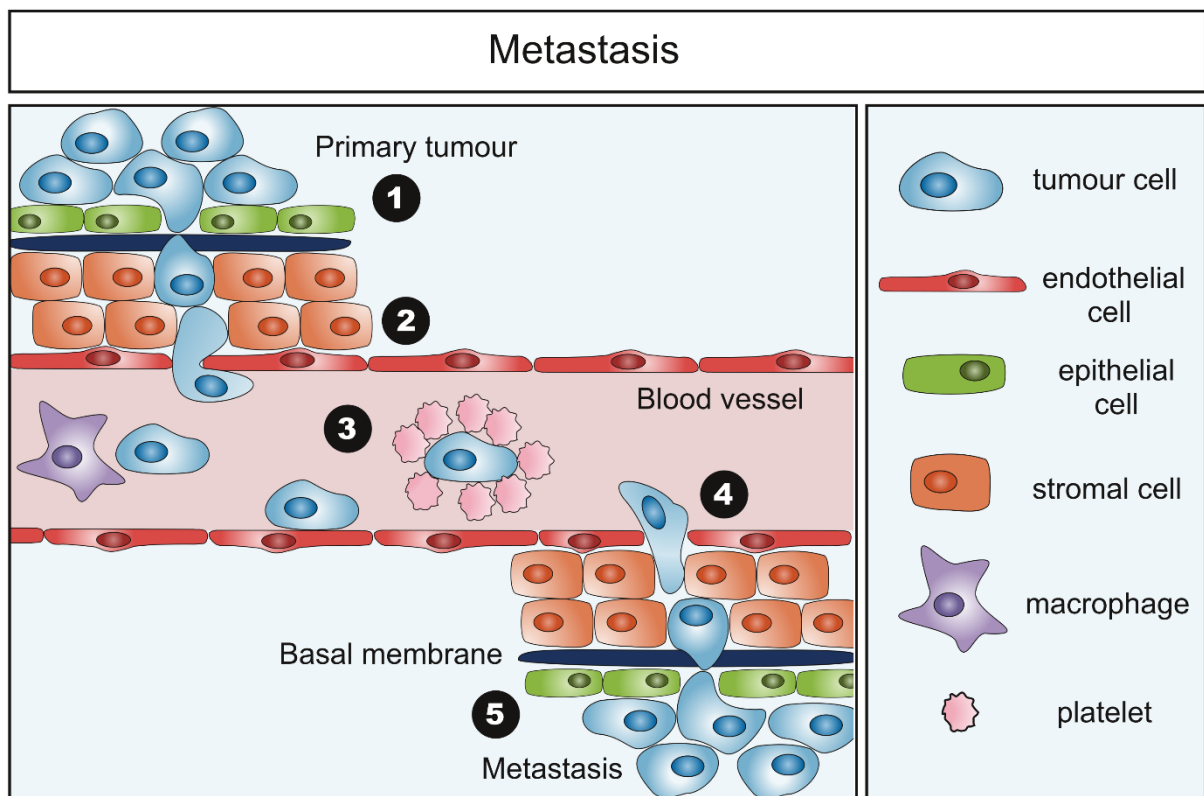


Figure 1.5: Schematic of the metastatic cascade. A single TC detaches from the primary tumor (1), penetrates the epithelium, the basal membrane, the stromal cell layer and the endothelium to intravasate into the vasculature (2), where it is susceptible to attacks of immune cells (3). In small capillaries TCs adhere to ECs, extravasate (4) and proliferate to form a secondary tumor (5).

Firstly, either single cells or cell clusters detach from the primary tumor and migrate towards microvessels [85, 86]. This involves the transition from a non-invasive phenotype of the TC to an invasive one. In TCs of epithelial origin, this process is called epithelial-to-mesenchymal transition (EMT). During EMT TCs lose intercellular contacts, upregulate MMP expression to degrade the basal membrane, polarize to a more stem cell-like, migratory phenotype and are often referred to as cancer stem cells (CSCs) [87, 88]. EMT is induced by intrinsic factors and

stimuli TCs receive from host cells and is not defined by one distinct signaling pathway but rather the consequence of several signaling events [88]. Fundamental in this process is the reprogramming of gene expression patterns, which predominantly involves the SNAIL, TWIST and zinc finger E-box-binding homeobox transcription factor families. Their activation can be regulated by SMADs, which are activated by the TGF protein family of proteins [89].

Once disseminated, TCs migrate to microvessels within the primary tumor. This is promoted by blood vessel associated macrophages, releasing EGF [90]. They also help TCs during the next step in the metastatic cascade, the intravasation through the endothelial barrier into the circulation. Intravital microscopy revealed a crucial role for macrophages in supporting successful intravasation of TCs. Cluster of ECs, macrophages and TCs were termed tumor microenvironment of metastasis [91]. Although newly synthesized vasculature of the primary tumor is already more permeable, permeability even increases further at those sites of tumor microenvironment of metastasis [88, 92]. Originally, it was believed that intravasation of TCs occurs in late stages of disease. However, today there is agreement that metastatic dissemination and intravasation happens continuously and earlier than expected. In addition, little is known about this step as it occurs deep within the tumor and is therefore difficult to visualize.

While approximately 10^6 TCs enter the circulation daily, only 0.01 % survive and are able to extravasate [91, 93]. However, extensive research has been carried out on the detection and clearance of metastasizing cells, as TCs are most vulnerable during this step of the metastatic cascade. They are confronted with massive shear stress and prone to undergo anoikis, a form of programmed cell death, induced by the loss of extracellular matrix contact [94]. Much more problematic is, that while there is immunosuppression within the primary tumor, TCs in the circulation are exposed to a functional immune system. Although metastasizing cells themselves can attenuate cytotoxicity of immune cells, their survival in the circulation is in part dependent on the interaction with CAFs, leukocytes, platelets and ECs [88, 95].

Platelets form aggregates around TCs, helping them to evade immune cell recognition [96]. Additionally, activated platelets were reported to secrete TGF β which stimulates protective nuclear factor κ B (NF- κ B) signaling in metastasizing cells, which enhances their chance of survival [97].

Neutrophils were also reported to benefit survival of metastasizing cells. Stimulated by TC-derived granulocyte-colony stimulating factor, neutrophils form neutrophil extracellular traps [98]. These extracellular DNA traps cluster TCs, which promotes their adhesion to the endothelium [99]. Moreover, stimulated neutrophils suppress the activity of anti-tumorigenic

natural killer cells and are able to inhibit cytotoxic CD8⁺ T cell responses [88]. The exact mechanisms by which neutrophils achieve these two pro-tumorigenic functions are still not known.

After circulating for a short period of time, TCs have to extravasate to colonize the secondary organ. Extravasation of TCs is somewhat similar to leukocyte extravasation and usually occurs in small capillaries, where TCs slow down and arrest due to physical restriction. The firm adhesion to ECs is the first step of extravasation and followed by transendothelial migration. Rolling of TCs over the endothelium similar to leukocytes, was documented only *in vitro* so far [100]. The stable attachment to ECs is mediated by selectins, cadherins, CD44, integrins and Ig receptors [101]. Upregulation of those proteins on ECs can be directly triggered by TCs or associated cells. Increasing E-selectin levels on the surface of liver ECs 6-8 hours (h) after injection of either carcinoma or colorectal cancer cells in the portal vein for example, is an indirect effect of macrophage-secreted TNF α [102].

Following the firm adhesion, TCs undergo transendothelial migration. Hereby, TCs can overcome the endothelial barrier as single cells or cluster. It is even reported that TCs start to proliferate in microvessels prior to transendothelial migration [103].

There are two routes of transendothelial migration defined. The migration through EC junctions is termed paracellular migration, whereas the migration through the EC body is referred to as transcellular migration. Whereas the latter route is well described for leukocytes, it is still unclear whether TCs use this route. They seem to prefer paracellular transendothelial migration [101]. It involves the disruption of EC junctions and/or contraction of ECs, which is mediated by several factors secreted by TCs and blood cells.

TCs promote their extravasation by releasing growth factors, pro-inflammatory cytokines and chemokines [104]. VEGF, for instance, is produced in large amounts by TCs and induces vascular permeability by binding to VEGF-R on ECs, thereby disrupting vascular endothelial (VE)-cadherin/ β -catenin interactions in EC junctions [105]. Another important mediator of permeability is CCL2. This chemokine activates C-C chemokine receptor (CCR) 2 on ECs, which is a G_{q/11} α -coupled receptor (Chapter 1.1.2). This binding was shown to lead via p38 activation and the janus kinase (JAK)-signal transducer and activator of transcription protein (STAT) pathway to hyper-permeability of the endothelium, although the exact molecular mechanism remains elusive [106]. Additionally, CCL2 recruits inflammatory monocytes, which in turn produce VEGF, contributing to permeability of the endothelium [107].

In addition to monocytes, platelets play a crucial role in TC extravasation. Activated

thrombocytes secrete adenosine triphosphat (ATP), thereby activating P2Y₂ purino receptor on ECs modulating endothelial junctions and the cytoskeleton [108].

Contractility of the cytoskeleton is as important as disassembly or disruption of EC junctions for proper transendothelial migration. The activation of p38, for instance by TNF α or EGF-R ligands, stimulates the phosphorylation of myosin light chain, leading to stress fiber formation [109]. Stress fiber stability in ECs in turn is mediated by phosphorylated ERK [101].

Very recently, Strilic et al. demonstrated a novel extravasation strategy. TCs induce programmed necrosis, termed necroptosis (Chapter 1.3), in ECs. TCs express membrane-bound APP, which binds to death receptor (DR) 6 on ECs, triggering necroptotic cell death. TCs can subsequently escape the circulation through the resulting gap. Additionally, perishing ECs release death-associated molecular patterns (DAMPs), like ATP and nucleic acids, which in turn affect junction integrity of surrounding ECs and stimulate immune cells [110].

Once TCs have extravasated, the final and rate-limiting step in the metastatic cascade is the progression of micrometastases to macrometastases. Hereby, the switch from an invasive to a non-invasive phenotype is essential to proliferate. TCs of epithelial origin have been observed to reverse EMT and undergo mesenchymal-to-epithelial transition (MET) [111]. However, little is known about molecular mechanisms of MET. Induction of MET in breast cancer cells was shown to be dependent on the release of versican by myeloid progenitor cells [112]. Additionally, lung fibroblasts were reported to activate SMAD1/5 signaling in breast cancer cells leading to an epithelial phenotype and proliferation [113].

Failure to proliferate leads to dormancy of the disseminated TCs [114]. Interestingly, these dormant micrometastases can persist for years in the secondary tissue, clinically undetectable. To reverse this dormant state, TCs depend again on their microenvironment. For example, it was shown that tissue inflammation benefits the awakening of those dormant cell clusters [115]. Certainly, to grow beyond 1-2 mm, the micrometastases additionally have to induce angiogenesis [91].

Most treatment strategies of cancer and metastatic disease aim at the TCs themselves, which is difficult as TCs are genetically unstable and often develop resistance to chemotherapy and radiation. Manipulation of genetically stable host cells seems to be the more promising approach, but needs profound knowledge of pro-tumorigenic signaling pathways [116].

1.3 Death receptor-induced necroptosis

Two hallmarks of cancer, defined by Douglas Hanahan and Robert Weinberg in 2000, are the resistance of TCs to cell death and the unlimited proliferation capacity (Chapter 1.2.1) [70]. These characteristics highlight the importance of a precise balance between cell survival and death, as any disruption of this ratio leads to disease. The removal of damaged, infected and degenerated cells by cell death is therefore of great importance in tissue homeostasis as well as in embryogenesis [117]. Three distinct types of cell death have been described: cell death associated with autophagy, apoptosis and necrosis.

Apoptosis can be induced intrinsically or extrinsically, is genetically regulated and involves phagocytosis of the dying cell. Morphological hallmarks of apoptotic cells, are the shrinkage of the nucleus and cytoplasm, chromatin condensation and nucleus fragmentation as well as the release of apoptotic bodies [118].

Necrosis is the result of irreversible cell damage, resembles cell lysis and was thought to be an accidental form of cell death. In contrast to apoptotic cells, necrotic cells swell, have intact nuclei and an early rupture of the cell membrane occurs. Whereas apoptosis is thought to be less immunogenic, necrosis leads to the release of DAMPs, resulting in inflammation of the affected tissue. Hence, it is hardly surprising that necrosis is mainly associated with pathophysiology [119].

In the last decade evidence for a genetic regulation of necrosis emerged. By now, five distinct regulated necrotic death modes are described, although poorly understood: Caspase-1 and gasdermin-dependent **pyroptosis**, poly(adenin diphosphate-ribose)-polymerase-dependent **parthanatos**, iron-dependent **ferroptosis** and nicotinamide adenine dinucleotide phosphate oxidase-mediated **NETosis** of neutrophils [120]. The best studied mode, however, is death receptor-induced **necroptosis**. Necroptosis can be triggered by TNF α , Fas ligand, tumor necrosis factor related apoptosis inducing ligand (TRAIL), interferon, LPS, double-stranded RNA, ER stress, DNA damage, viruses and some anti-cancer drugs [121]. Still, not every molecular mechanism initiated by these stimuli is conclusively investigated. However, only TNF α -induced necroptosis via the death receptor TNF-R1 will be discussed in the following.

1.3.1 Pro-survival signaling by TNF-R

Death receptor is a casual term referring to transmembrane cytokine receptors of the TNF-R superfamily that exhibit a death domain and are thereby capable of inducing cell death [122].

Among others, this group includes Fas receptor, TRAIL receptor, DR6 and TNF-R1 [123]. TNF-R1 signaling is by far the best characterized. Its closest relative TNF-R2, contains a cytoplasmic TNF receptor-associated factor (TRAF)-interacting motif instead of a death domain and is therefore unable to directly induce cell death [124]. Both TNF-R1 and TNF-R2 are activated by TNF α . Whereas TNF-R1 binds membrane-bound and soluble TNF α , the affinity of TNF-R2 to membrane-bound TNF α is considerable higher than to its soluble form [125, 126]. TNF-R1 is ubiquitously expressed, whereas TNF-R2 is found on oligodendrocytes, astrocytes, T cells, myocytes, thymocytes, ECs and mesenchymal stem cells [127]. Receptors of the TNF-R superfamily are thought to exist as oligomers at the cell surface prior to ligand binding [128]. The biological response of TNF-R1 and TNF-R2 is dependent on adaptor proteins, as the receptors themselves are unable to transduce a signal [129]. Whereas direct TNF-R2 signaling exclusively leads to cell survival, TNF-R1 activation can, depended on cell type and stimuli, either lead to survival or death, induced by two, spatially and temporally separated complexes [130].

Under physiological conditions, however, TNF-R1 signaling induces cell survival rather than cell death. Rapidly after ligand binding, receptor-interacting serine/threonine-protein kinase 1 (RIPK1) and the adaptor protein TNF-R-associated death domain protein (TRADD) are recruited to TNF-R1 (Figure 1.6A). TRADD binds the receptor with its intracellular death domain and in turn is able to recruit TRAF2, which subsequently binds cellular inhibitor of apoptosis protein (cIAP) 1 and 2 with its cIAP interaction motif and additionally activates MAPKs, like p38, ERK and JNK. cIAP1/2 are ubiquitin ligases, adding K63-linked polyubiquitin chains to RIPK1, which do not lead to proteasomal degradation of RIPK1 but rather function as scaffold for the linear ubiquitin chain assembly complex (LUBAC). LUBAC consists of haeme-oxidized IRP2 ubiquitin ligase 1 (HOIL1), HOIL1-interacting protein (HOIP) and SHANK-associated RH domain-interacting protein (SHARPIN). It is an ubiquitin ligase complex and adds M1-linked polyubiquitin chains to RIPK1 as well as to TRADD and other proteins of complex I. K63-linked polyubiquitin chains function as scaffold for the recruitment of TGF β -activated kinase 1 (TAK1)-binding proteins (TAB) 1, 2 and TAK1. M1 ubiquitination, however, is essential for the recruitment of a complex, consisting of nuclear factor of κ light polypeptide gene enhancer in B-cells inhibitor alpha (I κ B α) kinase (IKK) α , β and NF- κ B essential modulator (NEMO). In the following, TAK1 activates MAPKs and IKK β . IKK β in turn phosphorylates I κ B α , leading to its degradation. Since I κ B α binds and thereby inhibits the NF- κ B complex p50/p65, its degradation leads to translocation of the transcription factor complex to the nucleus, which drives the

expression of pro-survival and pro-inflammatory genes. This activation pathway of NF- κ B is referred to as canonical pathway.

By contrast, TNF-R2 signaling leads to NF- κ B activation via the non-canonical pathway [131]. Upon stimulation of TNF-R2, the adaptor proteins TRAF2 and TRAF3 bind directly to the receptors intracellular domain (Figure 1.6B).

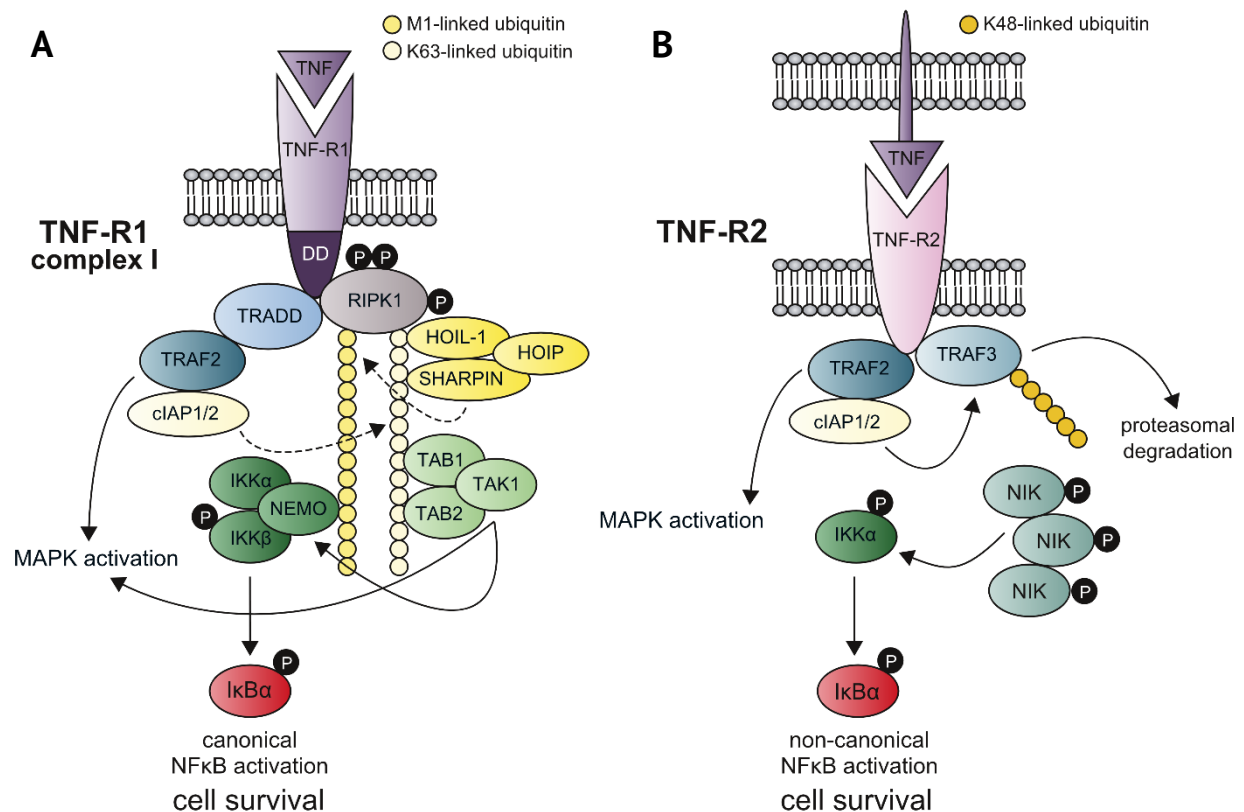


Figure 1.6: TNF-R1 and TNF-R2 induced signaling. **A:** Upon binding of either membrane-bound or soluble TNF α to TNF-R1 the adaptor protein TRADD and RIPK1 are recruited to the intracellular death domain of the receptor. TRADD subsequently binds TRAF2, which recruits cIAP1/2. cIAP1/2 add K63-linked ubiquitin to RIPK1, which serves as platform for the LUBAC complex (HOIP, HOIL-1, SHARPIN) and TAB1, TAB2 and TAK1. LUBAC adds M1-linked ubiquitin to RIPK1 to which NEMO, IKK β and IKK α are recruited. IKK β initiates the phosphorylation of I κ B α , which is subsequently degraded, releasing NF- κ B. This is the canonical NF- κ B activating pathway. **B:** TNF-R2 is triggered by membrane-bound TNF α and requires cytoplasmic binding of TRAF2 and TRAF3 to transduce a signal. TRAF2 activates MAPKs and recruits cIAP1/2. cIAP1/2 add K48-linked polyubiquitin chains to TRAF3, leading to its proteasomal degradation. This subsequently leads to the release, activation and accumulation of NIK, which under unstimulated conditions is usually bound to TRAF3 and degraded. NIK phosphorylates IKK α leading to NF- κ B activation. This is the non-canonical pathway activating NF- κ B.

TRAF2 recruits cIAP1 and 2, which subsequently add K48-linked polyubiquitin chains to TRAF3. This leads to the proteasomal degradation of TRAF3. Under unstimulated conditions, TRAF3 is bound to NF- κ B inducing kinase (NIK), which leads to ubiquitination and proteasomal

degradation of NIK [131]. Therefore, TRAF3 degradation upon TNF-R2 stimulation leads to NIK activation and accumulation. NIK in turn phosphorylates IKK α , finally leading to NF- κ B activation [129]. Just as TNF-R1 signaling, TNF-R2 signaling additionally results in MAPKs activation by TRAF2.

1.3.2 Induction of cell death by TNF-R

In case complex I formation and NF- κ B activation is inhibited, TNF-R1 activation leads to the formation of complex II in the cytoplasm, resulting in cell death (Figure 1.7).

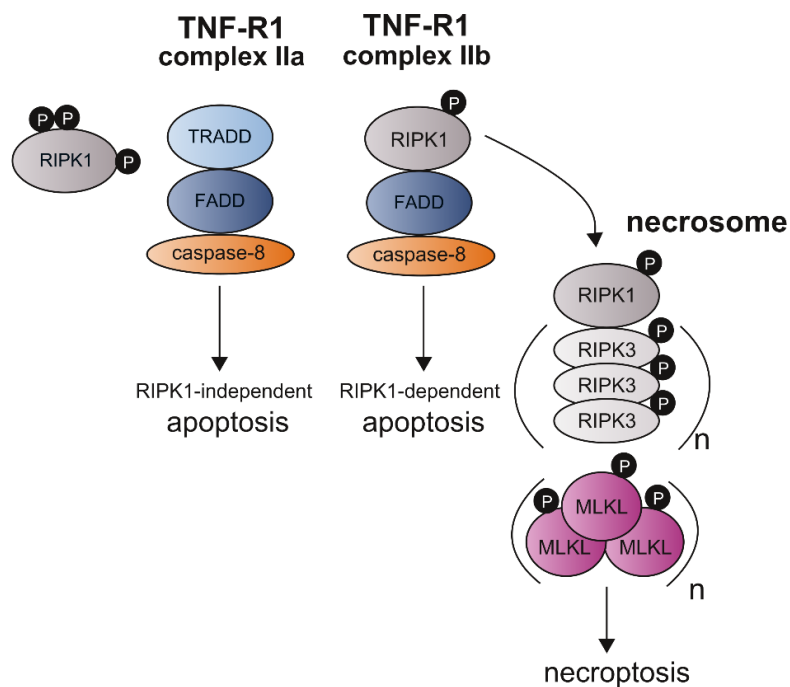


Figure 1.7: TNF-R1-induced signaling complex II. Receptor dissociation of RIPK1 leads to formation of cell death complexes. Complex IIa is independent of RIPK1 kinase activity. Active IKK complex still phosphorylates RIPK1, preventing its activity. Complex IIa consists of TRADD and FADD, leading to the cleavage and thereby activation of caspase-8. In consequence the cell undergoes apoptosis. Complex IIb formation is dependent on RIPK1 activity and the recruitment of FADD and caspase-8. Inhibition of caspase-8 in complex IIb leads to the recruitment and phosphorylation of RIPK3, which subsequently forms β -amyloid-like structures. In consequence MLKL is phosphorylated, integrates in the plasma membrane and executes necroptosis. Both apoptotic complexes and the necrosome are cytoplasmic and not associated with the receptor.

Complex IIa is independent of RIPK1, whereas complex IIb needs its kinase activity, i.e. deubiquitinated and autophosphorylated RIPK1 at Serine 166. The formation of complex IIa is a very slow process and starts by engagement of FAS-associated death domain protein (FADD) and receptor-dissociated TRADD in the cytosol. FADD in turn recruits and activates caspase-8. Caspase-8 is most probably activated via autocatalytic cleavage by oligomerization of procaspase-8 [133, 134]. In the absence of cIAPs or the LUBAC complex, RIPK1 can not be

ubiquitinated and is thought to undergo autophosphorylation [132]. Activated RIPK1 engages FADD, which in turn recruits caspase-8. In this complex, as well as in complex IIa caspase-8 activates caspase-3, -6 and -7 resulting in cleavage of many of their substrates and subsequently to cell death. Nevertheless, in the absence or upon inhibition of caspase-8 and cIAPs or the LUBAC complex, RIPK1 kinase activity promotes the assembly of the necrosome. RIPK1 subsequently recruits RIPK3. It has yet to be resolved whether RIPK1 is needed for the autophosphorylation of RIPK3 or whether trans-phosphorylation of the kinase occurs [135]. However, activated RIPK3 was shown to form amyloid fibrils, which might function as platform for RIPK1 stabilization as well as for recruitment of mixed lineage kinase domain like pseudokinase (MLKL) [136]. MLKL is considered the key element of necroptosis. It is phosphorylated by RIPK3, which leads to exposure of its N-terminal four-helical bundle domain, oligomerization and translocation to the plasma membrane. It is still under debate, how MLKL oligomers exactly execute cell death. However, it is generally agreed, that its phosphorylation is followed by ion influx and disruption of membrane integrity [121].

Regulation of TNF-R1-induced cell death is insufficiently understood. Though several distinct checkpoints involving the central protein RIPK1 have been identified. In TNF-R1 complex I RIPK1 is not only highly ubiquitinated by the LUBAC complex and cIAPs, it is also phosphorylated at several sites. Independent of I κ B α activation, IKK α and IKK β phosphorylate RIPK1, inhibiting its FADD-binding capacity [137]. Furthermore, it was shown that the p38-downstream target MAPK-activated protein kinase 2 phosphorylates RIPK1 at Serine 321 in complex I to prevent complex II formation and cell death [138]. Very recently a third checkpoint for RIPK1 was identified. The group of H. Walczak discovered a mechanism by which the IKK α /IKK β homologous kinases TANK-binding kinase 1 and IKK ϵ are shuttled to TNF-R1 complex I by TRAF family member-associated NF- κ B activator and nucleosome assembly protein, phosphorylating RIPK1 at several sites [139].

Fine-tuning of the ubiquitination status of RIPK1 is an additional control mechanism in TNF-R1 signaling. Main regulators in this process are three deubiquitinases, namely OTULIN, CYLD and A20. Whereas the first two cleave M1-linked ubiquitin, A20 is thought to rather stabilize linear ubiquitination [140].

Besides keeping RIPK1 in check, activation of NF- κ B also directly suppresses cell death execution by upregulating FLICE-like inhibitory protein (FLIP) expression [141]. FLIP is a potent inhibitor of caspase-8, as it resembles its structure while lacking enzyme activity. Additionally, cIAP expression is regulated by NF- κ B [142]. Interestingly, recently two independent groups showed

that even initialized necroptotic cell death can be prevented when there is limited MLKL activation [143, 144]. The authors show, that during necroptosis the endosomal sorting complexes required for transport (ESCRT)-III machinery is activated, leading to exosome formation. MLKL oligomers are removed in those vesicles, which prevents TNF-R1 induced necroptosis.

1.3.3 Death receptor 6 signaling

DR6 is less characterized than the other TNF-R superfamily members. Nevertheless, DR6 is known to be expressed ubiquitously and even showed elevated expression in some cancer types on TCs. *In vitro* studies revealed its expression being regulated by NF- κ B activation [145]. The same authors showed, that overexpression of DR6 leads to activation of NF- κ B, activation of JNK and apoptosis. Unfortunately, the exact signaling cascade remains elusive.

The physiological role of DR6 was discovered in studies with DR6^{-/-} mice and seems to lie in regulating the adaptive immune system, hence it is discussed as target in inflammatory and autoimmune disease [146]. On ECs, DR6 can induce necroptosis after binding membrane-bound APP on TCs (Chapter 1.2.3) [110]. So far membrane-bound APP is the only described ligand for DR6.

1.4 Aim

Metastasis is a multistep process in which many aspects still remain elusive. It is obvious that only profound knowledge of this complex mechanism enables to control and prevent tumor metastasis as well as to improve survival of cancer patients.

Changes in ADAM17 expression and activity were associated with various pathologies. Particularly, its contribution to tissue inflammation was thoroughly investigated. Nevertheless, only little is known about the role of ADAM17 in cancer. In fact, its function in metastasis has not been addressed so far.

Therefore, we want to study the impact of ADAM17 on host cells in metastasis. To this aim, we inject TCs i.v. in hypomorphic ADAM17 mice or in mice with cell type-specific deletion of ADAM17. To assess early and late events in the metastatic process we will examine lungs of these mice at two different time points histologically and biochemically.

Using TCs expressing β -galactosidase, we will be able to trace them within the tissue by X-Gal staining, shortly after injection. This will provide further information on TC extravasation and outgrowth.

Taken together, we aim to find out whether ADAM17 is a promising target for metastasis and cancer therapy.

2 Material & Methods

2.1 Material

2.1.1 Chemicals and recombinant proteins

| | |
|--|---------------------------------------|
| Anti-FLAG M2 agarose beads | Sigma-Aldrich, Steinheim, Germany |
| CFSE | Thermo Scientific, Darmstadt, Germany |
| cOmplete™ Protease inhibitor cocktail | Roche, Mannheim, Germany |
| Dako Protein block serum-free | Agilent, Waldbronn, Germany |
| Dulbecco's modified Eagle's medium | Sigma-Aldrich, Steinheim, Germany |
| Endothelial cell growth medium 2 | Promocell, Heidelberg, Germany |
| Endothelial cell growth medium MV2 | Promocell, Heidelberg, Germany |
| Enzastaurin | Biomol, Hamburg, Germany |
| Enbrel® (Etanercept) | Pfizer, Berlin, Germany |
| Ethidium homodimer III | Biotium, Fremont, CA, USA |
| FCS | PAN Biotech, Aidenbach, Germany |
| FITC-Dextran FD-40S | Sigma-Aldrich, Steinheim, Germany |
| GW280264 | Iris Biotech, Marktredwitz, Germany |
| Histokitt II | Carl Roth, Karlsruhe, Germany |
| Hoechst33342 | Sigma-Aldrich, Steinheim, Germany |
| Lipofectamine RNAiMAX | Thermo Scientific, Darmstadt, Germany |
| Nuclear fast red | Sigma-Aldrich, Steinheim, Germany |
| NucleoZOL | Macherey-Nagel, Düren, Germany |
| OCT TissueTek compound | Plano GmbH, Wetzlar, Germany |
| PageRuler™ Prestained protein ladder | Thermo Scientific, Darmstadt, Germany |
| PBS without CaCl ₂ /MgCl ₂ | Sigma-Aldrich, Steinheim, Germany |
| Penicillin-Streptomycin solution | Sigma-Aldrich, Steinheim, Germany |
| PhosSTOP™ | Roche, Mannheim, Germany |
| PEI | Polysciences, Eppelheim, Germany |
| Precision Plus Protein™ Dual color | Bio-Rad, Munich Germany |
| Protein G Sepharose® beads | Sigma-Aldrich, Steinheim, Germany |
| Tamoxifen | Sigma-Aldrich, Steinheim, Germany |

2 Material & Methods

| | |
|------------------------------|--------------------------------------|
| TAPI-1 | Enzo Life Sciences, Lörrach, Germany |
| TPCA-1 | Biomol, Hamburg, Germany |
| Trypsin-EDTA solution 0.25 % | Sigma-Aldrich, Steinheim, Germany |
| zVAD | Bachem, Bubendorf, Germany |
| X-Gal | AppliChem, Darmstadt, Germany |

All other chemicals were purchased from Carl Roth (Karlsruhe, Germany), Sigma-Aldrich (Steinheim, Germany) or AppliChem (Darmstadt, Germany).

Table 2.1: Recombinant proteins.

| Name | Supplier | Product # |
|---|---|----------------|
| recombinant human TNF α | Immunotools, Friesoythe, Germany | 11343013 |
| recombinant human moTAP-TNF α | generous gift from Henning Walczak (UCL Cancer Institute, London) | |
| recombinant murine TNF α | Immunotools, Friesoythe, Germany | 12343010 |
| recombinant murine ADAM17 | generous gift from Christoph Becker-Pauly (CAU, Kiel, Germany) | |
| recombinant human jagged-1-Fc chimera protein | R&D, Wiesbaden, Germany | 1277-JG |
| recombinant human APP-Fc chimera protein | Biozol, Eching, Germany | SIN-10703-H02H |
| recombinant human IgG1 | R&D, Wiesbaden, Germany | 110-HG |
| PEPDAB005 | Biozyme, Apex, USA | PEPDAB005m001 |

2.1.2 Primer

All oligonucleotides were purchased from and synthesized by Sigma-Aldrich.

Table 2.2: Primers for genomic DNA.

| Target | Forward Primer (5'-3') | Reverse Primer (5'-3') | Expected bandsize |
|-------------------------|-------------------------|------------------------|------------------------------|
| <i>Adam17</i> | CTTCGTATAATGTATGCTATACG | TCTCTGGACCCCTTCTTCCT | 250 bp (wt) 150 bp (flox) |
| | TGGGGAAGCAAAGTTGTAGG | | |
| ADAM17 ^{ex/ex} | TATGTGATAGGTGTAATG | CTTATTATTCTCGTGGTCACC | 500 bp (wt) 250 bp (tg) |
| Cre | CGAGTGATGAGGTTGCAAG | TGAGTAAACGAACCTGGTCG | 390 bp |
| <i>Prckb</i> | CAGGGTCGAATTGCCATCCTCCA | AGCCACTCTCGGTGCTGTG | 1300 bp (tg) 391 (wt) |
| | CTTGGGTGGAGAGGCTATTC | | |

Table 2.3: Primers for quantitative Real-Time PCR.

| Target | Forward Primer (5'-3') | Reverse Primer (5'-3') | UPL | Sequence reference |
|-----------------|----------------------------|-------------------------|-----|--------------------|
| <i>Adam17</i> | TGTGGTTATTTAAATGCAGATAGTGA | TCACTCGACGAACAACTCTTC | 38 | NM_009615.6 |
| <i>Axl</i> | CGCTGTGAAGACCATGAAAA | TGCAGACAGCTTCACTCAGG | 78 | NM_009465.4 |
| <i>Col6a1</i> | GACATCCAGGGCTCCAAA | AGGTGTGCGAGCACGAAGAAT | 97 | NM_009933.4 |
| <i>Hes-1</i> | TGCCAGCTGATATAATGGAGAA | CCATGATAGGCTTTGATGACTTT | 20 | NM_008235.2 |
| <i>Twist1</i> | AGCTACGCCTTCTCCGTCT | TCCTTCTCTGGAAACAATGACA | 58 | NM_011658.2 |
| <i>Vimentin</i> | CCAACCTTTTCTCCCTGAAC | TTGAGTGGGTGTCAACCAGA | 109 | NM_011701.4 |
| <i>Gapdh</i> | AAGAGGGATGCTGCCCTTAC | CCATTTTGTCTACGGGACGA | 33 | NM_001289726.1 |

2.1.3 siRNA

Table 2.4: siRNA

| Target | Target Sequence | Distributor (Product #) |
|----------------------------------|---------------------------|-------------------------------|
| <i>Adam17 (mouse)</i> | GGACGUAAUUGAGCGAUUU | Dharmacon (L-040408-00-0010) |
| | GGUAGCAGAUCAUCGAUUU | |
| | UAUGGGAACUCUUGGAUUA | |
| | UGACCGAGUUGAUGACAUA | |
| <i>Adam17 (human)</i> | GGAAGCUGACCUGGUUACAACUCAU | Thermo Scientific (HSS110434) |
| | CCAGGGAGGGAAAUAUGUCAUGUAU | Thermo Scientific (HSS110435) |
| | CAGAAUCGUGUUGACAGCAAAGAAA | Thermo Scientific (HSS186181) |
| <i>Prckb (human)</i> | GGUCAUGCUUUCAGAACGA | Dharmacon (L-003758-00-0005) |
| | CCUGUCAGAUCCCUACGUA | |
| | GAUUUGGGAUUGGGAUUUUG | |
| | UCAUUGUCCUCGUAAGAGA | |
| <i>Tnfrsf1a (human)</i> | CAAAGGAACCUACUUGUAC | Dharmacon (L-005197-00-0005) |
| | GAGCUUGAAGGAACUACUA | |
| | AAGCUCUACUCCAUUGUUU | |
| | CCGUUGCGCUGGAAGGAAU | |
| <i>Control (human and mouse)</i> | not known | Dharmacon (D-001810-10-05) |

2.1.4 Antibodies

Table 2.5: Primary antibodies.

| Target | Host | Dilution | Application | Distributor (Product #) |
|--------------------------|--------|----------|----------------------|---|
| ADAM17 (human) | rabbit | 1:2 000 | Immunoblot | Abcam (ab39162) |
| ADAM17 (mouse) | rabbit | 1:1 000 | Immunoblot | Kerafast (EHS008) |
| P-Axl | rabbit | 1:1 000 | Immunoblot | Abcam (77773) |
| Axl | rabbit | 1:1 000 | Immunoblot | Cell Signaling (49775) |
| β -actin | mouse | 1:10 000 | Immunoblot | Sigma-Aldrich (A1978) |
| β -galactosidase | rabbit | 1:5 000 | Immunohistochemistry | Cell Signaling (27198) |
| cleaved caspase-8 | rabbit | 1:1 000 | IP/Immunoblot | Cell Signaling (9429) |
| caspase-8 (mouse) | mouse | 1:1 000 | IP/Immunoblot | Enzo Life Sciences (1G12) |
| CD31 | rat | 1:500 | Immunohistochemistry | BD Bioscience (550274) |
| cIAP1 | rabbit | 1:1 000 | IP/Immunoblot | generous gift from H.Walczak/J.Silke |
| ERK1/2 | rabbit | 1:1 000 | Immunoblot | Cell Signaling (4695) |
| F4/80 | rat | 1:200 | Immunohistochemistry | Bio-Rad (MCA497R) |
| FADD | mouse | 1:1 000 | IP/Immunoblot | Enzo Life Sciences (1F7) |
| FADD | goat | 1:14 | IP | Santa Cruz (sc-6036) |
| FLAG | mouse | 1:1 000 | IP/Immunoblot | Sigma-Aldrich (F1804) |
| HOIP | mouse | 1:1 000 | IP/immunoblot | Thermo Scientific (costume made) |
| IgG (human) | rabbit | 1:20 000 | in vitro assay | Thermo Scientific (31142) |
| P-I κ B α | rabbit | 1:1 000 | Immunoblot | Cell Signaling (9246) |
| I κ B α | mouse | 1:1 000 | Immunoblot | Cell Signaling (4814) |
| P-IKK α / β | rabbit | 1:1 000 | Immunoblot | Cell Signaling (2078) |
| IKK α | rabbit | 1:1 000 | Immunoblot | Cell Signaling (2682) |
| P-JNK | mouse | 1:1 000 | Immunoblot | Santa Cruz (sc-6254) |
| Ly6G | rat | 1:400 | Immunohistochemistry | eBioscience (14-5931) |
| P-MLKL (mouse) | rabbit | 1:1 000 | Immunoblot | Abcam (ab196436) |
| MLKL | rabbit | 1:1 000 | Immunoblot | Abcam (ab184718) |
| cleaved Notch1 | rabbit | 1:1 000 | Immunoblot | Cell Signaling (4147) |
| Notch1 | rabbit | 1:1 000 | Immunoblot | Cell Signaling (3439) |

2 Material & Methods

| Target | Host | Dilution | Application | Distributor (Product #) |
|----------------|--------|----------|----------------------|--------------------------------------|
| P-p38 | rabbit | 1:1 000 | Immunoblot | Cell Signaling (9215) |
| PCNA | mouse | 1:400 | Immunohistochemistry | Santa Cruz (sc-56) |
| RIPK3 | rabbit | 1:1 000 | IP/Immunoblot | Enzo Life Sciences (ADI-905-242-100) |
| P-RIPK1 (S166) | rabbit | 1:1 000 | Immunoblot | Cell Signaling (31122) |
| RIPK1 | mouse | 1:1 000 | IP/Immunoblot | BD Bioscience (610459) |
| TRADD | mouse | 1:1 000 | IP/immunoblot | Santa Cruz (sc-6254) |
| TRAF2 | rabbit | 1:1 000 | IP/Immunoblot | Enzo Life Sciences (ADI-APP-422) |

Table 2.6: Secondary antibodies.

| Target | Tag | Dilution | Distributor (Product #) |
|--------|------------------------|----------|----------------------------|
| rat | Alexa Flour® 488 | 1:200 | Life Technologies (A21208) |
| rabbit | Alexa Flour® 647 | 1:200 | Life Technologies (A31573) |
| mouse | Horseradish peroxidase | 1:10 000 | Thermo Scientific (31432) |
| rabbit | Horseradish peroxidase | 1:10 000 | Dianova (111-035-144) |
| rat | Biotin | 1:200 | Dako (E0468) |

2.1.5 Cell lines

Table 2.7: Cell lines.

| Cell line | Source of cells | Culture medium | Source |
|--|------------------------------|---|--|
| LLC | murine lung carcinoma | DMEM + 10 % FCS | Cell lines service, Eppelheim, Germany |
| B16F1 | murine melanoma | DMEM + 10 % FCS | Cell lines service, Eppelheim, Germany |
| LLC-LacZ | murine lung carcinoma | DMEM + 10 % FCS | generous gift from by Achim Krüger (Technische Universität München, Germany) |
| B16F1-LacZ | murine melanoma | DMEM + 10 % FCS | generous gift from Achim Krüger (Technische Universität München, Germany) |
| MEF ADAM17 ^{ex/ex} | murine embryonic fibroblasts | DMEM + 10 % FCS + 1 % Penicillin/Streptomycin | generous gift from Athena Chalaris (CAU, Kiel, Germany) |
| MEF ADAM17 ^{wt/wt} | murine embryonic fibroblasts | DMEM + 10 % FCS + 1 % Penicillin/Streptomycin | generous gift from Athena Chalaris (CAU, Kiel, Germany) |
| MEF PSEN1 ^{+/-/2^{-/-}} | murine embryonic fibroblasts | DMEM + 10 % FCS + 1 % Penicillin/Streptomycin | generous gift from Paul Saftig (CAU, Kiel, Germany) |
| HUVEC | human umbilical vein | Endothelial Cell Growth Medium 2 | Promocell, Heidelberg, Germany |
| HMVEC-L | human lung | Endothelial Cell Growth Medium MV2 | generous gift from Boris Strilic (MPI Bad Nauheim, Germany) |
| HEK ADAM17 ^{-/-} | human kidney | DMEM + 10 % FCS | generous gift from Björn Rabe (CAU, Kiel, Germany) |
| HEK 293T | human kidney | DMEM + 10 % FCS | DSMZ, Braunschweig, Germany |
| MDA-MB231 | human breast cancer | DMEM + 10 % FCS + 1 % Penicillin/Streptomycin | generous gift from Nina Hedemann (UKSH, Kiel, Germany) |

2.1.6 Mice

Table 2.8: Mice used for experiments.

| Mouse line | Term (in this study) | Source | Reference |
|--|---|---|-----------|
| <i>Adam17^{ex/ex}</i> | ADAM17 ^{ex/ex} | Athena Chalaris (CAU, Kiel, Germany) | [39] |
| <i>Adam17^{tm1.2Bbl/J}</i> | ADAM17 ^{fl/fl} | Jackson Laboratory (Bar Harbor, USA) | [147] |
| B6.Tg(Cdh5-cre/ER ^{T2})1Rha | VE-Cdh5ER ^{T2} -Cre | Ralf Adams (MPI, Münster, Germany) | [148] |
| B6.129P2- <i>Lyz2^{tm1(cre)lfo/J}</i> | LysM-Cre | Jackson Laboratory (Bar Harbor, USA) | [149] |
| B6.Tg(Cd4-cre)1Cwi/Bflw; <i>Adam17^{tm1.2Bbl/J}</i> | CD4-Cre;ADAM17 ^{fl/fl} (ADAM17 ^{ΔT/ΔT}) | Hans-Willi Mittrücker (UKE, Hamburg, Germany) | [150] |
| B6. <i>Ripk3^{-/-}</i> | RIPK3 ^{-/-} | Dieter Adam, Stefan Krautwald (UKSH, Kiel, Germany) | [151] |
| B6. <i>Prkcb^{-/-}</i> | PKCβ ^{-/-} | Michael Leitges (Biotek, Oslo, Norway) | [152] |
| C57BL/6N | WT | Charles River (Sulzfeld, Germany) | |

2.2 Methods

2.2.1 Animal experimentation

2.2.1.1 Housing

Mice were housed at a 12 h light cycle under specific pathogen free conditions and fed a standard laboratory chow (Sniff V1534-000, Soest, Germany) *ad libitum*. Room temperature (RT) was kept stable at 22°C. Animals were treated according to German and European animal regulations.

2.2.1.2 Breeding

Mice were used for breeding at an age of at least 8 weeks. For the duration of breeding they received a special chow (Sniff V1124-000, Soest, Germany). Pups were weaned 3 weeks after birth. All mice used in this study were crossed to a C57BL/6N background.

For breeding of hypomorphic ADAM17^{ex/ex} mice heterozygous female mice were mated with homozygous male mice due to infertility of homozygous ADAM17^{ex/ex} female mice [39]. Experiments were conducted only on homozygous ADAM17^{ex/ex} mice of both sexes.

PKCβ^{-/-} mice were bred homozygously. Homozygous PKCβ^{-/-} mice of both sexes were used for experiments.

Tissue-specific knock-out of ADAM17 was achieved by using the Cre/loxP system [153]. Mice with loxP-sites flanking exon 2 of the *Adam17* gene (ADAM17^{fl/fl}) were bred to mice heterozygously expressing Cre recombinase under the control of the *Cdh5*- (VE-Cdh5ER^{T2}-Cre) or *LysM*-promotor (LysM-Cre). LysM-Cre^{+/-};ADAM17^{fl/fl} (ADAM17^{ΔMC/ΔMC}) mice exhibit ADAM17 deficiency only on myeloid cell. Knock-out of ADAM17 on ECs in 9 week old VE-Cdh5ER^{T2}-Cre^{+/-};ADAM17^{fl/fl} (ADAM17^{iΔEC/iΔEC}) mice was induced by injection of 25 mg/kg bodyweight Tamoxifen (TAM) in ethanol/oil intraperitoneal (i.p.) 4 consecutive days. Mice were then used for experiments within 1 week. RIPK3^{-/-} were kindly provided by Dieter Adam and Stefan Krautwald for the indicated experiments. CD4-Cre^{+/-};ADAM17^{fl/fl} mice (ADAM17^{ΔT/ΔT}) were kindly provided by Hans-Willi Mittrücker for the indicated experiments. Names, sources and references for the mouse strains used in this study are listed in Table 2.8.

2.2.1.3 Genotyping

To analyze the genotype, a short tail biopsy of 3 to 5 week old mice was taken. Hot scissors were used in order to avoid inflammation, bleeding and cross-contamination. Tails were digested in 0.5 mL DNA digestion buffer at 55°C and 1000 rpm overnight (ON). Digested material was pelleted at 13 000 rpm for 5 min. The supernatant (SN) was transferred to a fresh tube and mixed

2 Material & Methods

with 170 μ L saturated NaCl solution. After centrifugation for 20 min at 13 000 rpm to pellet proteins, SN was transferred to a new reaction tube and mixed with 1 mL 100 % ethanol to precipitate the DNA. Samples were centrifuged at 13 000 rpm for 5 min. SN was discarded and the pellet washed with 0.5 mL 70 % ethanol for 5 min at 13 000 rpm. After removing the SN, the pellet was allowed to dry for 15 min and then resuspended in 50-100 μ L TE-buffer. Better solubility of the DNA was achieved by heating up the solution to 50°C for 5-20 min. Genomic DNA from 10-20 mg tissue was isolated according to this protocol, too. DNA was stored at -20°C or directly used for genotyping PCRs.

| | | |
|---------------------------------------|---------------|---------------------------------------|
| DNA digestion buffer | 100 mM | Tris-HCl pH 8.5 |
| | 200 mM | NaCl |
| | 5 mM | EDTA |
| | 0.2 % | SDS |
| | 0.3 mg/mL | Proteinase K (added right before use) |
| TE-buffer | 100 mM | Tris-HCl pH 7.5 |
| | 0.1 mM | EDTA |
| PCR mix ADAM17^{ex/ex} | 1.0 μ L | DNA |
| | 2.0 μ L | 10x DreamTaq™ buffer |
| | 2.0 μ L | dNTPs (2 mM) |
| | 1.5 μ L | 5'Primer (10 μ M) |
| | 1.5 μ L | 3'Primer (10 μ M) |
| | 0.2 μ L | DreamTaq™ Polymerase |
| | ad 20 μ L | ddH ₂ O |

Table 2.9: ADAM17^{ex/ex} PCR conditions.

| Step | Temperature | Time | Cycles |
|----------------------|-------------|----------|--------|
| Initial denaturation | 95°C | 5' | 1 |
| Denaturation | 95°C | 1' | 29 |
| Annealing | 58°C | 1' | |
| Elongation | 72°C | 1' | |
| Final elongation | 72°C | 5' | 1 |
| Storage | 4°C | ∞ | 1 |

| | | |
|---------------------------------------|-----------------------------|---------------------------|
| PCR mix ADAM17^{fl/fl} | 2.0 µL | DNA |
| | 1.0 µL | dNTPs (20 mM) |
| | 1.0 µL | MgCl ₂ (25 mM) |
| | 2.0 µL | 5' Primer 1 (10 µM) |
| | 2.0 µL | 3' Primer (10 µM) |
| | 0.1 µL | DreamTaq™ Polymerase |
| | ad 20 µL ddH ₂ O | |

The same PCR is performed with 5' Primer 2.

Table 2.10: ADAM17^{fl/fl} PCR conditions.

| Step | Temperature | Time | Cycles |
|----------------------|-------------|------|--------|
| Initial denaturation | 94°C | 3' | 1 |
| Denaturation | 94°C | 30" | 35 |
| Annealing | 58°C | 30" | |
| Elongation | 72°C | 30" | |
| Final elongation | 72°C | 10' | 1 |
| Storage | 4°C | ∞ | 1 |

| | | |
|--------------------|-----------------------------|----------------------|
| PCR mix Cre | 2.0 µL | DNA |
| | 3.0 µL | 10x DreamTaq™ buffer |
| | 3.0 µL | dNTPs (2 mM) |
| | 1.5 µL | 5' Primer (10 µM) |
| | 1.5 µL | 3' Primer (10 µM) |
| | 0.2 µL | DreamTaq™ Polymerase |
| | ad 30 µL ddH ₂ O | |

Table 2.11: Cre PCR conditions.

| Step | Temperature | Time | Cycles |
|----------------------|-------------|------|--------|
| Initial denaturation | 95°C | 2' | 1 |
| Denaturation | 95°C | 30" | 30 |
| Annealing | 56°C | 30" | |
| Elongation | 72°C | 30" | |
| Final elongation | 72°C | 10' | 1 |
| Storage | 4°C | ∞ | 1 |

| | | |
|--|---------------|--------------------------|
| PCR mix PKC$\beta^{-/-}$ | 1.0 μ L | DNA |
| | 2.0 μ L | 10x DreamTaq™ buffer |
| | 2.0 μ L | dNTPs (20 mM) |
| | 1.0 μ L | 5' Primer 1 (10 μ M) |
| | 1.0 μ L | 5' Primer 2 (10 μ M) |
| | 1.0 μ L | 3' Primer (10 μ M) |
| | 0.2 μ L | DreamTaq™ Polymerase |
| | ad 20 μ L | ddH ₂ O |

Table 2.12: PKC $\beta^{-/-}$ PCR conditions.

| Step | Temperature | Time | Cycles |
|----------------------|-------------|----------|--------|
| Initial denaturation | 94°C | 5' | 1 |
| Denaturation | 94°C | 30" | 40 |
| Annealing | 58°C | 30" | |
| Elongation | 72°C | 1' | |
| Final elongation | 72°C | 10' | 1 |
| Storage | 4°C | ∞ | 1 |

Primer sequences for all genotyping PCRs are listed in Table 2.2. PCRs were separated by agarose gel electrophoresis.

2.2.1.4 Experimental metastasis model

At the age of 9-12 weeks, mice were injected with 5×10^5 LLC or B16F1 cells in 250 μ L sterile PBS intravenously (i.v.) into the tail vein. Mice were sacrificed 6 h, 24 h, 1 week, 2 weeks and 3 weeks after TC injection. For inhibitory experiments 12 mg/kg bodyweight TAPI-1 or 1 mg/kg bodyweight ADAM17-PD (generous gift from I. Sagi, Weizmann Institute of Science, Israel) were injected i.v. 5 min prior to TC injection. To assess endothelial permeability, mice were injected with 200 μ L 2.5 mg/mL FITC-labeled 40 kDa dextran 10 min prior sacrificing. For the identification of necroptotic ECs, ethidium homodimer III (EthDIII) was injected i.v. at a concentration of 300 μ M in 50 μ L sterile PBS 5 min before sacrificing the mice. Experiments were approved by the German and European governments with the reference numbers V242-74639/2016(75-6/15), V243-65407/2015(75-6/11) and V242-70603/2017(53-5/16).

2.2.1.5 Organ harvesting and blood sampling

Mice were killed by cervical dislocation. The thorax was opened immediately and blood was taken directly from the heart. It was transferred to micro tubes with lithium-heparin (25 I.U.

heparin/mL blood). Samples were centrifuged at RT for 10 min at 2 000 ×g. Plasma was transferred to fresh tubes and stored at -80°C. The lung was dissected and tumors counted. The organ was weighed and processed for further use.

2.2.1.6 *Immunohistochemistry*

Lung tissue was fixed in 4 % formaldehyde in PBS (v/v) ON and stored in 1 % formaldehyde in PBS (v/v) at 4°C. Samples were washed several times in ddH₂O and incubated ON in 50 % ethanol. Next day the tissue samples were dehydrated.

| | | |
|--------------------|---------|------------------|
| Dehydration | 60 min | 70 % ethanol |
| | 30 min | 96 % ethanol I |
| | 60 min | 96 % ethanol II |
| | 90 min | 100 % ethanol I |
| | 120 min | 100 % ethanol II |
| | 90 min | xylol I |
| | 90 min | xylol II |
| | 30 min | paraffin I |
| | ON | paraffin II |
| | 30 min | paraffin III |

The tissue was embedded in paraffin and cut into 8 µm-thick sections. Sections were stained with hematoxylin-eosin (HE) according to standard procedures. Additionally, sections were stained with primary antibodies (Table 2.5) and secondary, biotinylated antibodies (Table 2.6). Subsequently, the secondary antibody was detected using a peroxidase DAB kit according to manufacture's instructions (Dako, Hamburg, Germany).

2.2.1.7 *Immunofluorescence*

Lung tissue was snap frozen in OCT TissueTek compound and cut into 8 µm-thick sections. Sections were fixed in acetone-methanol (v/v) for 2 min and stained with primary antibodies (Table 2.5), which were detected by fluorescent-coupled secondary antibodies (Table 2.6).

2.2.1.8 *β-galactosidase staining*

Lung tissue was snap frozen in OCT TissueTek compound and cut into 8 µm-thick sections. Sections were fixed in 0.2 % glutaraldehyde for 10 min at 4°C. Slides were then washed 3 times in LacZ washing buffer at RT. Subsequently, sections were circled with a pap pen (DAKO, Hamburg, Germany) and incubated at 37°C ON with 90 µL staining solution per section in a

humidified chamber. The next day, slides were washed for 5 min in PBS and ddH₂O, respectively. Sections were counterstained with nuclear fast red for 5 min and subsequently washed with H₂O. Finally, sections were dehydrated and mounted with Histokitt II (Carl Roth, Karlsruhe, Germany).

| | | |
|----------------------------|--------|---------------------|
| LacZ washing buffer | 2 mM | MgCl ₂ |
| | 0.01 % | Sodium deoxycholate |
| | 0.02 % | NP-40 |
| | ad | PBS |

| | | |
|--------------------------|-----------|------------------------------------|
| Staining solution | 5 mM | K ₃ Fe(CN) ₆ |
| | 5 mM | K ₄ Fe(CN) ₆ |
| | 0.5 mg/mL | X-Gal |
| | ad | washing buffer |

| | | |
|----------------------------------|-------|---|
| Nuclear fast red solution | 25 g | Al ₂ (SO ₄) ₃ |
| | 0.5 g | Nuclear fast red |
| | ad | 500 mL ddH ₂ O |
| | | filter before use |

2.2.1.9 RNA isolation

Total RNA was isolated from 25 mg lung tissue samples using TRIzol according to manufacturers' protocol. RNA was precipitated ON at -20°C.

2.2.1.10 cDNA synthesis

Isolated RNA was transcribed to cDNA using RevertAid™ Reverse transcriptase (Thermo Scientific, Darmstadt, Germany).

| | | |
|---------------------|----------|--|
| cDNA PCR mix | 1.0 µg | RNA |
| | 2.0 µL | oligo(dT) ₁₈ primer |
| | 3.0 µL | 10x reaction buffer |
| | 2.0 µL | dNTPs (10 mM) |
| | 1.0 µL | RevertAid™ Reverse transcriptase |
| | ad 20 µL | Diethyl pyrocarbonate-treated H ₂ O |

The mix was incubated for 60 min at 42°C. Reaction was terminated for 10 min at 70°C. cDNA was used for quantitative real-time PCR (qRT-PCR) immediately or stored at -20°C.

2.2.1.11 Quantitative real-time PCR

cDNA samples were analyzed on a Roche Light Cycler 480 II with primers and corresponding UPL

probes listed in Table 2.3. Cp values were corrected for the reference gene and the primer efficiency (E) according to the following term: $E^{-(Cp-Cp(\text{reference gene}))}$.

2.2.2 Cell culture

2.2.2.1 Culture conditions

Cell lines (Table 2.7) were cultured in incubators at 37°C, 5 % CO₂ and 95 % humidity. Work with the cells was performed under sterile conditions.

2.2.2.2 Passaging

Cells were expanded and passaged upon confluency. Cells were washed once with PBS and detached using EDTA/Trypsin. After incubation, detached cells were resuspended in cell culture medium and centrifuged at 200 ×g for 5 min. SN was removed, cells were resuspended in fresh medium and seeded in new cell culture flasks or dishes. HUVECs and HMVECs were passaged 3 times maximum.

2.2.2.3 Freezing and thawing

Cells were detached from cell culture flasks, centrifuged and resuspended in freezing medium. The suspension was cooled down slowly in a freezing container to -80°C. Frozen cell stocks were stored at -150°C long-term.

Freezing medium 10 % DMSO
 ad FCS

Cells were thawed rapidly at 37°C and resuspended in pre-heated cell culture medium. The cell suspension was centrifuged at 200 ×g for 5 min. SN was removed, the cells resuspended in fresh medium and seeded in a cell culture flask or dish.

2.2.2.4 Cell count

Determination of cell concentration was achieved using a Neubauer hemocytometer. Therefore, 20 µL of a cell suspension was used. All cells in the counting grid squares were counted, the average calculated and multiplied by 10⁴ to determine the cell concentration in 1 mL suspension.

2.2.2.5 Transient transfection of cells

5×10⁴ HEK 293 and HEK A17^{-/-} were seeded in 6-wells. The cells were transfected with either hDR6-EGFP-pCMV3 (generous gift from B. Strilic, MPI Bad Nauheim, Germany) or hTNF-R1-pEYFP plasmid (generous gift from W. Schneider-Brachert, Institute for Clinical Microbiology and Hygiene, University Hospital Regensburg, Germany) in order to overexpress DR6 or TNF-R1,

respectively. Transfection was performed at a ratio of 1:3 with polyethylenimine (PEI) and transfection efficiency was controlled by fluorescence microscopy. On the next day cells were either analyzed for cell death (for protocol see 2.2.2.10) or subjected to immunoblot analysis (for protocol see 2.2.3) to analyze shedding of DR6 and TNF-R by ADAM17.

2.2.2.6 Cell transfection with siRNA

Gene expression in HUVECs and HMVECs was down regulated using small interfering RNA (siRNA). 2 pmol siRNA for 10^4 cells and 40 pmol for 2×10^5 cells was used. Transfection was performed using Lipofectamine RNAiMAX (Thermo Scientific, Darmstadt, Germany), according to manufacturers' protocol on two consecutive days.

2.2.2.7 Cell staining with CFSE

For transmigration and co-culture experiments MDA-MB231 cells were detached with EDTA/trypsin and centrifuged for 5 min at $200 \times g$. SN was removed and the cell pellet was resuspended in 300 μ L PBS. CFSE was added to the cell suspension with a final concentration of 8 μ M. The cells were incubated in the dark for 10 min at RT and for 5 min at 4°C. The staining reaction was stopped by adding 1.7 mL cell culture medium to the suspension. Subsequently cells were spun down by centrifugation and counted (for protocol see 2.2.2.4).

2.2.2.8 Transmigration assay

HUVECs and HMVECs were cultured for two days and subsequently seeded at 5×10^4 into collagen I-coated 24-well inserts with a pore diameter of 8 μ m (Sarstedt, Rommelsdorf, Germany). On the next day, ECs were transfected with siRNA on two consecutive days (for protocol see 2.2.2.6). For the transmigration experiments 5×10^4 MDA-MB123 cells were stained with 8 μ M CFSE (for protocol see 2.2.2.7) and seeded on top of the ECs. Inhibitors were added in both the insert and the well 10 min before adding the TCs. After incubation for 6 h at 37°C, 5 % CO₂ and 95 % humidity, all remaining cells on top of the membrane were removed with a cotton bud. Transmigrated cells that passed the membrane were then imaged on a Leica DMI8 fluorescence microscope (Leica, Wetzlar, Germany) and quantified using ImageJ (Version 1.51j8, NIH, USA).

2.2.2.9 Co-culture and necroptosis experiments

To assess cell death *in vitro* 10^4 HUVECs were seeded in collagen I-coated lumox 96-well plates (Sarstedt, Rommelsdorf, Germany) and transfected with siRNA (for protocol see 2.2.2.6). 1.5×10^5 CFSE-stained MDA-MB231 cells (for protocol see 2.2.2.7) were seeded on top of the HUVECs in endothelial growth medium. Cells were incubated for 6 h and analyzed for cell death (for protocol

see 2.2.2.10). To trigger cell death independent of TCs, HUVECs or MEF cells were either treated with 100 μ M of the pan-caspase inhibitor zVAD alone or together with 5 μ M of the IKK β inhibitor TPCA-1 in 6-well plates. After incubation for 10 min, the cells were stimulated with 50 ng/mL TNF α . The cells were then incubated for 6 h and cell death was analyzed (for protocol see 2.2.2.10).

2.2.2.10 Cell death analysis

Cells were stimulated or co-cultured (for protocol see 2.2.2.9). After incubation the cells were stained with 2 μ M Hoechst33342 and 1.6 μ M EthDIII and subsequently imaged on an Olympus Fluoview 1000 confocal laser scanning microscope (Olympus, Hamburg, Germany) in a climate chamber (37°C, 5 % CO₂, 55 % humidity). EthDIII⁺ cells were quantified with ImageJ and expressed as percentage of all cells.

2.2.2.11 APP/jagged-1 assay

A 96-well plate was coated with 6.48 ng/mL IgG1 antibody diluted in PBS for 30 min at 37°C, 5 % CO₂ and 95 % humidity. The wells were washed once with PBS and subsequently blocked for 1 h with cell culture medium in the incubator. Medium was removed and 18 nM IgG1-Fc or APP-Fc diluted in PBS was added and incubated for 1 h in the incubator. Wells were washed once with PBS. 5 \times 10⁴ HUVECs or MEFs were seeded in 200 μ L in the wells. The cells were stimulated for 6 h at 37°C, 5 % CO₂ and 95 % humidity. Afterwards cell death was analyzed (for protocol see 2.2.2.10).

The same protocol was used for the stimulation of cells with jagged-1. This experiment was performed in 6-well plates and recombinant jagged-1-Fc was used. 3.5 \times 10⁵ LLC or B16F1 cells were stimulated ON. Cells were used for protein or RNA isolation (for protocol see. and 2.2.1.9)

2.2.2.12 TNF-R1 stimulation

500 μ L WT and ADAM17^{ex/ex} MEFs were seeded in a 12-well plate at a concentration of 2 \times 10⁵/mL and stimulated with 200 ng/mL modified tandem affinity purification (moTAP)-TNF α for 15 min, 30 min, 60 min and 120 min in FCS-free DMEM. moTAP-TNF α was designed to perform TNF-R complex I purification. The moTAP-Tag consists of 3 FLAG epitopes, a PreScission cleavage site and 2 Strep epitopes [154]. Subsequently, cells were lysed and subjected to immunoblot analysis (for protocol see 2.2.3.1-2.2.3.4).

2.2.2.13 Isolation of TNF-R1 complex I and complex II

4 \times 10⁶ WT or ADAM17^{ex/ex} MEFs were seeded in 15 cm plates and for isolation of TNF-R1

2 Material & Methods

complex II pre-incubated with 20 μ M zVAD for 30 min in FCS-free DMEM. Subsequently, cells were stimulated with 1 μ g/mL moTAP-TNF α for 1 h, 2 h and 4 h. In order to isolate TNF-R1 complex I, cells were stimulated with 1 μ g/mL moTAP-TNF α for 15 min, 30 min, 60 min, 120 min. Cells were scratched in 1 mL IP lysis buffer and incubated for 30 min at 4°C. Subsequently, cell debris was spun down at full speed for 20 min at 4°C and 800 μ L of the SN was used for the immunoprecipitation of either complex I or complex II.

For precipitation of TNF-R1 complex I 400 μ L anti-FLAG M2 agarose beads (Sigma Aldrich, Steinheim, Germany) were washed in IP lysis buffer twice and resuspended in 1 mL IP lysis buffer. Cell lysates were incubated with 100 μ L beads in each case ON at 4°C rotating. The next day beads were washed 3 times in IP lysis buffer (3 000 rpm, 4°C, 1 min). Remaining buffer was aspirated with a needle and the beads were resuspended in 60 μ L 2x Laemmli. Samples were incubated at 95°C for 5 min and subsequently subjected to SDS-PAGE and immunoblotting.

TNF-R1 complex II was precipitated via FADD. 800 μ L Protein G Sepharose beads (Sigma Aldrich, Steinheim, Germany) were washed and resuspended in 1 mL 1 % BSA in IP lysis buffer. A final concentration of 11 μ g/mL FADD antibody was added and bound to the beads for 1 h at RT rotating. After that, the beads were washed 3 times in IP lysis buffer and resuspended in 800 μ L IP lysis buffer, of which 100 μ L was added to each sample. Samples with beads were incubated ON at 4°C rotating. The next day beads were washed 3 times in IP lysis buffer (3 000 rpm, 4°C, 1 min). Remaining buffer was aspirated with a needle and the beads were resuspended in 60 μ L 2x Laemmli. Samples were incubated at 95°C for 5 min and subsequently subjected to SDS-PAGE and immunoblotting (for protocol see 2.2.3.3-2.2.3.4).

| | | | |
|------------------------|------------------------|------------------|--|
| IP lysis buffer | 30mM Tris-HCl (pH 7.4) | ad fresh: | 1 x cOmplete™ protease inhibitor and phosSTOP (Roche, Mannheim, Germany) |
| | 120 mM NaCl | | |
| | 2 mM EDTA | | |
| | 2 mM KCl | | |
| | 1 % Triton-X-100 | | |

| | |
|--------------------------|-------------------------------|
| 2x Laemmli buffer | 100 mM Tris-HCl pH6.8 |
| | 4.0 % SDS |
| | 20 % Glycerine |
| | 2 % β -Mercapthoethanol |
| | 0.5 % Bromphenol blue |

2.2.3 Proteinbiochemistry

2.2.3.1 Protein lysates

Cultured cells were washed once with cold PBS and incubated for 30 min in RIPA buffer with protease and phosphatase inhibitors on ice. Cells were scratched in the buffer afterwards. Murine lung samples were mechanically disrupted with ceramic beads in 10 μ L RIPA buffer per 20 μ g tissue in a tissue homogenizer at 5500 rpm for 3 min at 4°C (Precellys with Cryolys cooling unit, Peqlab, Erlangen, Germany). Cell debris was spun down at full speed for 20 min at 4°C and SN, containing proteins was transferred to a fresh reaction tube. Protein lysates were stored short-term at -20°C and long-term at -80°C. Lysates subjected to SDS-PAGE (for protocol see 2.2.3.3) were mixed with 5x Laemmli buffer and heated up to 95°C for 10 min. Cooled down samples were shortly centrifuged.

| | | | | | |
|--------------------------|--------|---------------------------|------------------|--------------|-------------|
| RIPA buffer | 50 mM | HEPES pH7.4 | <i>ad fresh:</i> | 1 mM | PMSF |
| | 150 mM | NaCl | | 1 mM | NaV |
| | 1 mM | EDTA | | 1.46 μ M | Pepstatin A |
| | 2 mM | EGTA | | 1.54 μ M | Aprotinin |
| | 0.5 % | NP-40 | | 2.1 μ M | Leupeptin |
| | 50 mM | NaF | | | |
| 5x Laemmli buffer | 250 mM | Tris-HCl pH6.8 | | | |
| | 10 % | SDS | | | |
| | 50 % | Glycerine | | | |
| | 5 % | β -Mercapthoethanol | | | |
| | 0.5 % | Bromphenol blue | | | |

2.2.3.2 Determination of protein concentration

Protein concentration in protein lysates from cultured cells or murine tissue was determined using BCA Assay Kit (Thermo Scientific, Darmstadt, Germany) according to manufacturers' protocol.

2.2.3.3 SDS-PAGE

Proteins were separated by sodium dodecyl sulfate polyacrylamide gel electrophoresis (SDS-PAGE) according to their molecular weight. A reducing 10 % bis-Tris separating gel was prepared and after polymerization overlaid with a stacking gel containing a comb with 10 or 15 pockets. The gel was inserted in an electrophoresis chamber, which was filled with running buffer. The comb was removed, denaturated samples and 5 μ L PageRuler™ Prestained Plus protein marker

were loaded in the pockets. The gel was run at 100 V until the tracking dye reached the end.

| | | | | | |
|------------------------------|--------|------------------|----------------------|--------|----------------|
| Seperating gel (10 %) | 10 % | Acrylamide | Stacking gel: | 4 % | Acrylamide |
| | 350 mM | bis-Tris pH6.5 | | 350 mM | bis-Tris pH6.5 |
| | 0.1 % | SDS | | 0.1 % | SDS |
| | 0.1 % | APS | | 0.1 % | APS |
| | 0.06 % | TEMED | | 0.1 % | TEMED |
| Running buffer | 250 mM | MOPS | | | |
| | 250 mM | Tris | | | |
| | 5 mM | EDTA | | | |
| | 0.5 % | SDS | | | |
| | 5 mM | Sodium bisulfite | | | |

Samples from TNF-R1 complex I and II IP were analyzed with Criterion™ TGX™ Precast Gels and (Bio-Rad, Munich, Germany). SDS-PAGE was performed according to manufacturers' protocol.

2.2.3.4 Immunoblot

Separated proteins by SDS-PAGE were transferred to a polyvinylidene fluoride (PVDF)-membrane. The stacking gel was removed and placed on a sponge and 3 layers of Whatmann Paper. The PVDF-membrane was covered with methanol for activation for approximately 2 min. The activated membrane was then placed on top of the gel followed by 3 layers of Whatmann Paper and a sponge. The composition was assembled in transfer buffer. Air bubbles were removed and the blotting apparatus along with an ice pack put in a blotting chamber which was filled with transfer buffer. For a transfer of negative loaded proteins, the membrane had to be placed between gel and anode. The transfer was achieved by applying 100 V for 90 min.

After the transfer the membrane was covered with 5 % BSA in PBS-T (w/v) for at least 1 h at RT to block unspecific binding sites. The membrane was incubated with primary antibody (Table 2.5), diluted in 5 % BSA in PBS-T (w/v) at 4°C ON, subsequently. Excessive primary antibody was removed by washing the membrane 3 times in PBS-T at RT. The secondary horseredish peroxidase (HRP)-coupled antibody (Table 2.6) diluted in PBS-T was applied for at least 30 min at RT. After washing the membrane again 3 times with PBS-T and once with ddH₂O, the membrane was developed with either SuperSignal™ West Femto Maximum Sensitivity Substrate or SuperSignal™ West Pico Maximum Sensitivity Substrate (Thermo Scientific, Darmstadt, Germany) according to manufacturers' protocol. ECL Chemocam imager (Intas, Hamburg,

Germany) was used for imaging. Exposure time was determined individually.

| | | | | | |
|------------------------|--------|--------------------|--------------|------------------|----------------------------------|
| Transfer buffer | 25 mM | Tris | PBS-T | 136 mM | NaCl |
| | 200 mM | Glycine | | 2.68 mM | KCl |
| | 20 % | Methanol | | 10 mM | Na ₂ HPO ₄ |
| | ad | ddH ₂ O | | 1.76 mM | KH ₂ PO ₄ |
| | | | | adjust to pH 7.4 | |
| | | | | add 0.05 % | Tween-20 |

Separated proteins of TNF-R1 complex I and II IP were transferred to a nitrocellulose membrane with the Trans-Blot® Turbo™ Midi/Mini Nitrocellulose transfer system (Bio-Rad, Munich, Germany) according to manufactures' instructions. After the transfer the membrane was covered with 2.5 % milk powder in PBS-T (w/v) for at least 1 h at RT to block unspecific binding sites. The membrane was incubated with primary antibody (Table 2.5), diluted in 2.5 % BSA in PBS-T (w/v) at RT for 1 h or at 4°C ON, subsequently. Excessive primary antibody was removed by washing the membrane 3 times in PBS-T at RT. The secondary HRP-coupled antibody (Table 2.6) diluted in 2.5 % milk powder in PBS-T was applied for at least 1 h at RT. After washing the membrane again 3 times with PBS-T, the membrane was developed with ECL solution on X-ray film. Exposure time was determined individually.

2.2.3.5 Stripping of immunoblot

Membranes were covered with mild stripping buffer and incubated for 15 min at RT shaking. This step was repeated with fresh buffer once. Membranes were washed two times with PBS for 10 min at RT shaking and two times with PBS-T for 5 min at RT. Membranes were blocked with 5 % BSA in PBS-T (w/v) for 1 h at RT and were then ready for incubation with primary antibody (Table 2.5). Membranes from TNF-R1 complex I and II IP were stripped incubating it for 10 min at RT in stripping buffer. Afterwards they were blocked again for at least 20 min in 2.5 % milk powder in PBS-T.

| | | | | | |
|------------------------------|------------------|----------|-------------------------|------------------|---------|
| Mild stripping buffer | 200 mM | Glycine | Stripping buffer | 50 mM | Glycine |
| | 3.47 mM | SDS | | adjust pH to 2.3 | |
| | 1 % | Tween-20 | | | |
| | adjust pH to 2.2 | | | | |

2.2.3.6 Enzyme-linked immunosorbent assay

The detection of soluble TNF-R1, VE-cadherin and junction adhesion molecule (JAM)-A in cell culture SN or mouse plasma was performed with corresponding enzyme-linked immunosorbent

assays (ELISAs) according to manufacturers' protocol. All used ELISAs are listed in Table 2.13.

Table 2.13: ELISA Kits.

| Target | Supplier | Product # |
|-------------------|---|-----------|
| Mouse TNF-R1 | R&D Systems, Wiesbaden-Nordenstadt, Germany | DY425 |
| Mouse VE-cadherin | Boster Biological Technology, Pleasanton, USA | EK1318 |
| Mouse JAM-A | R&D Systems, Wiesbaden-Nordenstadt, Germany | DY1077 |

2.2.3.7 Activity assay

The inhibitory effect of ADAM17-PD on ADAM17 activity was determined by a peptide based activity assay. 50 nM recombinant ADAM17 was mixed with increasing concentrations of either the metalloprotease inhibitor TAPI-1, the ADAM17 and ADAM10 inhibitor GW or recombinant ADAM17-PD. After incubation for 10 min at 37°C 5 µM PEPDAB005 ADAM17 substrate peptide was added. Subsequently the change in fluorescence intensity was recorded every 30 s for 18 min. The initial linear slope was determined by linear regression and plotted against the inhibitor concentrations. IC₅₀ values were calculated by four parameter non-linear curve using GraphPad PRISM (GraphPad Software, Inc., CA, USA).

2.2.4 Statistics

Data in all graphs are shown as mean ± standard error of the mean (SEM). Comparison of two groups with normal distribution were performed by applying the Student's t-Test. Not normally distributed values of two groups were compared with the Mann-Whitney-U test. More than two groups were compared applying an ANOVA test with a subsequent post-hoc test. Analysis was conducted using SigmaPlot 12.0 Software (Systat Software, Erkrath, Germany) or GraphPad PRISM (GraphPad Software, Inc., CA, USA) A p-value ≤ 0.05 was considered statistically significant (p ≤ 0.05 *, p ≤ 0.01 **, p ≤ 0.001 ***).

3 Results

3.1 ADAM17 mediates tumor cell extravasation

A complete knock-out of ADAM17 is lethal. In order to investigate the role of ADAM17 in metastasis *in vivo* we therefore used hypomorphic ADAM17^{ex/ex} mice, that were described before [39]. Previous work of our lab revealed that these mice show a strong reduction in tumor burden 3 weeks after i.v. injection of LLC or B16F1 cells [155]. Here, we went on to decipher the pro-metastatic role of ADAM17.

It was described, that TCs, once in the circulation are either cleared by the immune system or extravasated within the first 24 h [156]. Therefore, we injected TCs i.v. in ADAM17^{ex/ex} and WT mice and examined the lungs 6 h and 20 h later (Figure 3.1A).

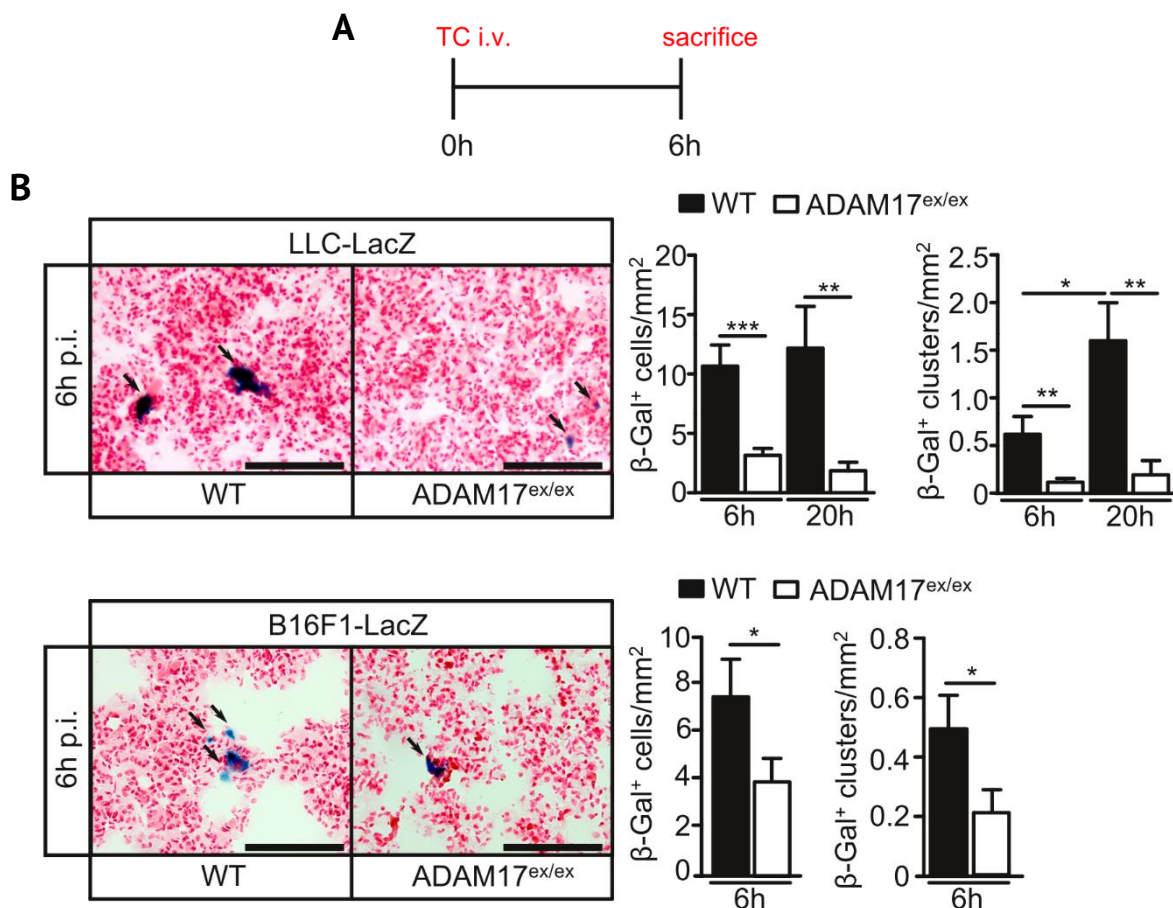


Figure 3.1: Impaired extravasation of TCs in the absence of ADAM17. **A:** Immunoblot analysis of whole lung lysates of WT and ADAM17^{ex/ex} mice. **B:** Representative microscopic images of β-galactosidase and nuclear fast red staining of WT and ADAM17^{ex/ex} lungs 6 h after LLC-LacZ or B16F1-LacZ cell injection. Lungs of mice injected with LLC-LacZ cells were additionally examined 20 h after injection. Scale bar indicates 100 μm. Quantification shows mean ± SEM (n = 4 WT, 3 ADAM17^{ex/ex}). Statistical significance was determined by Mann-Whitney U. p.i. = post injection.

To detect TCs in the lung tissue at that early time point, we used LLC-LacZ and B16F1-LacZ cells, which stably express β -galactosidase. By substrate administration we were able to visualize the TCs in the lung tissue. We detected significantly less TCs in lungs of ADAM17^{ex/ex} mice irrespective of the injected TC entity (Figure 3.1B).

In case of LLC cells, TC numbers were even further reduced in ADAM17^{ex/ex} animals 20 h after injection, while TC numbers were increased in WT animals. Interestingly, number of TC clusters in WT animals were elevated compared to ADAM17^{ex/ex} mice.

As TCs have to pass the endothelial barrier during extravasation, we set up a transmigration assay to investigate the dependence of TC extravasation on endothelial ADAM17 independent of other cell types *in vitro* (Figure 3.2A). We therefore used two human primary endothelial cell lines. Human umbilical vein endothelial cells (HUVECs) and human microvessel endothelial cells of the lung (HMVEC-L).

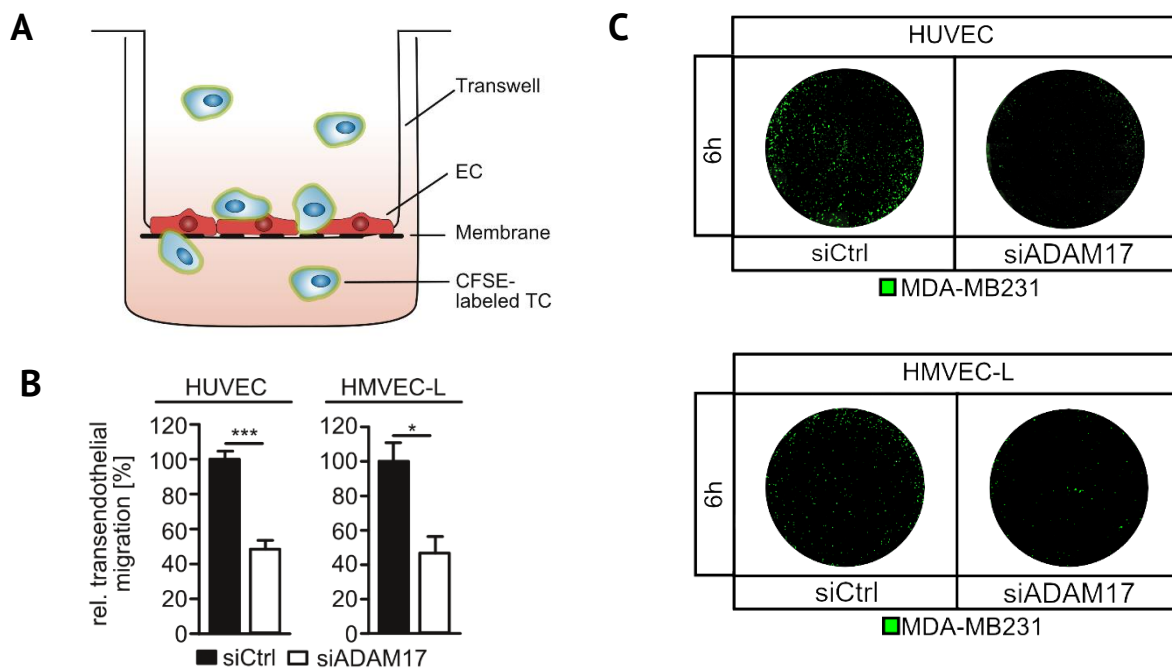


Figure 3.2: Less TC-transmigration in the absence of ADAM17 on ECs *in vitro*. **A:** Schematic of the experimental procedure. Experiments were conducted in 24-well plates. **B:** Quantification and representative microscopic images of the transmigration of CFSE-labeled MDA-MB231 cells through a HUVEC or HMVEC-L monolayer treated with control siRNA or siRNA against ADAM17. Scale bar indicates 100 μ m. Quantification shows mean \pm SEM. (n = 3). Statistical significance was determined by unpaired, one-tailed Student's t-Test. **C:** Representative images of insert membrane with transmigrated MDA-MB231 TCs.

The transmigration of human CFSE-labeled MDA-MB231 breast cancer cells through a HUVEC or HMVEC-L monolayer with siRNA mediated knock-down of ADAM17 was significantly less compared to control conditions (Figure 3.2B,C).

These findings suggest a decisive role of ADAM17 on ECs for the extravasation of TCs.

3.2 Endothelial permeability upon tumor cell contact is regulated by ADAM17

Breaking the endothelial barrier is a critical prerequisite for the extravasation of TCs. We therefore tested whether ADAM17 deficiency alters the permeability of the endothelium. To this end we injected FITC-labeled dextran i.v. in LLC injected or untreated mice shortly before sacrificing the mice. The amount of tissue-penetrated dextran was expressed by area as measure for the permeability of the endothelium. Interestingly, the endothelium of ADAM17^{ex/ex} mice was *per se* slightly more permeable (Figure 3.3).

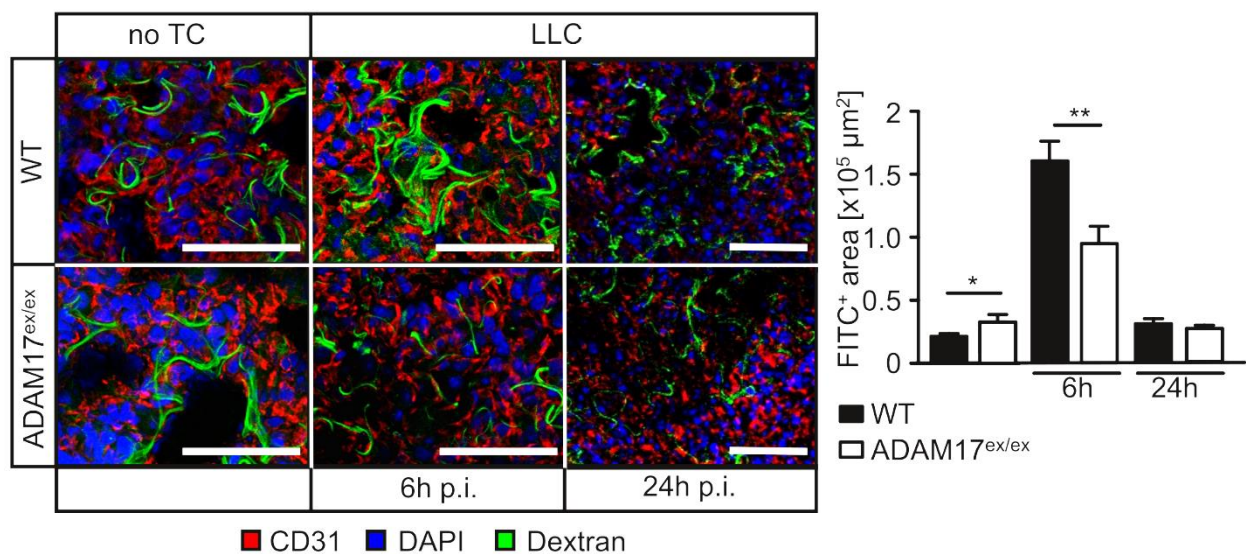


Figure 3.3: Endothelium in ADAM17^{ex/ex} mice is less permeable upon tumor cell injection. Representative microscopic images of immunofluorescence staining of CD31 in FITC-Dextran injected untreated or LLC injected WT and ADAM17^{ex/ex} mice. Lungs were examined 6 h or 24 h after TC injection. Scale bar indicates 50 μm. For the quantification a minimum of 6 non-overlapping pictures per mouse were analyzed. Quantification shows mean ± SEM (n = 2 WT, 4 ADAM17^{ex/ex}). Statistical significance was determined by ANOVA on ranks and Dunn's post-hoc test. p.i. = post injection.

Injection of LLC cells caused an increase in endothelial permeability after 6 h in both WT and ADAM17^{ex/ex} mice. However, while the FITC⁺ area in WT mice increased almost six fold, it was only tripled in ADAM17^{ex/ex} mice. 24 h after LLC injection EC permeability was reduced to normal in both mouse strains. We concluded that the endothelial barrier in ADAM17^{ex/ex} mice stays intact in the presence of TCs. These data further emphasize an essential role of ADAM17 in the regulation of EC permeability during metastasis.

As a consequence, we generated mice with an inducible ADAM17 deficiency only on ECs (ADAM17^{iΔEC/iΔEC}). Recombination was induced by tamoxifen (TAM)-injection (Chapter 2.2.1.2). We injected either LLC-LacZ or B16F1-LacZ cells into ADAM17^{iΔEC/iΔEC} mice and examined the lungs 6 h later (Figure 3.4A). β-galactosidase activity staining showed significant reduction in TC numbers in the lung tissue of mice with endothelial-specific ADAM17 deficiency compared to

controls, irrespective of the TC entity (Figure 3.4B).

Similar to previous experiments in WT mice (Figure 3.1), we again noticed more clusters of TCs in control animals than in ADAM17-deficient mice.

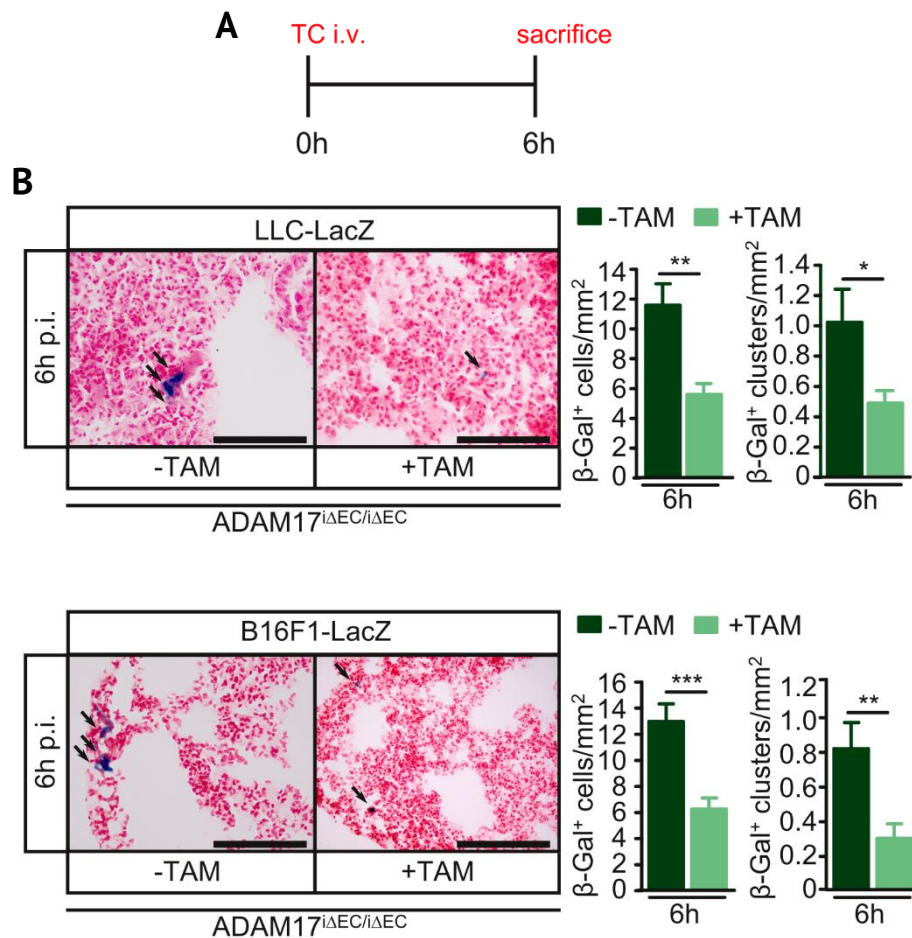


Figure 3.4: ADAM17 deficiency on ECs leads to impaired TC extravasation. **A:** Timeline for the *in vivo* experiment. **B:** Representative microscopic images of β -galactosidase activity and nuclear fast red stained lung sections of ADAM17^{i Δ EC/i Δ EC} mice. Mice were either injected with tamoxifen (+TAM) or vehicle (-TAM) i.p. on 4 consecutive days prior to LLC-LacZ or B16F1-LacZ injection. Mice were sacrificed 6 h after TC injection. Scale bar indicates 100 μ m. Quantification shows mean \pm SEM (n(LLC-LacZ) = 5 -TAM, 6 +TAM; n(B16F1) = 2 -TAM, 3 +TAM). Statistical significance was determined by unpaired, one-tailed Student's t-Test. p.i. = post injection. Black arrows point to β -Gal⁺ cells.

Consequently, tumor numbers of LLC and B16F1 cells were strongly reduced in TAM-injected mice compared to control animals 3 weeks after TC injection (Figure 3.5A,B), confirming that ADAM17 deficiency only on ECs is sufficient to inhibit extravasation of TCs and subsequent metastases formation.

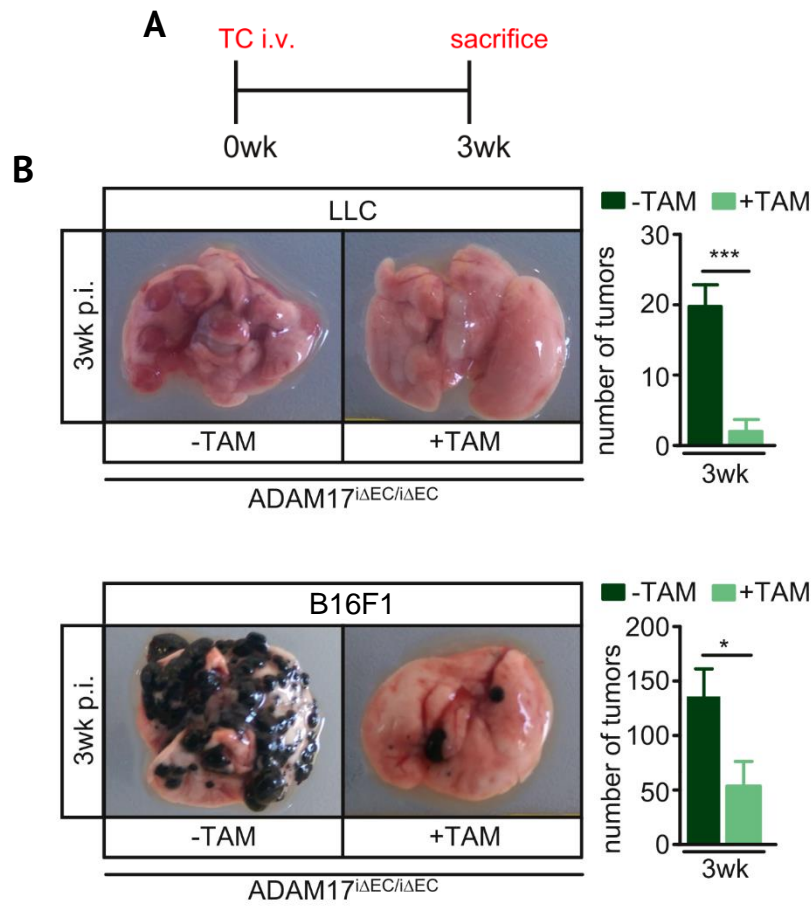


Figure 3.5: ADAM17 deficiency on ECs strongly decreases tumor burden. **A:** Timeline for the *in vivo* experiment. **B:** Representative macroscopic lung images of ADAM17^{ΔEC/ΔEC} mice. Mice were either injected with tamoxifen (+TAM) or vehicle (-TAM) i.p. on 4 consecutive days prior to TC injection. Mice were injected with LLC or B16F1 cells and sacrificed 3 weeks later. Tumor number was quantified and is shown as mean ± SEM (n(LLC) = 4 -TAM, 4 +TAM; n(B16F1) = 4 -TAM, 5 +TAM). Statistical significance was determined by unpaired, one-tailed Student's t-Test. p.i. = post injection, wk = weeks.

3.3 PKC β is a potent activator of ADAM17 in metastasis

Signal transduction via GPCRs and the subsequent activation of PKC family members was shown to activate ADAM17 [157]. The PKC family is divided in three subfamilies based on their required activator. So far it is not fully understood which PKC isotype regulates ADAM17 activity under certain conditions. However, the development of new cancer therapies requires not only a sufficient understanding of underlying signaling mechanisms but also depends on the availability of highly specific inhibitors to interrupt these signaling pathways. We therefore aimed to investigate the role of PKC-dependent activation of ADAM17 in our metastatic mouse model and define the PKC isoform responsible. Previous data of our lab suggested the classical isoform PKC β to activate ADAM17 *in vitro* (data not shown) (Chapter 4.1). We assessed

phosphorylation of PKC β in untreated and LLC-LacZ-injected WT mice by immunofluorescence co-staining with the endothelial marker CD31 (Figure 3.6). Mice with a PKC β deficiency (PKC $\beta^{-/-}$) served as control.

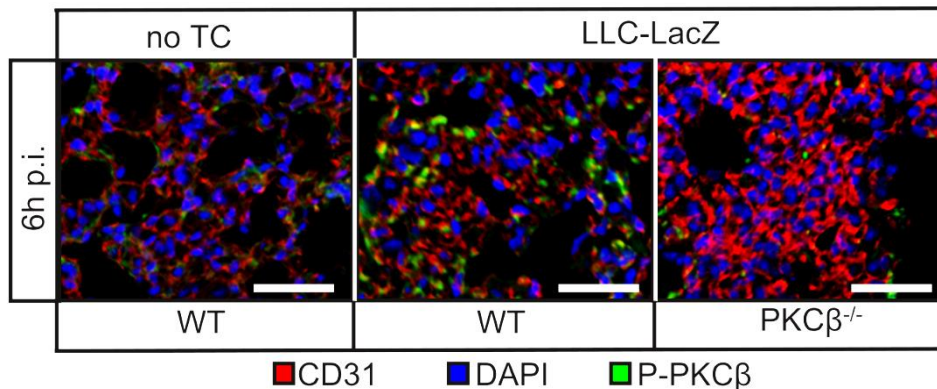


Figure 3.6: PKC β is activated upon tumor cell injection. Representative microscopic images of lung tissue of either non treated WT mice or LLC-LacZ injected WT and PKC $\beta^{-/-}$ mice. Tissue sections were stained for CD31 and P-PKC β . Scale bar indicates 100 μ m. p.i. = post injection.

There was almost no phosphorylation of PKC β detectable in untreated WT mice. The injection of LLC-LacZ cells increased the amount of phosphorylated PKC β massively, indicating an activation of this specific isoform in the presence of TCs. P-PKC β co-stained with CD31, suggesting a role of PKC β in ECs.

We used PKC $\beta^{-/-}$ mice to address, whether the absence of PKC β has a similar effect on the extravasation and metastasis of TCs as ADAM17 deficiency (Figure 3.7A). In lungs of PKC $\beta^{-/-}$ mice we found significantly less TCs 6 h after TC injection compared to WT mice (Figure 3.7B). Furthermore, TC cluster formation was significantly enhanced. 3 weeks after TC injection tumor numbers were strongly reduced in PKC $\beta^{-/-}$ mice compared to WT animals, irrespective of the injected TC entity (Figure 3.7C).

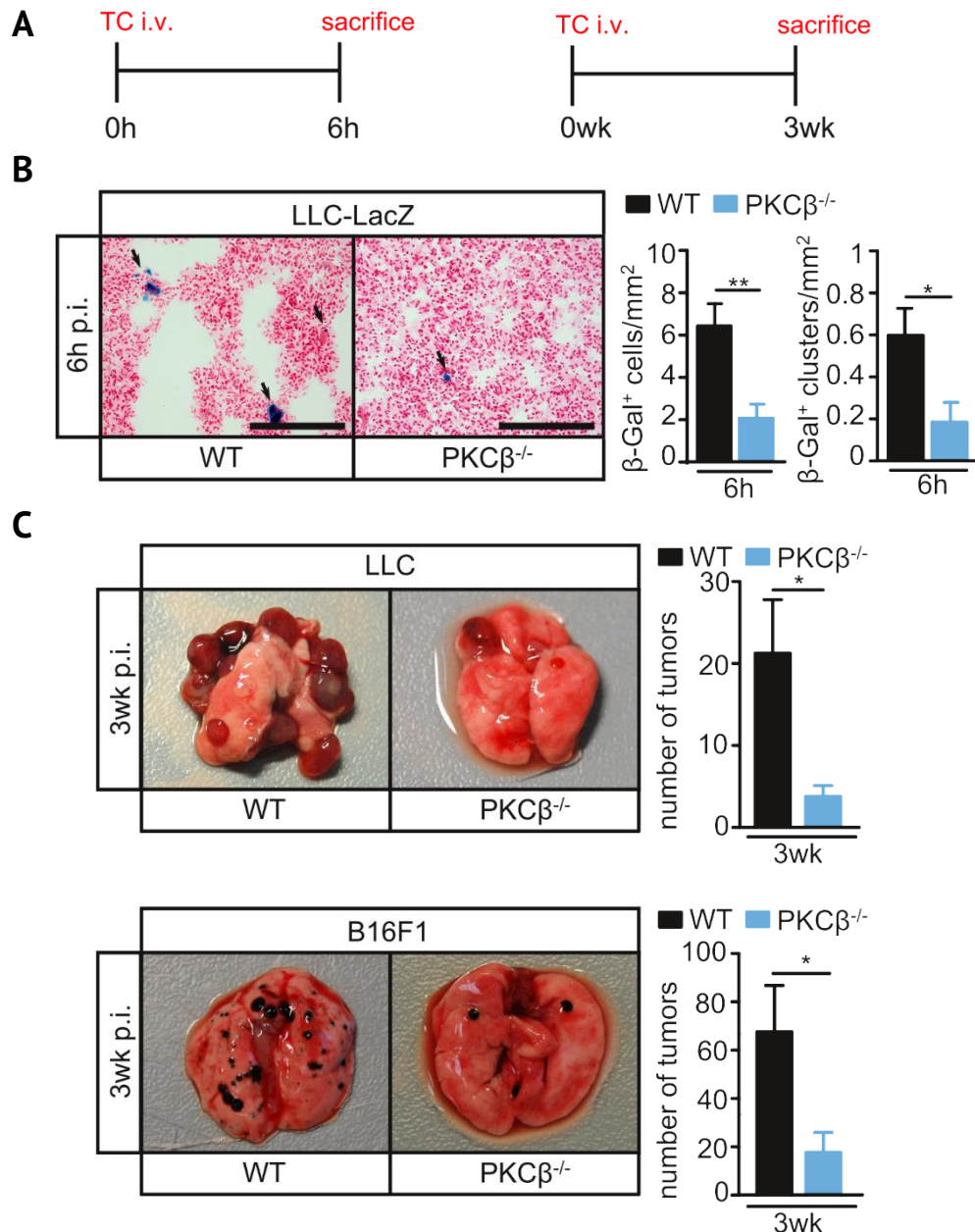


Figure 3.7: PKC β deficiency leads to impaired TC extravasation and reduced tumor burden in the lung. **A:** Timeline for the *in vivo* experiments. **B:** Representative microscopic images of β -galactosidase activity and nuclear fast red stained lung sections of PKC β ^{-/-} mice 6 h after LLC-LacZ cell injection. Scale bar indicates 100 μ m. Quantification shows mean \pm SEM (n = 4 WT, 3 PKC β ^{-/-}). Statistical significance was determined by unpaired, one-tailed Student's t-Test. p.i. = post injection. Black arrows point to β -Gal⁺ cells. **C:** Representative macroscopic lung images of PKC β ^{-/-} mice 3 weeks after LLC or B16F1 cell injection. Tumor number was quantified and is shown as mean \pm SEM (n = 4 per group). Statistical significance was determined by unpaired, one-tailed Student's t-Test. p.i. = post injection, wk = weeks.

We concluded that PKC β is critically involved in our metastasis mouse model and its absence reduces metastases formation in the same extend as an ADAM17 deficiency.

3.4 Tumor cells induce ADAM17-mediated cell death in endothelial cells

Next we aimed to understand the molecular mechanism downstream of ADAM17 that leads to TC extravasation. The favored route of TCs in *in vitro* experiments is the paracellular transendothelial migration, involving the opening of EC junctions [101]. Interestingly, the tight junction proteins JAM-A as well as VE-cadherin were found to be substrates of ADAM proteases [158, 159]. We therefore determined plasma levels of soluble JAM-A and VE-cadherin of ADAM17^{ex/ex} and ADAM17^{iΔEC/iΔEC} mice by ELISA (Figure 3.8).

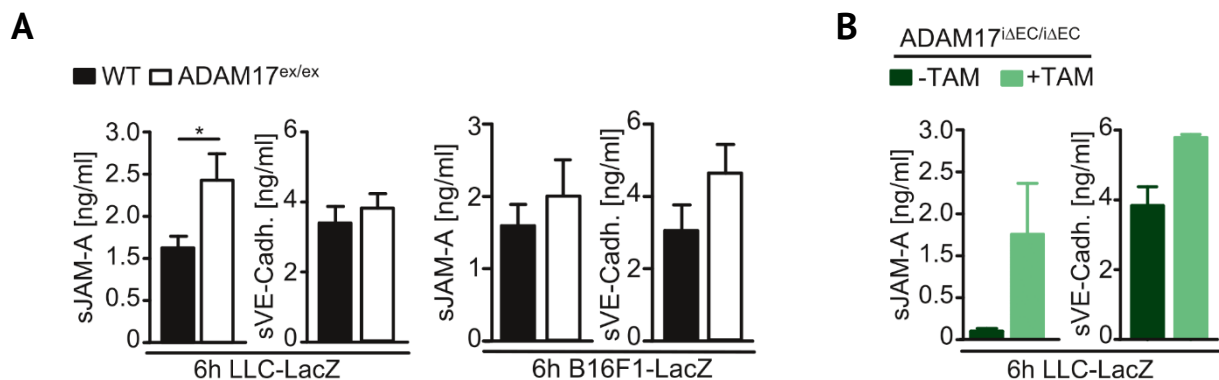


Figure 3.8: Impaired extravasation of TCs in the absence of ADAM17 can not be linked to reduced shedding of tight junction proteins. **A:** Quantification of murine JAM-A and VE-cadherin ELISA from plasma of LLC-LacZ or B16F1-LacZ injected WT and ADAM17^{ex/ex} mice. Bar graphs show mean \pm SEM (n = 2). Statistical significance was determined by unpaired, one-tailed Student's t-Test. **B:** Quantification of murine JAM-A and VE-cadherin ELISA from plasma of LLC-LacZ or B16F1-LacZ injected ADAM17^{iΔEC/iΔEC} mice. The mice were either injected with tamoxifen (+TAM) or ethanol/oil (-TAM) on 4 consecutive days prior to TC injection. Bar graphs show mean \pm SEM (n = 2).

The injection of TCs resulted in elevated soluble JAM-A and VE-cadherin levels in ADAM17^{ex/ex} and ADAM17^{iΔEC/iΔEC} mice compared to controls 6 h post TC injection (Figure 3.8A,B). This difference was even significant for soluble JAM-A levels in LLC-injected ADAM17^{ex/ex} (Figure 3.8A).

Recently, Strilic and colleagues [110] showed that TCs induce necroptosis in ECs during metastasis. We therefore co-cultured HUVECs with MDA-MB231 breast cancer cells in the presence or absence of endothelial ADAM17. To identify dead ECs, we added EthDIII after 6 h co-incubation. Its incorporation is a sign for necrotic and late apoptotic cells. The co-culture of ECs with siRNA-mediated knock-down of ADAM17 with TCs lead to significantly less EthDIII⁺ ECs compared to control conditions (Figure 3.9).

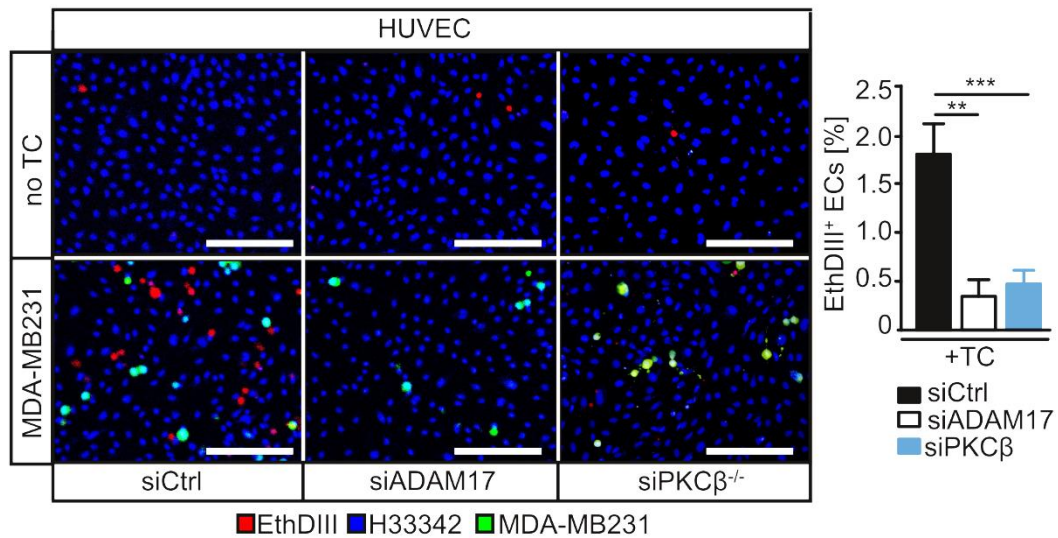


Figure 3.9: TC-induced EC death is reduced in the absence of ADAM17 *in vitro*. Representative images of co-culture of HUVECs with siRNA-mediated knock-down of ADAM17 or PKC β and MDA-MB231 cells. MDA-MB231 cells were stained with CFSE and co-cultured for 6 h. All cells were stained with Hoechst33342 and EthDIII before imaging. Scale bar indicates 200 μ m. For the quantification a minimum of 4 non-overlapping pictures per condition were analyzed. Quantification shows mean \pm SEM (n = 3). Statistical significance was determined by ANOVA on ranks and Dunn's post-hoc test.

Interestingly, EC death was also markedly reduced in the absence of PKC β .

In order to examine TC-induced EC death *in vivo* we injected EthDIII i.v. in TC-injected mice 5 min prior to sacrifice and analyzed co-localization of the endothelial marker CD31 and EthDIII by immunofluorescence staining of lung tissue sections (Figure 3.10). Indeed, we detected CD31⁺ ECs in the lung of WT mice, that were EthDIII⁺ and in close proximity to β -galactosidase⁺ TCs. We therefore analyzed TC-induced necroptosis in WT, ADAM17^{ex/ex} and, as a control, RIPK3^{-/-} mice (Figure 3.11A;B).

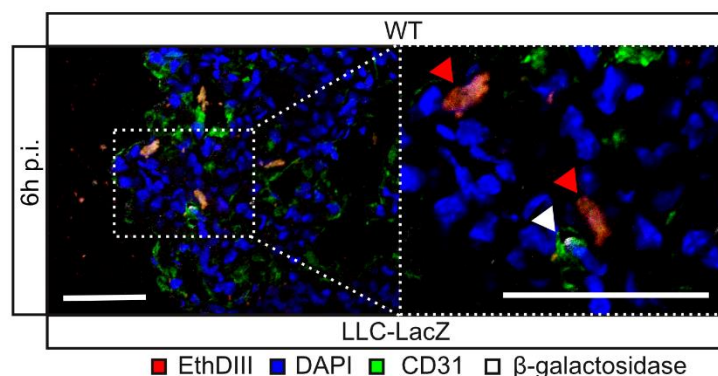


Figure 3.10: TCs induce cell death in ECs of the lung. Representative image of lung tissue sections stained for CD31. WT mice were i.v. injected with LLC-LacZ cells and sacrificed after 6 h. EthDIII was injected i.v. 5 min prior to sacrifice. Scale bar indicates 50 μ m. p.i. = post injection.

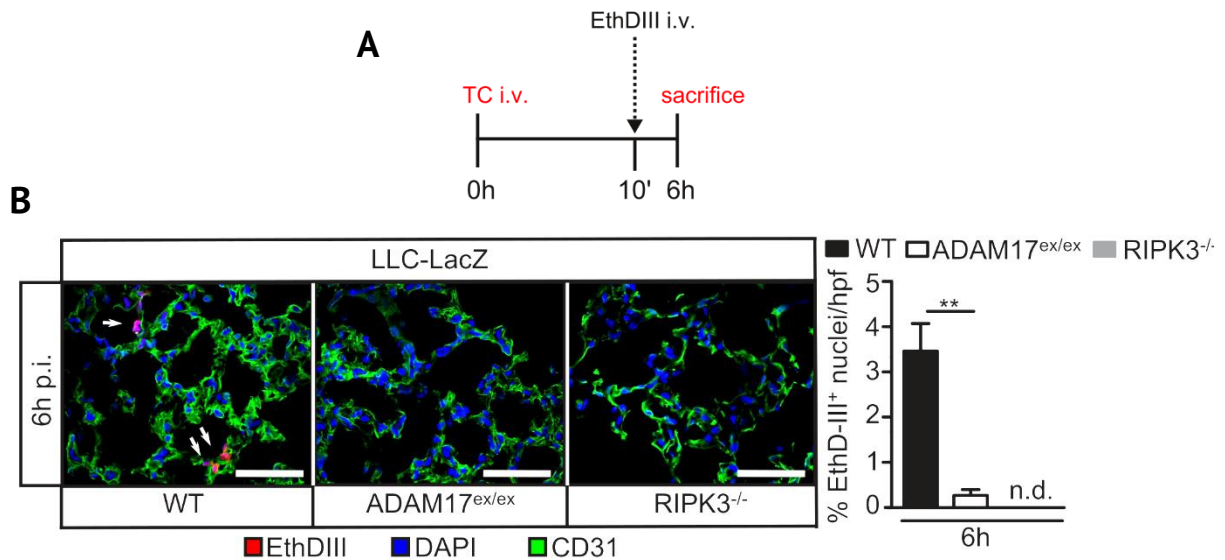


Figure 3.11: TC-induced EC death is decreased in the absence of ADAM17 *in vivo*. **A:** Timeline for the *in vivo* experiment. **B:** Representative images of lung tissue sections stained for CD31. WT, ADAM17^{ex/ex} and RIPK3^{-/-} mice were i.v. injected with LLC-LacZ cells and sacrificed after 6 h. EthDIII was injected i.v. 5 min prior to sacrifice. Scale bar indicates 100 μm. A minimum of 5 non-overlapping images per animal were analyzed. Quantification shows mean ± SEM (n = 3 per group). Statistical significance was determined by Mann-Whitney U. p.i. = post injection. White arrows point to EthDIII⁺ cells.

RIPK3 is an essential component of the necrosome and therefore necroptosis is impossible in RIPK3^{-/-} mice. In line with our *in vitro* experiments, we observed significantly less EthDIII⁺ ECs in ADAM17^{ex/ex} compared to WT mice (Figure 3.11A). We detected 3.5 % EthDIII⁺ ECs in WT mice 6 h after LLC injection, but only 0.2 % in ADAM17^{ex/ex} mice. We did not observe any ECs that incorporated EthDIII in RIPK3^{-/-} mice. Therefore, ADAM17 seems to be crucial for the induction of programmed cell death.

We reasoned that endothelial ADAM17 mediates EC necroptosis upon TC contact. Thus, we injected TCs i.v. in ADAM17^{iΔEC/iΔEC} mice and examined TC-induced EC death after 6 h (Figure 3.12A). Irrespective of the TC entity, ADAM17^{iΔEC/iΔEC} mice displayed significantly less necroptotic ECs in the lung tissue 6 h after TC injection as determined by EthDIII and CD31 staining (Figure 3.12B).

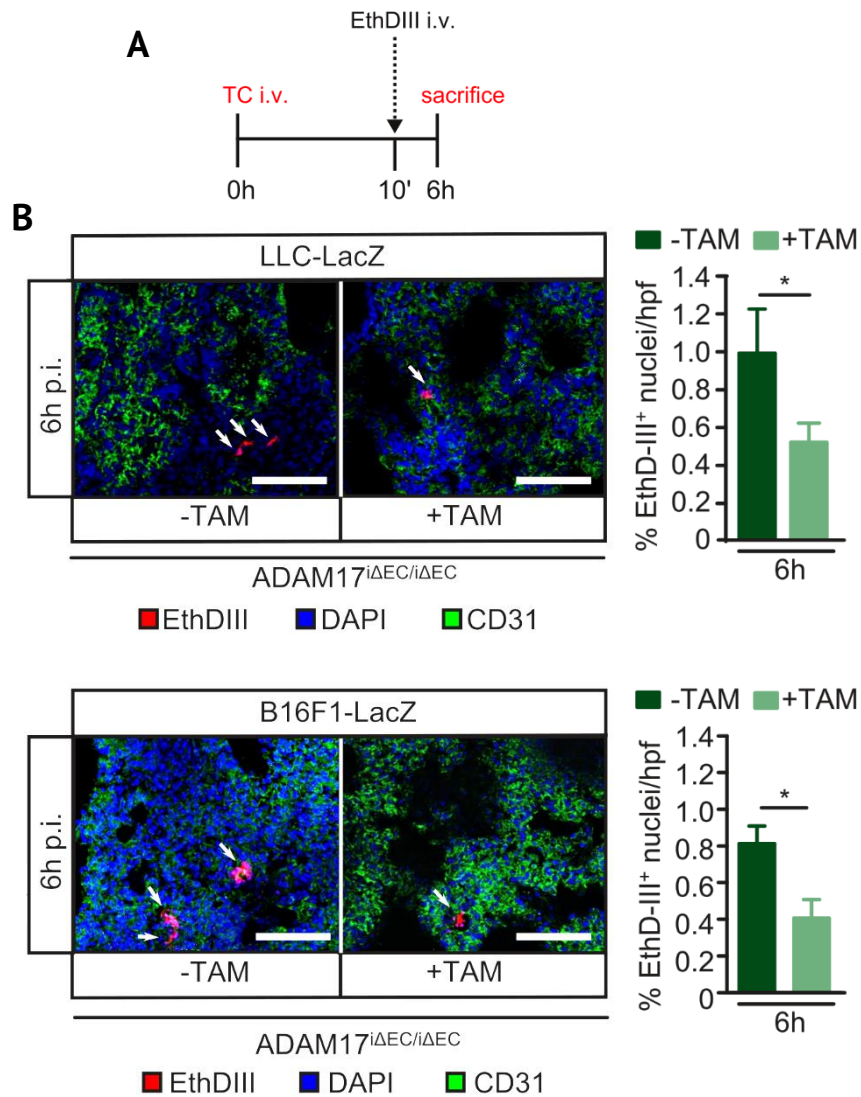


Figure 3.12: In the absence of endothelial ADAM17 TC-induced EC death is reduced *in vivo*. **A:** Timeline for the *in vivo* experiments. **B:** Representative images of lung tissue sections stained for CD31. ADAM17^{iΔEC/ΔEC} mice were i.v. injected with LLC-LacZ or B16F1-LacZ cells and sacrificed 6 h later. EthDIII was injected i.v. 5 min prior to sacrifice. Mice were either injected with tamoxifen (+TAM) or vehicle (-TAM) on 4 consecutive days prior to TC injection. Scale bar indicates 100 μm. A minimum of 5 non-overlapping images per animal were analyzed. Quantification shows mean ± SEM (n(LLC-LacZ) = 2 -TAM, 3 +TAM; n(B16F1-LacZ-LacZ) = 2 -TAM, 3 +TAM). Statistical significance was determined by Mann-Whitney U. p.i. = post injection. White arrows point to EthDIII⁺ cells.

Furthermore, PKCβ^{-/-} mice also show significantly less EthDIII⁺ ECs as assessed by CD31 co-staining (Figure 3.13A,B), being in accordance with the assumption that PKCβ confers ADAM17 activity in ECs.

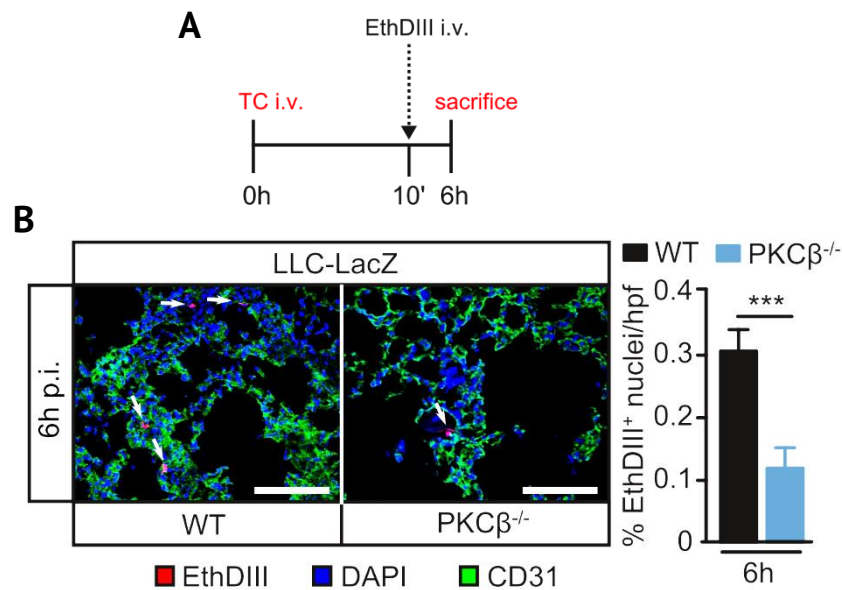


Figure 3.13: TC-induced EC death is reduced in the absence of ADAM17-activating PKC β . **A:** Timeline for the *in vivo* experiment. **B:** Representative images of lung tissue sections stained for CD31. PKC $\beta^{-/-}$ mice were i.v. injected with LLC-LacZ cells and sacrificed after 6 h. EthDIII was injected i.v. 5 min prior to sacrifice. Scale bar indicates 100 μ m. Quantification shows mean \pm SEM (n = 3 WT; 3 PKC $\beta^{-/-}$). Statistical significance was determined by unpaired, one-tailed Student's t-Test. p.i. = post injection. White arrows point to EthDIII⁺ cells.

The bisindolylmaleimide Enzastaurin is an PKC β -selective inhibitor. It competes with ATP for the ATP-binding site of the enzyme. PKC β is 6 times more sensitive to inhibition by Enzastaurin than other PKC isoforms (IC_{50} = 6 nM) [160].

In order to substantiate the importance of PKC β activity for the activation of ADAM17, EC necroptosis and metastasis, wild type animals were injected i.v. with a dose of Enzastaurin 5 min prior to LLC-LacZ injection. TC mediated EC necroptosis was assessed after 6 h by EthDIII injection and CD31-staining (Figure 3.14A). Mice pre-treated with Enzastaurin displayed almost 50 % less EthDIII⁺ ECs than mice pre-treated with the vehicle only (Figure 3.14B).

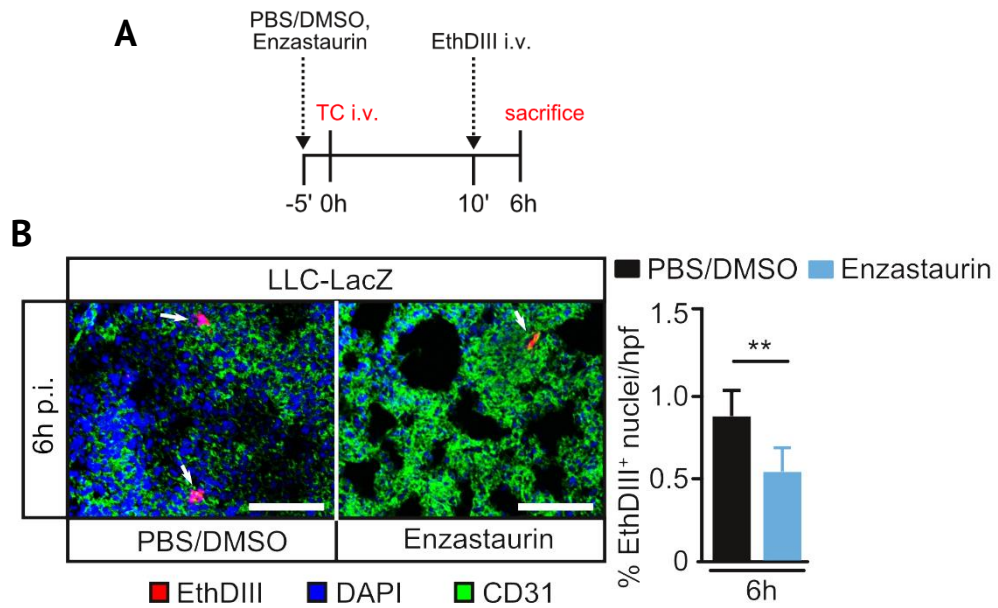


Figure 3.14: TC-induced EC death is decreased after pre-treatment with PKC β inhibitor Enzastaurin. A: Timeline for the *in vivo* experiment. **B:** Representative images of lung tissue sections stained for CD31. WT mice were i.v. injected with 0.5 $\mu\text{g/g}$ body weight Enzastaurin 5 min prior to injection of LLC-LacZ cells and sacrificed after 6 h. EthDIII was injected i.v. 5 min prior to sacrifice. Scale bar indicates 100 μm . A minimum of 4 non-overlapping images per animal were analyzed. Quantification shows mean \pm SEM ($n = 3$ PBS/DMSO injected, 5 Enzastaurin injected). Statistical significance was determined by Mann-Whitney U. p.i. = post injection. White arrows point to EthDIII⁺ cells.

These data demonstrate a pivotal role for PKC β and ADAM17 in TC-induced EC necroptosis, efficient extravasation and successful metastasis.

3.5 ADAM17 is essential for death receptor-induced necroptosis

Necroptosis is a programmed cell death that can be triggered by death receptors. The work of Strilic et al. already suggested a role of DR6 and APP in TC-induced EC necroptosis [95]. We therefore assumed, that ADAM17 regulates necroptosis via death receptor cleavage and investigated whether DR6 is processed by ADAM17. We transiently overexpressed DR6-GFP either in HEK293 or ADAM17-deficient HEK cells (HEK A17^{-/-}) (Figure 3.15A).

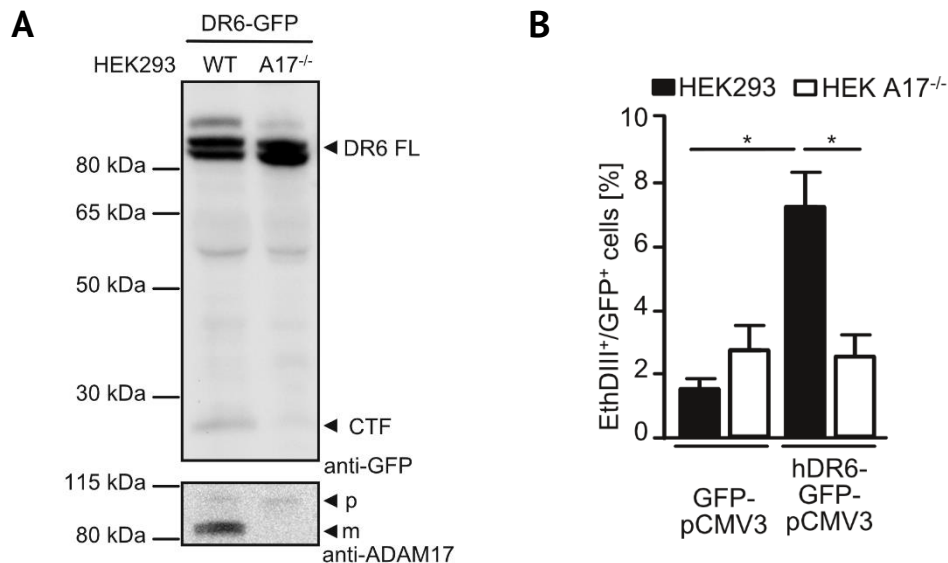


Figure 3.15: Cell death triggered by DR6 overexpression is impaired in the absence of ADAM17. **A:** Immunoblot of DR6-GFP transfected HEK293 and HEK A17^{-/-} cells using the indicated antibodies. Whole cell lysates were used for SDS-PAGE. CTF = C-terminal fragment, ICD = intracellular domain, p = proform, m = mature form. **B:** Quantification of EthDIII⁺/GFP⁺ cells after DR6-GFP overexpression in HEK293 or HEK A17^{-/-} cells. Bar graphs show mean \pm SEM (n = 3). Statistical significance was determined by ANOVA on ranks and Dunn's post-hoc test.

In both HEK293 and HEK A17^{-/-} cells we detected full length DR6 (Figure 3.15A). However, whereas we observed bands representing the CTF of DR6 (25 kDa) in HEK293 cells, they appeared weaker in the absence of ADAM17, pointing to ADAM17-dependent shedding of DR6.

We next overexpressed DR6 in ADAM17-deficient HEK cells and monitored cell death by EthDIII staining (Figure 3.16B). In HEK293 the overexpression of DR6 lead to a strong increase in the percentage of dead cells, whereas no difference was detectable in the HEK A17^{-/-} cells. In the absence of ADAM17 cell death due to DR6 overexpression was three times less than in the presence of ADAM17.

Signaling via DR6 is activated by binding of membrane-bound APP [110]. We therefore established an assay simulating this situation. Human IgG1 antibody was bound to the bottom of a culture dish. Subsequently, human APP-Fc was bound to the antibody, thereby clustering

and immobilizing it. We next seeded HUVECs with siRNA mediated knock-down of ADAM17 or TNF-R1 on top of this enriched, immobilized APP (Figure 3.16A). We first analyzed the siRNA efficiency via immunoblot and confirmed reduced protein levels of ADAM17 and TNF-R1 in siRNA-treated HUVECs (Figure 3.16B).

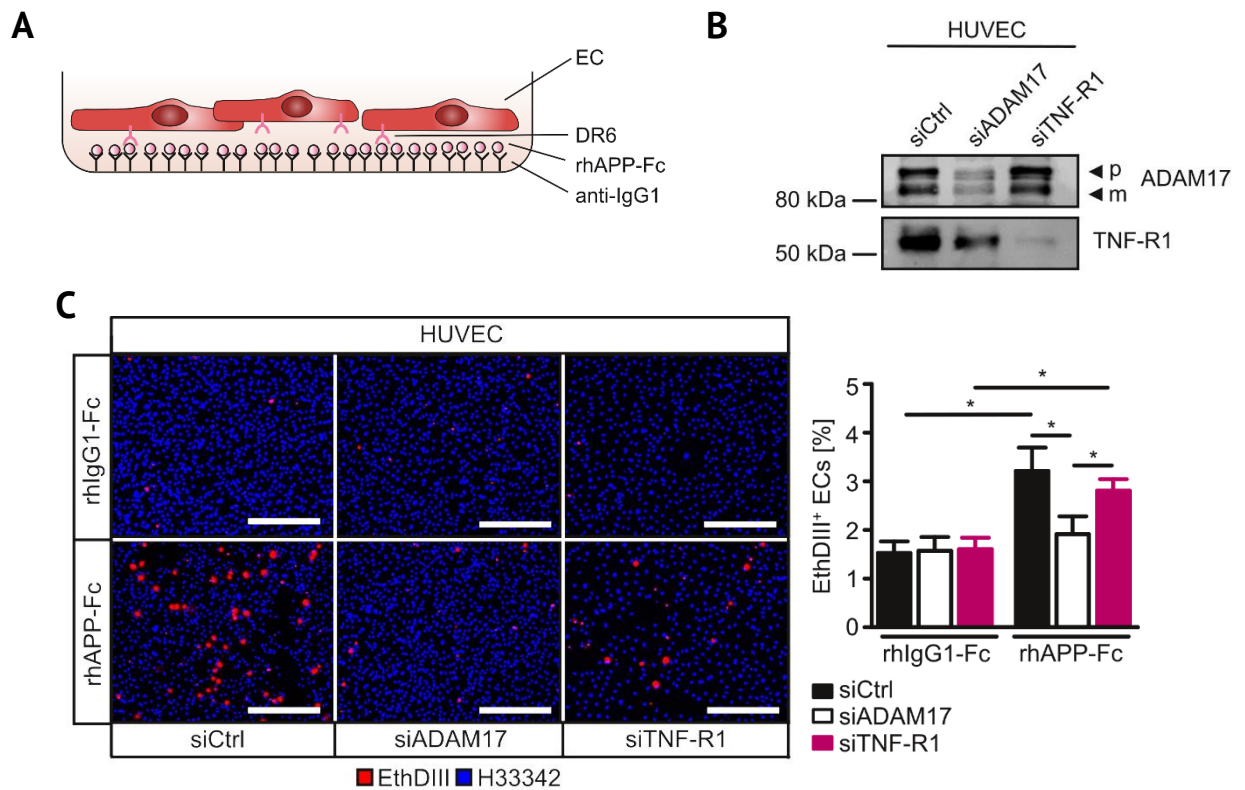


Figure 3.16: In ADAM17-deficient HUVECs APP induced necroptosis via DR6 is disabled. **A:** Schematic of the experimental procedure. **B:** Immunoblot analysis of whole cell lysates. HUVECs were transfected with the indicated siRNAs. **C:** Representative images of control siRNA, ADAM17 siRNA and TNF-R1 siRNA treated HUVECs. Cells were stimulated for 6 h with immobilized APP and stained with Hoechst33342 and EthDIII. Scale bar indicates 400 μ m. For the quantification a minimum of 4 non-overlapping pictures per condition were analyzed. Quantification shows mean \pm SEM (n = 3). Statistical significance was determined by one-way ANOVA and Turkey's post-hoc test.

The stimulation with immobilized APP lead to a significant, 2-fold increase in necroptotic ECs treated with control siRNA (Figure 3.16C). APP-induced increase in necroptosis was absent in ADAM17-depleted HUVEC cells. Furthermore, siRNA-mediated suppression of TNF-R1 reduced APP-induced necroptosis, further emphasizing a crucial role for TNF-R1 in TC-induced EC necroptosis. We assumed that ADAM17 might regulate necroptosis via death receptor cleavage in general. Cleavage of TNF-R1 by ADAM17 was described previously [30]. Indeed we detected a signal for the C-terminal fragment (30 kDa) of TNF-R1 in HEK293 cells overexpressing TNF-R1-EYFP (Figure 3.17A), which was strongly reduced in the absence of ADAM17. Notably, we additionally observed a signal at 25 kDa in transfected HEK239 cells, which was reduced in HEK

A17^{-/-} cells. This signal most likely represented the ICD of TNF-R1, liberated by another protease after cleavage by ADAM17. We next determined levels of soluble TNF-R1 *in vivo* and *in vitro* (Figure 3.17B,C).

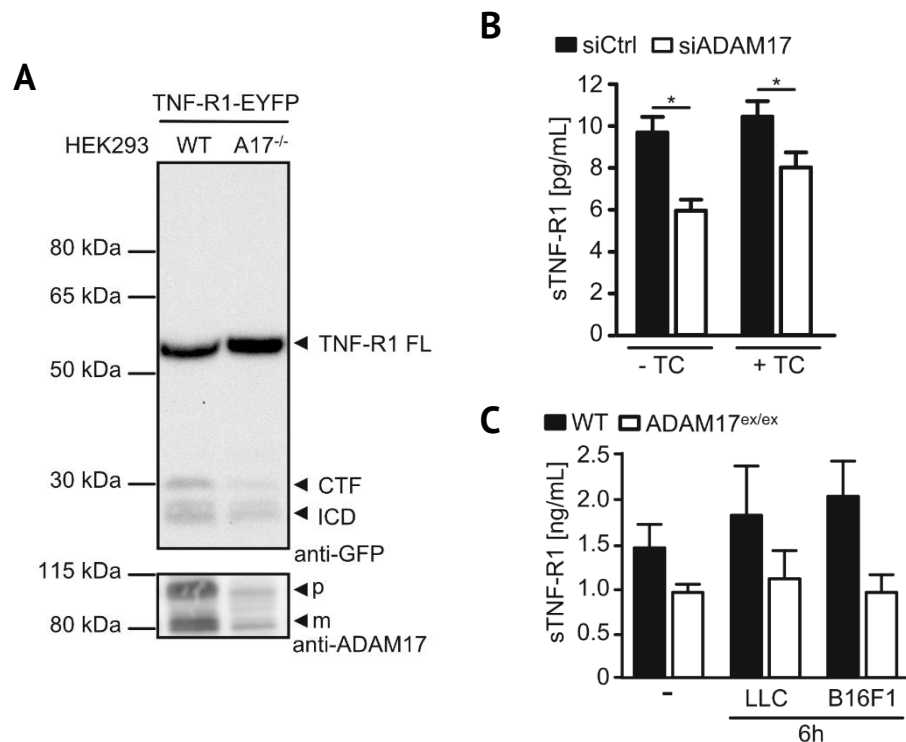


Figure 3.17: TNF-R1 shedding is impaired in the absence of ADAM17 *in vitro* and *in vivo*. **A:** Immunoblot analysis of TNF-R1-EYFP transfected HEK293 and HEK A17^{-/-} cells using the indicated antibodies. Whole cell lysates were used for the SDS-PAGE. CTF = C-terminal fragment, ICD = intracellular domain, p = proform, m = mature form. **B:** Quantification of soluble human TNF-R1 in the SN of co-culture experiments with HUVECs and MDA-MB231 (TC) cells via ELISA. Bar graphs show mean \pm SEM (n = 3). Statistical significance was determined by one-way ANOVA and Dunn's post-hoc test. **C:** Quantification of soluble murine TNF-R1 in plasma of WT and ADAM17^{ex/ex} mice via ELISA. Mice were either untreated or injected with LLC or B16F1 cells and sacrificed 6 h later. Bar graphs show mean \pm SEM (n = 3 mice per group). Statistical significance was determined by one-way ANOVA and Dunn's post-hoc test.

We detected significantly less soluble TNF-R1 levels in the SN of HUVECs with siRNA-mediated suppression of ADAM17 compared to SN of control cells. In co-culture with MDA-MB231 TCs soluble TNF-R1 levels were still reduced in the absence of ADAM17. Interestingly, we observed a slight increase in soluble TNF-R1 levels in both control and ADAM17-depleted HUVECs in the presence of TCs.

Measuring soluble TNF-R1 levels in plasma of either WT or ADAM17^{ex/ex} mice revealed the same tendency. Under untreated conditions we detected 1.5 ng/mL soluble TNF-R1 in WT and only half as much in ADAM17^{ex/ex} mice. 6 h after injection of either LLC or B16F1 cells soluble TNF-R1 levels slightly increased in WT mice, while soluble TNF-R1 levels in ADAM17^{ex/ex} were still reduced.

In conclusion, TNF-R1 shedding is impaired in the absence of ADAM17 *in vitro* and *in vivo* in the absence as well as in the presence of TCs.

TNF α stimulation of TNF-R1 rather leads to complex I assembly and cell survival than cell death. However, it is known that long stimulation with TNF α triggers TNF-R1 complex IIa formation and consequently apoptosis, whereas the simultaneous inhibition of caspase activity with the pan-caspase inhibitor zVAD leads to complex IIb and necrosome formation [161]. To investigate the role of ADAM17 for necroptosis triggered by TNF α -TNF-R1, we therefore stimulated HUVECs with siRNA-mediated suppression of ADAM17 with TNF α in the absence or presence of zVAD (Figure 3.18) for 6 h.

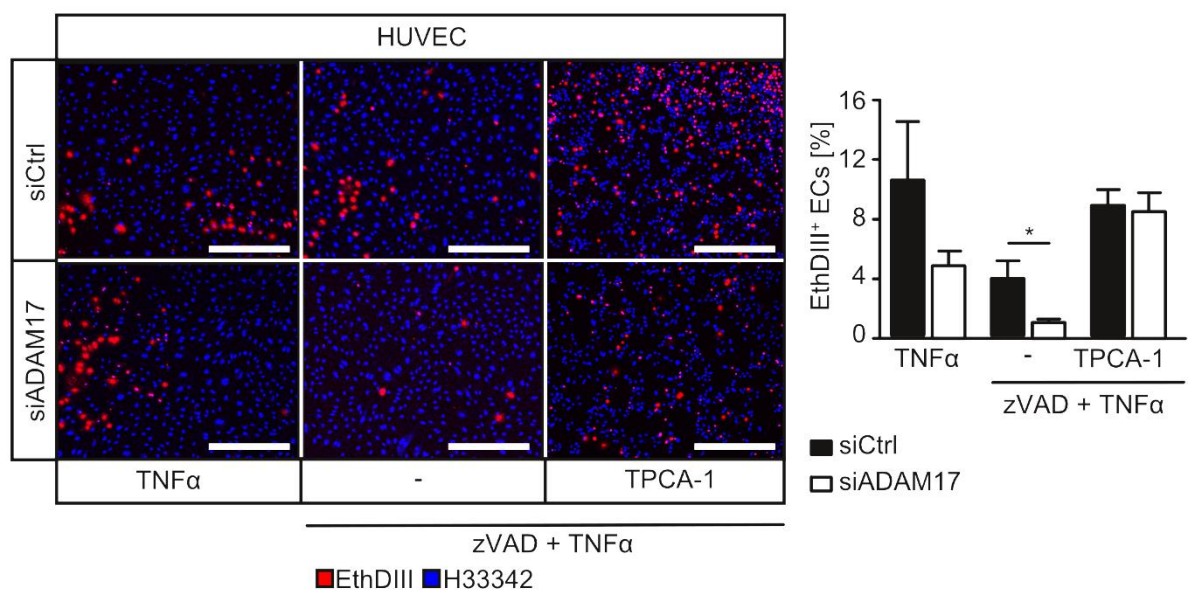


Figure 3.18: EC necroptosis via TNF-R1 is impaired in the absence of ADAM17. Representative images of control siRNA- or ADAM17 siRNA-treated HUVECs. Cells were stimulated with TNF α alone for 6 h or treated with zVAD and TPCA-1 prior to stimulation. Cells were stained with Hoechst33342 and EthDIII before imaging. Scale bar indicates 400 μ m. For the quantification a minimum of 4 non-overlapping pictures per condition were analyzed. Quantification shows mean \pm SEM (n = 4). Statistical significance was determined by one-way ANOVA and Dunn's post-hoc test.

Stimulation with TNF α alone resulted in up to 9 % EthDIII⁺ control siRNA-treated HUVECs, whereas an ADAM17 knock-down only lead to 4 % cell death. Nevertheless, this difference was not statistically significant.

In the presence of zVAD, only 4 % ECs died upon TNF α stimulation. Cell death was reduced to 1 % in the absence of ADAM17. Interestingly, upon simultaneous inhibition of IKK β with TPCA-1 cell death increased in control siRNA-treated as well as in ADAM17-depleted HUVECs up to 8 %. This result clearly shows a pivotal role of ADAM17 for TNF α -TNF-R1-induced necroptosis and suggests that the balance between complex I and II is shifted to complex I assembly with subsequent NF- κ B activation in the absence of ADAM17.

We next aimed at deciphering the underlying molecular mechanism. Chhibber-Goel and colleagues claimed, that RIP of TNF-R1 is a prerequisite for TNF α -induced apoptosis [162]. They showed initial cleavage of the receptor by ADAM17 and ICD release by Presenilin (PSEN) 1 and 2 containing γ -secretase complex. We investigated, whether this mechanism is also true for TNF α -induced necroptosis and therefore used MEFs isolated from WT, ADAM17^{ex/ex} or PSEN1^{+/-/2^{-/-}} mice (Figure 3.19).

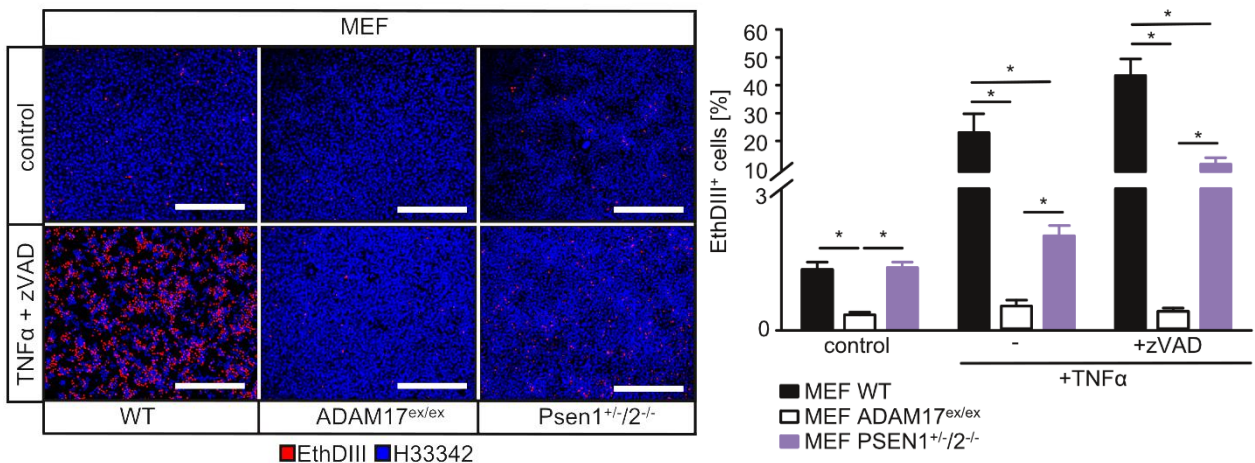


Figure 3.19: TNF-R1-triggered necroptosis is impeded in the absence of γ -secretase and ADAM17. Representative images of TNF α stimulated WT, ADAM17 or PSEN1^{+/-/2^{-/-}} MEFs. Cells were stimulated with TNF α alone for 6 h or treated with zVAD beforehand. Cells were stained with Hoechst33342 and EthDIII before imaging. Scale bar indicates 400 μ m. For the quantification a minimum of 4 non-overlapping pictures per condition were analyzed. Quantification shows mean \pm SEM (n = 3). Statistical significance was determined by one-way ANOVA and Dunn's post-hoc test.

Upon treatment with TNF α , cell death was induced in WT MEFs. Inhibition of caspases further increased cell death. By contrast TNF α stimulation of ADAM17^{ex/ex} MEFs did not result in cell death induction neither in the presence nor the absence of zVAD. In PSEN1^{+/-/2^{-/-}} MEFs cell death increased upon TNF α stimulation and was further enhanced in the presence of zVAD, but remained significantly lower than in WT MEFs.

These results suggest a general role of ADAM17 in TNF α -induced apoptosis and necroptosis. Furthermore, γ -secretase seems to play role in both apoptotic and necroptotic signaling pathways.

In order to determine the balance between TNF-R1 complex assembly and composition in the absence of ADAM17, WT and ADAM17^{ex/ex} MEFs were treated with moTAP-TNF α for different time points. The kinetic was subsequently used for immunoblot analysis of NF- κ B and MAPK activation (Figure 3.20).

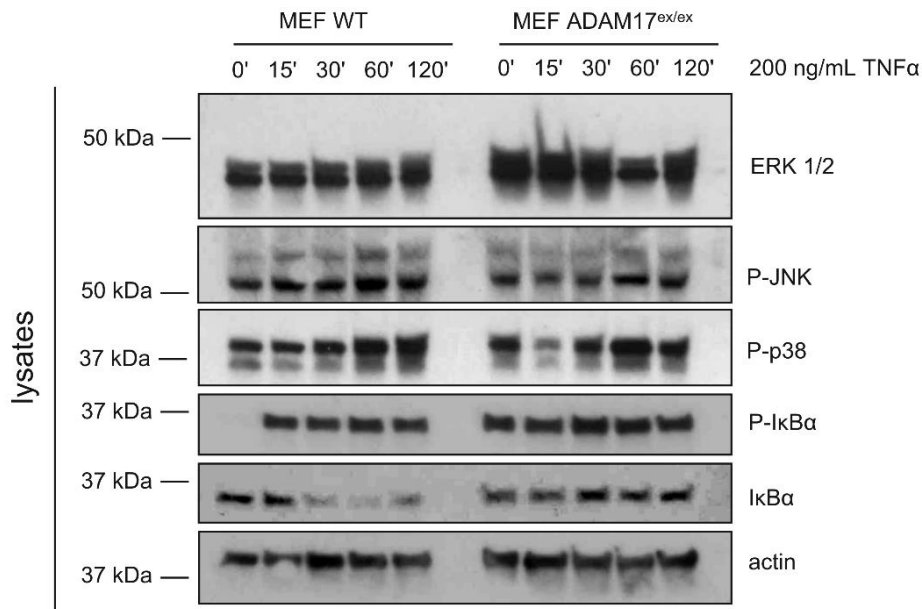


Figure 3.20: Constant phosphorylation of I κ B α ADAM17^{ex/ex} MEFs. Immunoblot analysis of whole cell lysates. WT and ADAM17^{ex/ex} MEFs were treated with moTAP-TNF α for the indicated time periods in FCS-free medium. Membrane was stained with the indicated antibodies.

We detected a time dependent phosphorylation of I κ B α and corresponding degradation in WT MEFs. In ADAM17^{ex/ex} MEFs P-I κ B α was already detectable without exogenous TNF α stimulation, suggesting constitutive activation of I κ B α in the absence of ADAM17. Phosphorylation of I κ B α leads to its degradation, further releasing NF- κ B. Interestingly, we did not detect degradation of this protein in ADAM17^{ex/ex} MEFs, as detected levels of I κ B α remained equal over time. MAPK activation was assessed by phosphorylation of p38, JNK and the presence of ERK1/2. Whereas there was an increase in phosphorylated p38 and JNK as well as levels of ERK1/2 in WT MEFs over time, ADAM17^{ex/ex} MEFs showed a different pattern. Unstimulated, 15 min and 30 min stimulation with TNF α lead to higher protein levels of ERK1/2 in ADAM17^{ex/ex} MEFs. Phosphorylation of JNK was less after 15 min and 30 min stimulation in those cells compared to WT MEFs. Furthermore, P-p38 levels were lower 15 min after stimulation with TNF α compared to 15 min stimulated WT MEFs. Of note, P-p38, P-JNK and ERK1/2 were present in both unstimulated cell types. These results emphasize an oscillating MAPK activation in the absence of ADAM17, whereas MAPK activation seems to be stabilized in WT MEFs. The same kinetic with an increased TNF α concentration was used for isolation of the TNF-R1 complex I. After

stimulation with moTAP-TNF α , the receptor-ligand-complex was immune-precipitated from whole cell lysates. Detection of proteins being involved in formation of TNF-R1 complex I was assessed by immunoblot analysis (Figure 3.21).

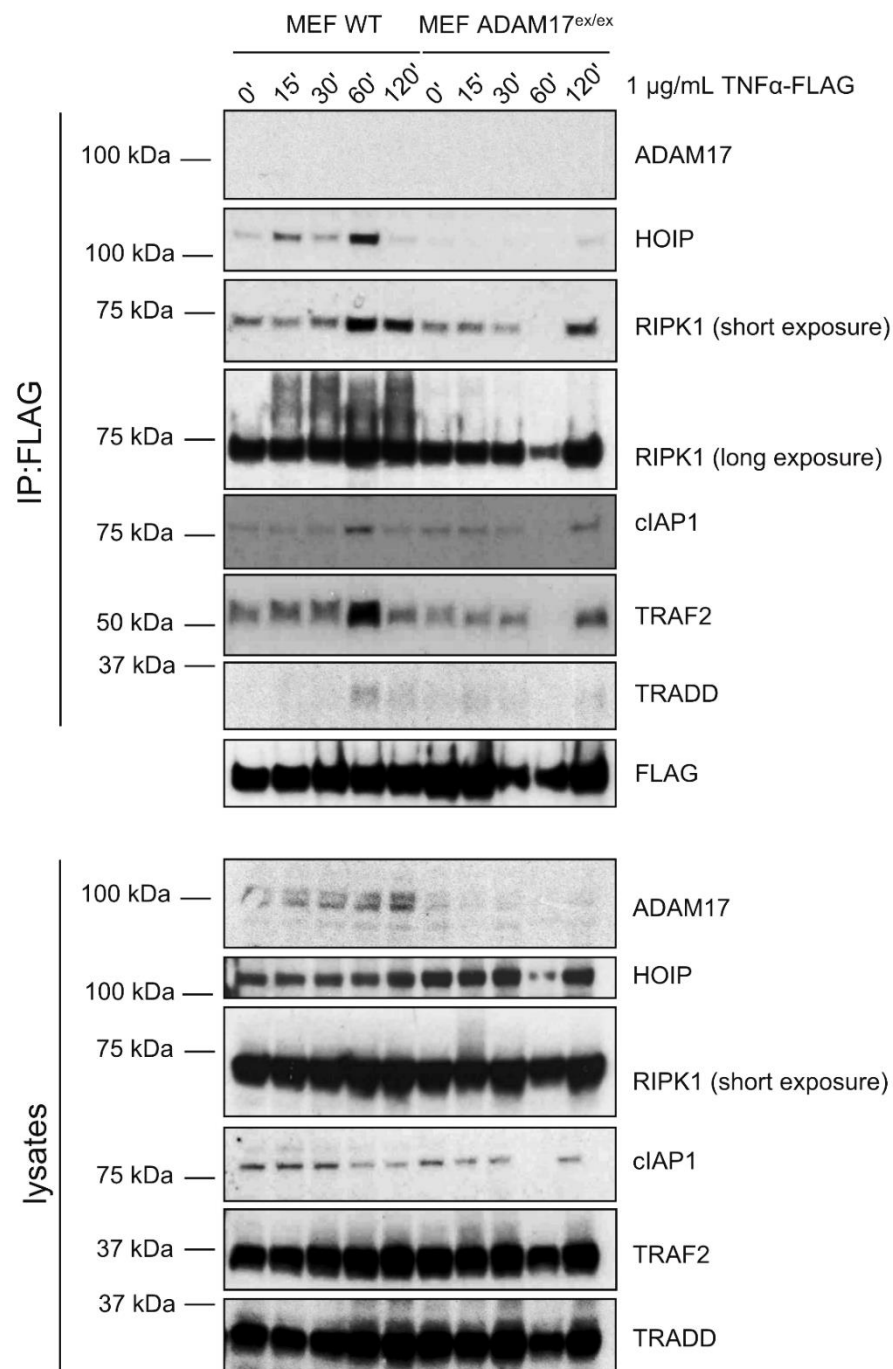


Figure 3.21: TNF-R1 complex I formation is less in the absence of ADAM17. Immunoblot analysis of TNF α -FLAG IP. WT and ADAM17^{ex/ex} MEFs were stimulated with moTAP-TNF α for the indicated time periods in FCS-free medium. Membrane was stained with the indicated antibodies.

In WT MEFs assembly of TNF-R1 complex I peaked after 60 min of stimulation with TNF α . Association of TRADD, RIPK1, TRAF2, cIAP1 and HOIP were detected. Ubiquitination of RIPK1,

detected as high molecular weight species of RIPK1, occurred over time and was visualized by long exposure. In contrast, TRADD association in ADAM17^{ex/ex} MEFs was almost not detectable. RIPK1 recruitment peaked after 120 min stimulation, yet protein levels were considerably less than in WT MEFs. More importantly, a longer exposure revealed strikingly decreased ubiquitination of associated RIPK1 than in WT MEFs. TRAF2, cIAP1 and HOIP protein levels peaked after 120 min stimulation with TNF α in ADAM17^{ex/ex} MEFs but were still lower than 60 min after stimulation in WT MEFs.

The analysis of TNF-R1 complex I isolation suggests reduced and delayed TNF-R1 complex I assembly upon stimulation in the absence of ADAM17. We additionally isolated TNF-R1 complex II by FADD immunoprecipitation, after stimulation with TNF α and pre-incubation with zVAD, to pin down molecular mechanism responsible for decreased necroptotic cell death in the absence of ADAM17 (Figure 3.22).

We additionally isolated TNF-R1 complex II by FADD immunoprecipitation, after stimulation with TNF α and pre-incubation with zVAD, to pin down molecular mechanism responsible for decreased necroptotic cell death in the absence of ADAM17 (Figure 3.22).

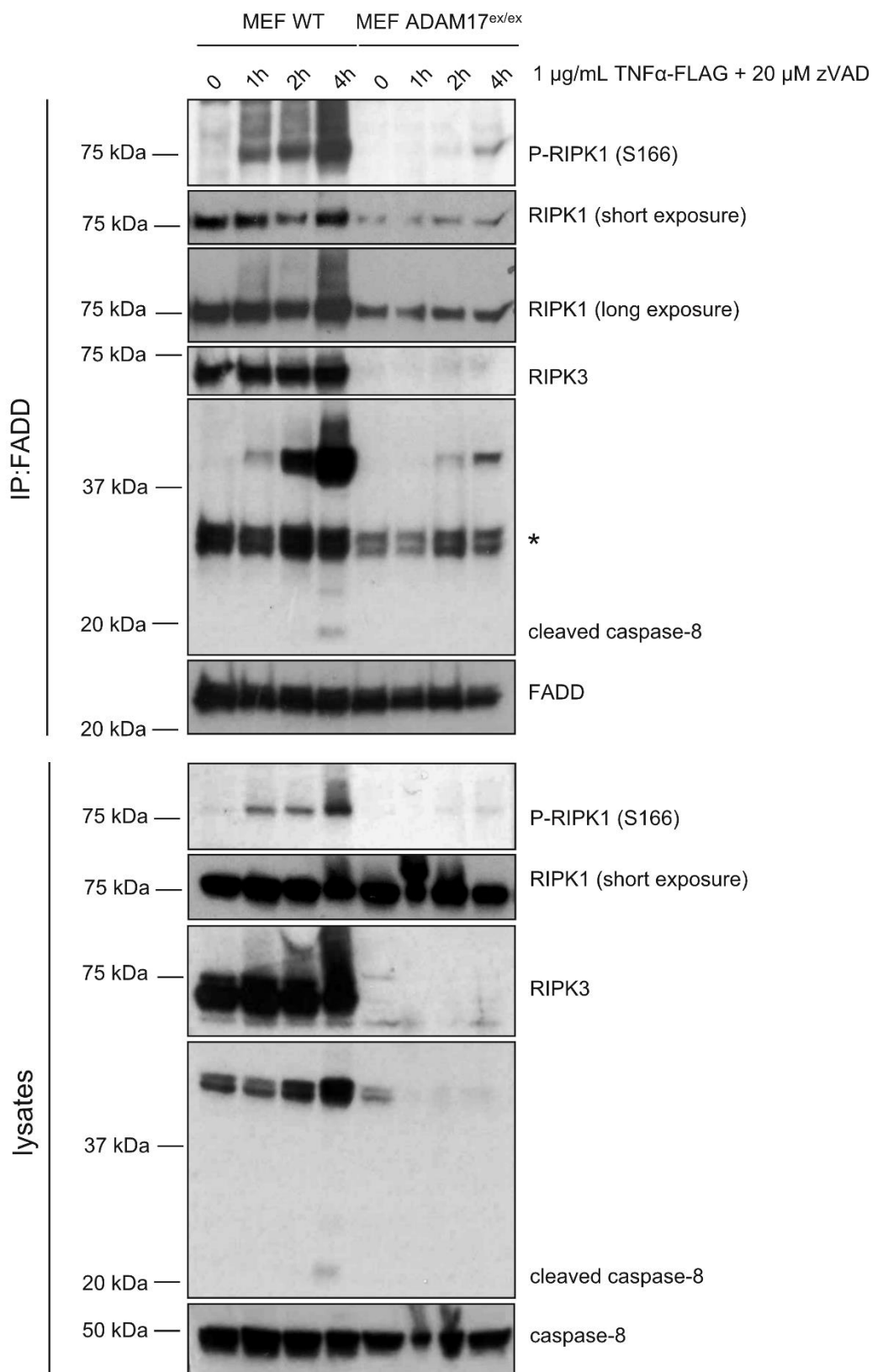


Figure 3.22: RIPK3 and caspase-8 are not recruited to TNF-R1 complex II in the absence of ADAM17. Immunoblot analysis of FADD IP. WT and ADAM17^{ex/ex} MEFs were stimulated with moTAP-TNF α for the indicated time periods after 30 min pre-incubation with zVAD. Membrane was stained with the indicated antibodies. * indicates unspecific binding.

The longer the stimulation with TNF α , the more RIPK1 associated with FADD in zVAD pre-treated WT MEFs. We also detected increasing RIPK3 and caspase-8 associating protein levels. Cleaved caspase-8 was only detected after 4 h of stimulation. Interestingly, FADD-associated RIPK1 exhibited increasing ubiquitination, as visualized by a long exposure, as well as phosphorylation at serine 166, which indicates autophosphorylation of RIPK1.

Surprisingly, we detected less RIPK1 protein levels associated to FADD in the TNF α stimulated and zVAD pre-treated ADAM17^{ex/ex} MEFs. Even after long exposure no ubiquitination was visible and only a slight phosphorylation after 4 h was detectable. Moreover, RIPK3 was neither associated to FADD nor found in the corresponding cell lysates of ADAM17^{ex/ex} MEFs. The same was true for cleaved caspase-8. Nevertheless, inactive caspase-8 was found in both WT and ADAM17^{ex/ex} MEF cell lysates in equal amounts on every examined time point.

The end point of necroptosis is thought to be phosphorylation of MLKL. To assess whether loss of RIPK3 expression in ADAM17^{ex/ex} MEFs simultaneously implies the absence of phosphorylated MLKL, we stimulated zVAD pre-treated WT and ADAM17^{ex/ex} MEFs with TNF α and subjected the cell lysates to immunoblot analysis (Figure 3.23).

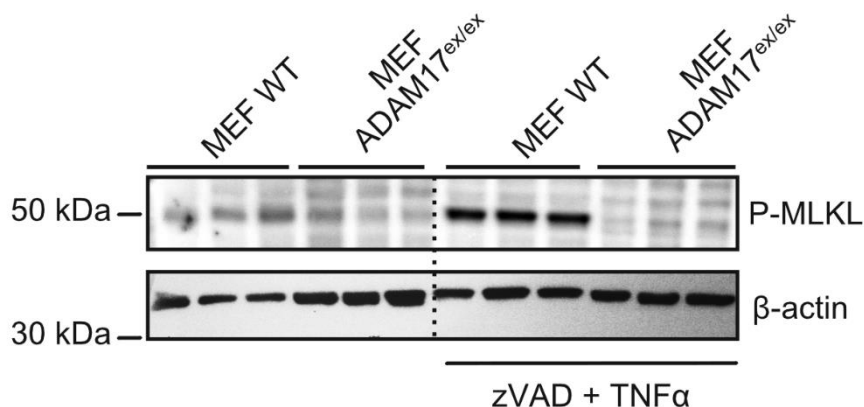


Figure 3.23: Loss of ADAM17 hinders MLKL phosphorylation upon stimulation with TNF α and zVAD treatment. Immunoblot analysis of WT and ADAM17^{ex/ex} MEFs were pre-treated with 100 μ M zVAD for 30 min and stimulated with 50 ng/mL TNF α for 4 h. Membrane was stained with the indicated antibodies.

While in WT MEFs MLKL phosphorylation occurs 4 h after induction of necroptosis by TNF α and zVAD, ADAM17^{ex/ex} MEFs showed no phosphorylation of MLKL.

Taken together, isolation of TNF-R1 complex II clearly revealed differences in the assembly in the absence and presence of ADAM17. There is no expression and recruitment of RIPK3 as well as cleavage of caspase-8. We show, that loss of RIPK3 expression inhibits downstream machinery of necroptosis. MLKL is not phosphorylated, thus there is no execution of necroptosis in the absence of ADAM17.

TNF-R1 complex I and II formation is strongly impaired in the absence of ADAM17 (Figure 3.21, Figure 3.22). Whether reduced cleavage of the receptor is accountable for that is left undecided so far. We rather reasoned that impaired TNF-R1 signaling would resemble ADAM17 deficiency in the *in vivo* metastasis model. Therefore, either WT or TNF-R1^{-/-} mice were injected with LLC-lacZ cells and sacrificed after 6 h. The lungs were analyzed for number of TCs in the tissue (Figure 3.24).

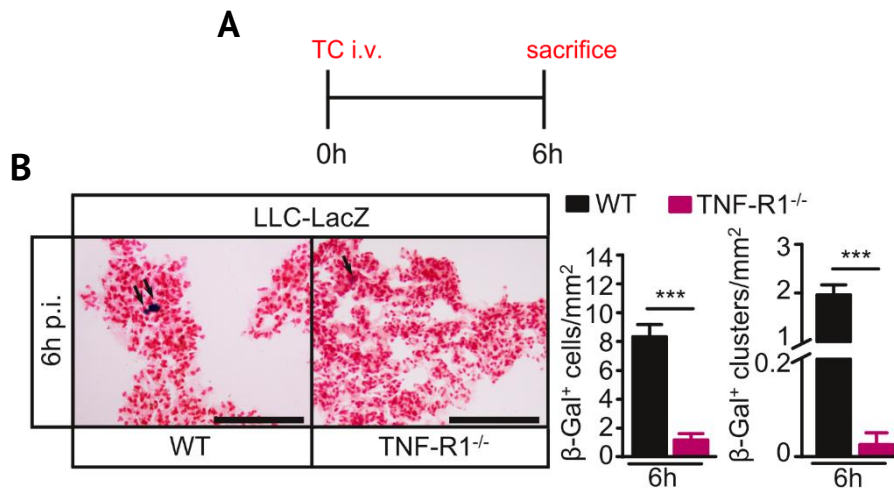


Figure 3.24: TC extravasation in the lung is decreased in the absence of TNF-R1. **A:** Timeline for the *in vivo* experiment. **B:** Representative microscopic images of β-galactosidase and nuclear fast red stained lung sections of WT and TNF-R1^{-/-} mice 6 h after LLC-LacZ cell injection. Scale bar indicates 100 μm. Quantification shows mean ± SEM (n = 3 mice per group). Statistical significance was determined by unpaired, one-tailed Student's t-Test. p.i. = post injection. Black arrows point to β-Gal⁺ cells.

In lung tissue of TNF-R1^{-/-} mice we found significantly less TCs after 6 h. Additionally, cluster formation was drastically reduced in those mice compared to WT mice.

We concluded that TNF-R1 signaling is essentially involved in TC extravasation, presumably by cell death induction triggered by its ligand TNFα, which itself is a substrate of ADAM17. TNFα can be blocked by Etanercept, a fusion protein of TNF-R2's extracellular portion and a Fc part. We injected it prior to TC injection in WT mice and analyzed EC cell death with EthDIII after 6 h (Figure 3.25). A single treatment 5 min before TC injection was sufficient to decrease EC necroptosis by almost 50 %. Both results (Figure 3.24, Figure 3.25) indicate that, apart from DR6-APP, TNF-R1-TNFα-induced EC death is also partly involved in TC extravasation.

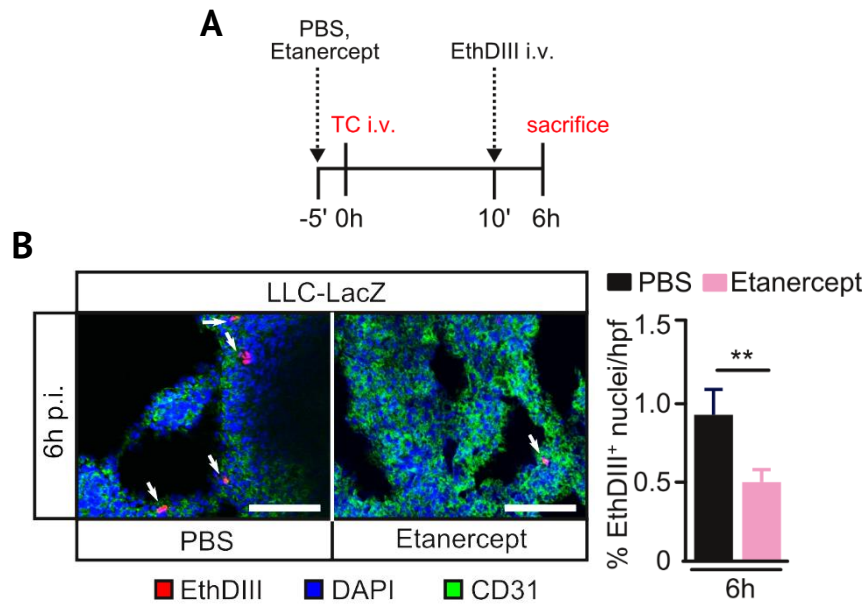


Figure 3.25: TC-induced EC death is decreased in Etanercept-treated WT mice. **A:** Timeline for the *in vivo* experiment. **B:** Representative images of lung tissue sections stained for CD31. WT mice were i.v. injected with 4 $\mu\text{g/g}$ Etanercept 5 min prior to injection of LLC-LacZ cells and sacrificed 6 h later. EthDIII was injected i.v. 5 min prior to sacrifice. Scale bar indicates 100 μm . A minimum of 3 non-overlapping images per animal were analyzed. Quantification shows mean \pm SEM ($n = 6$ mice per group). Statistical significance was determined by Mann-Whitney U. p.i. = post injection. White arrows point to EthDIII⁺ cells.

3.6 Myeloid ADAM17 has no impact on metastasis of tumor cells to the lung

We observed reduced LLC and B16F1 extravasation in the absence of ADAM17 6 h after TC injection (Figure 3.1). Interestingly, we noticed that 20 h after LLC injection the number of TC cluster further increased in WT mice, while TC cluster in ADAM17^{ex/ex} mice rather decreased, suggesting TC proliferation in WT but not in ADAM17^{ex/ex} mice. This further emphasizes that ADAM17 in the metastatic niche regulates more than just TC extravasation.

We therefore injected ADAM17^{ex/ex} or WT mice i.v. with LLC cells and sacrificed them 7, 14 or 21 days later.

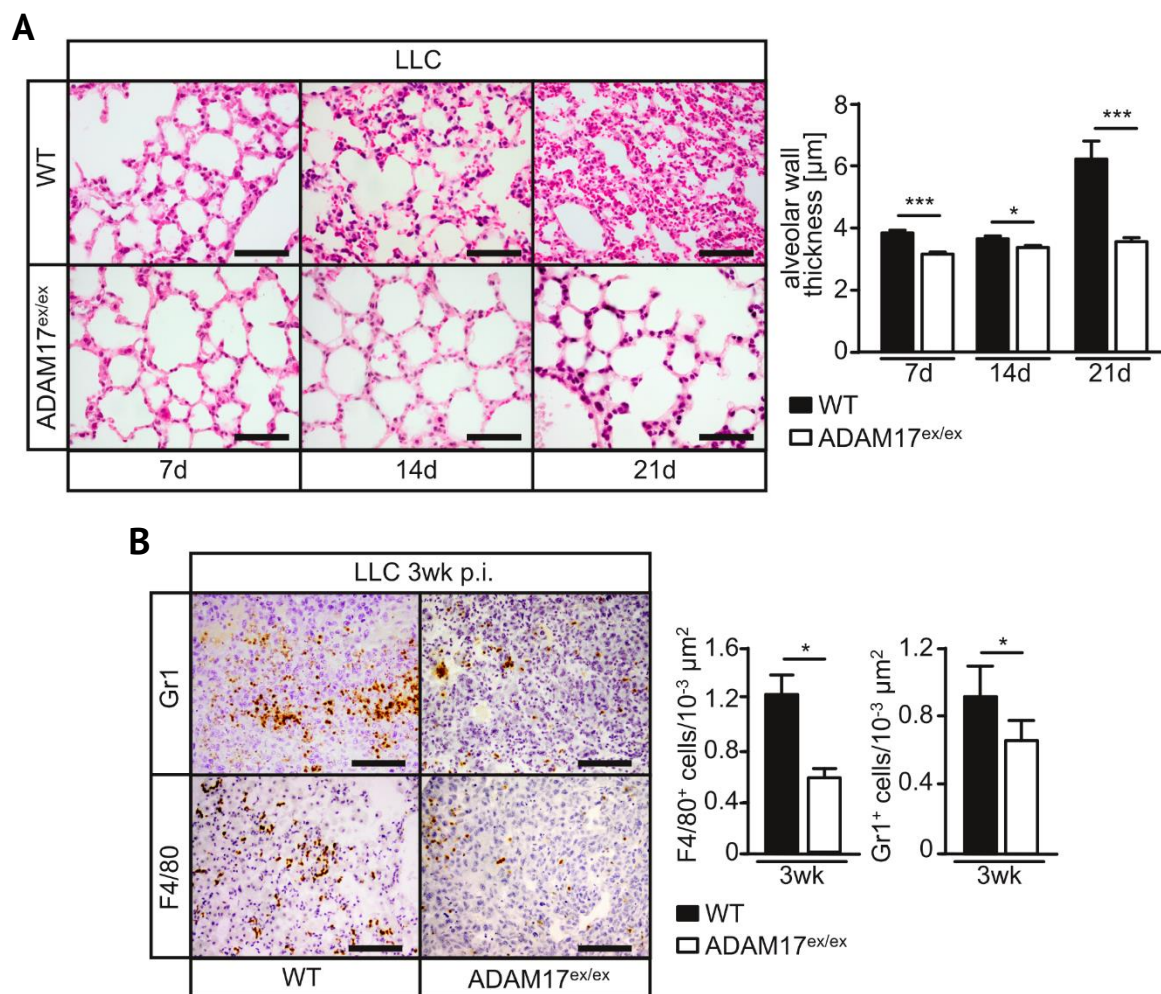


Figure 3.26: Less associated tissue inflammation in TC injected ADAM17^{ex/ex} mice. **A:** Representative microscopic images of HE-stained lung tissue of WT and ADAM17^{ex/ex} mice injected i.v. with LLC cells. Mice were sacrificed at the indicated time points. Scale bar indicates 50 μm. For each animal 5 images and 10 alveolar walls were measured. Quantification shows mean ± SEM (n = 3 per group). Statistical significance was determined by one-way ANOVA and Bonferroni post-hoc test. d = days. **B:** F4/80 and Gr1 stained lungs of WT and ADAM17^{ex/ex} mice injected with LLC cells and sacrificed 3 weeks later. Scale bar indicates 100 μm. 8 non-overlapping images per animal were analyzed. Quantification shows mean ± SEM (n = 3 per group). Statistical significance was determined by Student's t-Test. p.i. = post injection, wk = weeks.

We observed increased thickening of the alveolar walls over time in WT but not ADAM17^{ex/ex} mice, indicating reduced inflammation of the lung in the absence of ADAM17 (Figure 3.26A). The difference is most distinct 21 days after LLC cell injection.

Supportive to the HE-staining, we observed slightly reduced infiltration of Gr1⁺ granulocytes and 50 % reduction in F4/80⁺ macrophages in TC-injected ADAM17^{ex/ex} mice compared to WT animals (Figure 3.26B).

These observations indicate a reduction in TC-induced inflammation in ADAM17^{ex/ex} mice. During inflammation, TNF α is predominantly cleaved from the surface of macrophages by ADAM17 [163]. Interestingly, Kim and colleagues showed that the pro-inflammatory cytokine TNF α promotes metastasis [83]. Therefore, we hypothesized that ADAM17 on immune cells promotes inflammation, extravasation of TCs and metastasis by the release of TNF α .

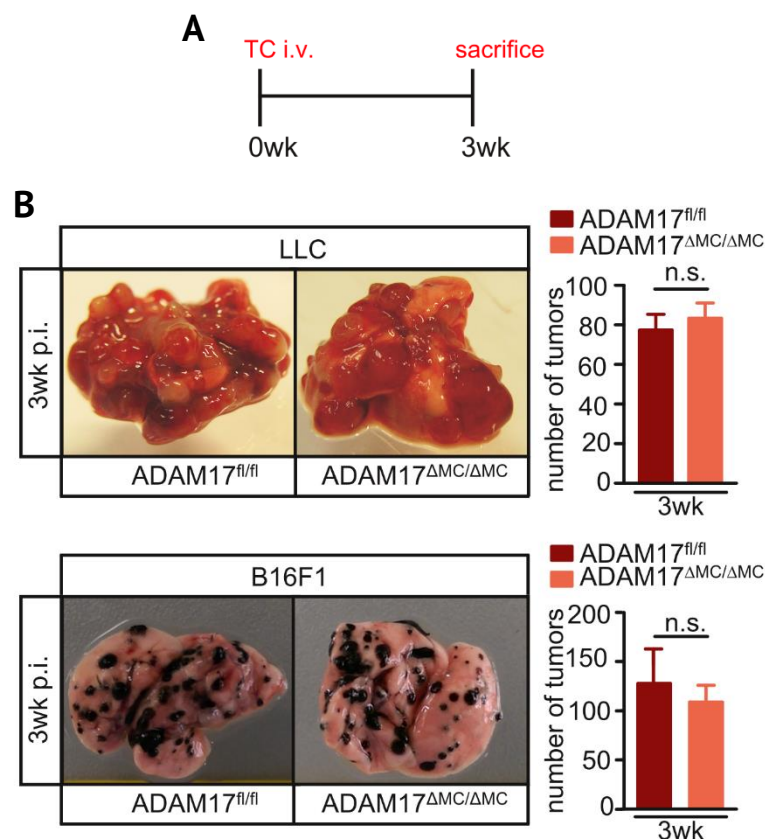


Figure 3.27: The absence of ADAM17 on myeloid cells is not protective against metastasis to the lung.

A: Timeline for the *in vivo* experiment. **B:** Representative macroscopic lung images of ADAM17^{ΔMC/ΔMC} mice 3 weeks after LLC or B16F1 cell injection. Tumor number was quantified and is shown as mean \pm SEM ($n = 3$ ADAM17^{fl/fl}, 4 ADAM17^{ΔMC/ΔMC}). Statistical significance was determined by unpaired, one-tailed Student's t-Test. p.i. = post injection, wk = weeks.

We therefore generated LysM-Cre;ADAM17^{fl/fl} (ADAM17^{ΔMC/ΔMC}) mice, which display ADAM17 deficiency on all myeloid cells and subjected them to our metastatic mouse model (Figure 3.27A).

Contrary to our assumption, we did not detect any difference in tumor number between ADAM17^{ΔMC/ΔMC} and ADAM17^{fl/fl} mice 3 weeks after LLC or B16F1 injection (Figure 3.27B). Thus ADAM17 on myeloid cells does not contribute to metastasis of TCs.

In order to target the adaptive immune system rather than the myeloid compartment, we next used CD4-Cre;ADAM17^{fl/fl} (ADAM17^{ΔT/ΔT}) mice. Those mice with an ADAM17 deficiency only on CD4⁺T cells were i.v. injected with LLC cells. 3 weeks later lungs were examined for macroscopic metastases (Figure 3.28A).

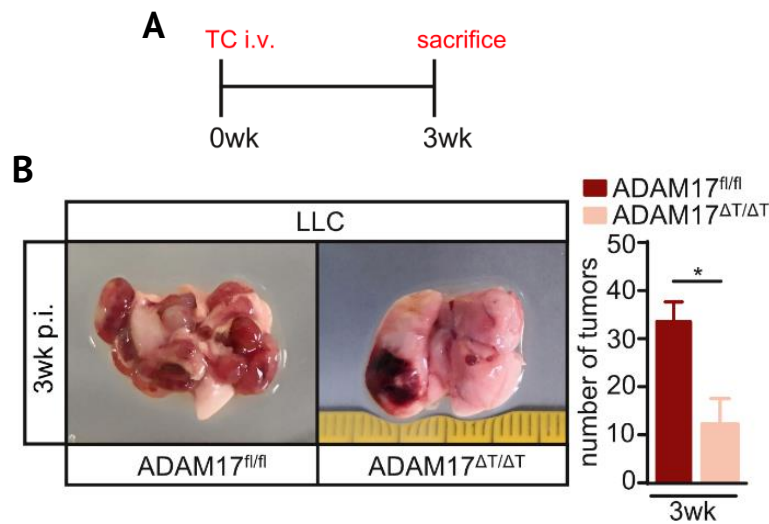


Figure 3.28: T cell-specific deletion of ADAM17 protects against tumor formation in the lung. **A:** Timeline for the *in vivo* experiment. **B:** Representative macroscopic lung images of ADAM17^{ΔT/ΔT} mice 3 weeks after LLC cell injection. Tumor number was quantified and is shown as mean \pm SEM (n = 3 per group). Statistical significance was determined by unpaired, one-tailed Student's t-Test. p.i. = post injection, wk = weeks.

Interestingly, T cell-specific deletion of ADAM17 reduced tumor number in the lung to a third compared to control mice (Figure 3.28B).

Taken together, these data imply a more important role of ADAM17 in the adaptive than the innate immune system in the context of metastasis.

3.7 Activated Notch1 signaling leads to tumor cell stemness and proliferation

We investigated the proliferation in tumorous tissue of WT and ADAM17^{ex/ex} mice. We stained paraffin embedded lung sections for proliferating cell nuclear antigen (PCNA) using DAB-staining (Figure 3.29). The staining revealed less PCNA⁺ cells in ADAM17^{ex/ex} lung tumors, compared to WT tumors 3 weeks after LLC injection, suggesting an important role of microenvironmental ADAM17 in TC proliferation.

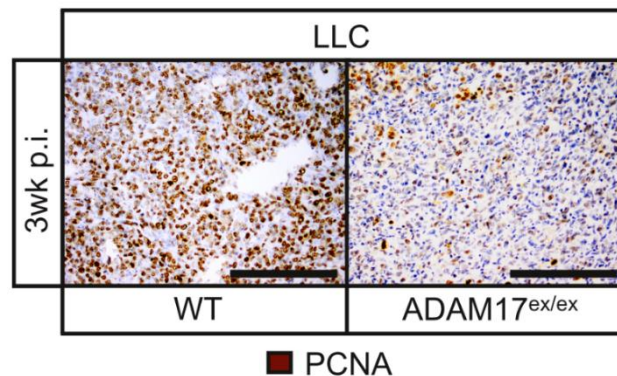


Figure 3.29: LLC tumors in ADAM17^{ex/ex} mice display less proliferating cells compared to tumors in WT mice. Representative images of DAB-stained tumorous tissue in WT and ADAM17^{ex/ex} lungs 3 weeks after LLC cell injection. Scale bar indicates 100 μ m. p.i. = post injection.

In order to simulate the paracrine activation, we immobilized the Notch1 ligand jagged-1-Fc with a IgG1 antibody on a tissue culture dish and seeded either LLC or B16F1 cells on top (Figure 3.30A). Notch1 activation was assessed by immunoblot analysis (Figure 3.30B).

Upon stimulation with jagged-1, LLC cells displayed increased amounts of cleaved Notch1 and phosphorylated receptor tyrosine kinase Axl, which is also involved in cell proliferation, migration and EMT. Moreover, Axl expression was shown to be regulated by TGF β signaling, which in turn was shown to cross-talk with Notch1 signaling [164, 165]. On mRNA-level, we noted a strong increase in fold induction of the Notch1-target gene *hairy and enhancer of split (Hes)-1* after jagged-1 stimulation. Furthermore, *Axl* was upregulated as well as *Vimentin*, *Twist1* and *Col6a1*, indicators for EMT. In B16F1 we did not see a jagged-1-dependent effect on Notch1 activation (Figure 3.30C). In fact, we detected cleaved Notch1 even in IgG1 stimulated B16F1 cells in equal amounts as in jagged-1 stimulated cells. Additionally, there was no difference in the amount of phosphorylated Axl. Consequently, we did not detect differences in the expression of *Hes-1* and *Axl*, as assessed by qRT-PCR (Figure 3.30D).

These results suggest the activation of Notch1 signaling in LLC cells in WT, but not ADAM17-deficient mice, leading to reduced proliferation, migration and survival of the TC. In contrast, Notch1 signaling in B16F1 cells seems to be independent of ADAM17.

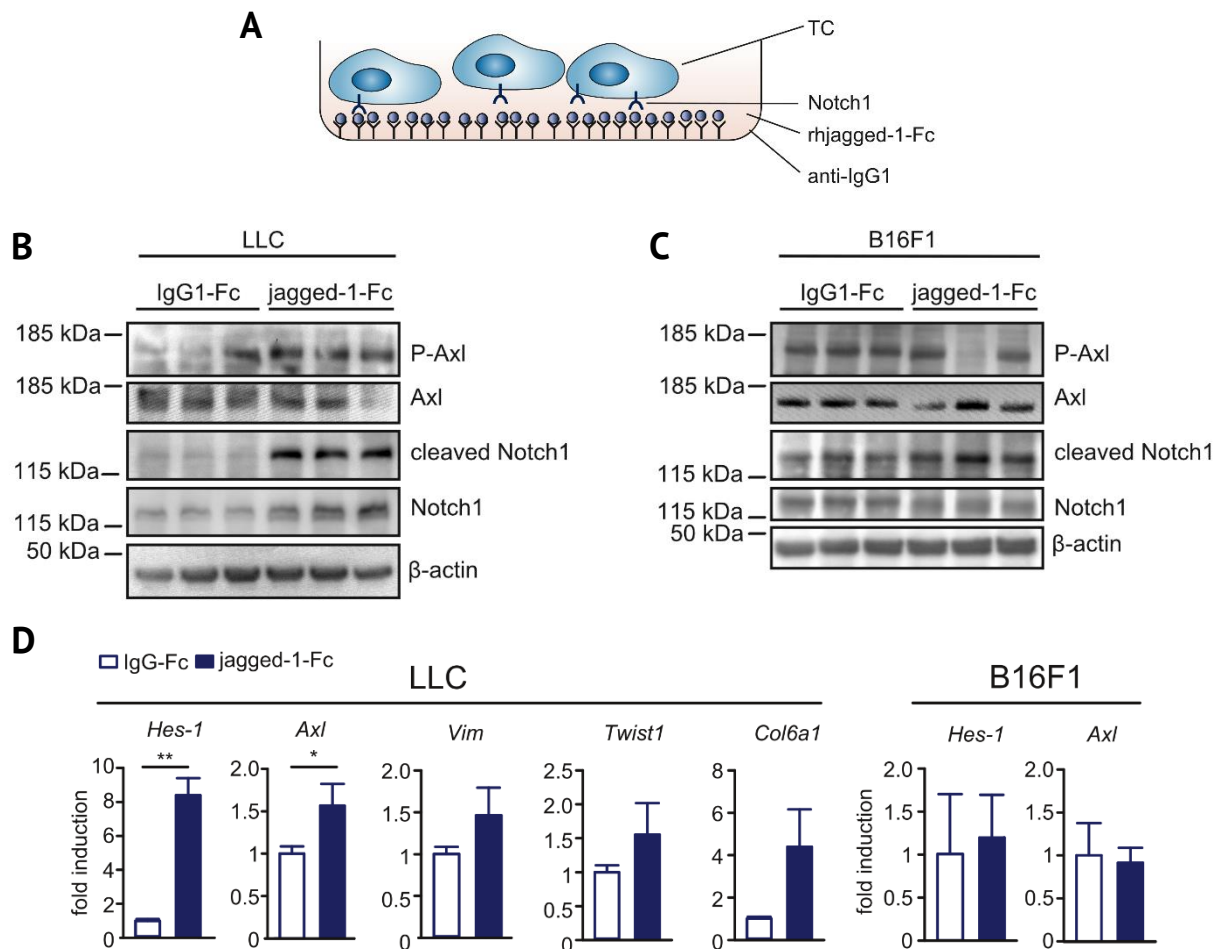


Figure 3.30: Notch1 activation in LLCs but not B16F1 cells leads to CSC phenotype. **A:** Schematic of the experimental procedure. **B:** Immunoblot analysis of LLC cell lysates. Cells were stimulated with immobilized jagged-1-Fc or IgG1-Fc for 72 h (n = 4). **C:** Immunoblot analysis of B16F1 cell lysates. Cells were stimulated with immobilized jagged-1-Fc or IgG1-Fc for 72 h. n = 4. **D:** qRT-PCR quantification of Notch target gene expression in LLC and B16F1 cells. Cells were stimulated with immobilized jagged-1-Fc or IgG1-Fc for 72 h (n = 3). Statistical significance was determined by unpaired, one-tailed Student's t-Test.

3.8 Specific inhibition of ADAM17 prevents tumor cell metastasis

Our results show a high relevance of ADAM17 for metastasis and tumor growth, identifying it as a promising target for anti-cancer therapies. Therefore, it is necessary to develop a highly specific inhibitor that does not interfere with the activity of other ADAMs, like ADAM10.

Very recently, Irit Sagi and colleagues were able to generate the recombinant ADAM17-PD. So far, it was used as inhibitor for ADAM17 activity in LPS-induced sepsis, collagen-induced arthritis, TNBS-induced colitis in mice, *Kras*-driven lung adenocarcinoma and kidney fibrosis [6, 26, 166]. In all four investigated pathologies, inhibition of ADAM17 showed beneficial effects. Here we aimed to test the ADAM17-PD in our metastatic mouse model. To begin with, we confirmed the identity and purity of the ADAM17-PD by coomassie stained SDS-PAGE (Figure 3.31A). To ensure the proper inhibitory effect of ADAM17-PD, we performed an activity assay with the recombinant catalytic domain of ADAM17 (Figure 3.31B). Not only the metalloprotease inhibitor TAPI-1, but also ADAM17-PD inhibited the cleavage of a fluorogenic TNF α -based substrate. The IC₅₀ of TAPI-1 and ADAM17-PD in those activity assays was 128.0 \pm 0.9 nM and 110.8 \pm 1.6 nM, respectively (Figure 3.31C).

We next investigated the inhibitory effect of ADAM17-PD *in vivo*. Therefore, WT mice were injected i.v. with either ADAM17-PD or TAPI-1 5 min before TC injection. The mice were sacrificed 6 h later and the lung tissue was analyzed for TC number and EC death (Figure 3.32). A β -galactosidase staining revealed significantly less TCs in lungs of mice treated with TAPI-1 and ADAM17-PD. We detected a reduction of extravasated TCs by half in ADAM17-PD treated mice and by almost 75 % in TAPI-1 treated mice. To investigate whether this is due to impaired necroptosis of ECs, we injected EthDIII 5 min before sacrificing the mice. Co-staining of lung sections with CD31 displayed indeed a strong reduction in necroptotic ECs in TAPI-1 and ADAM17-PD treated mice, reflecting the reduction in extravasation (Figure 3.32C).

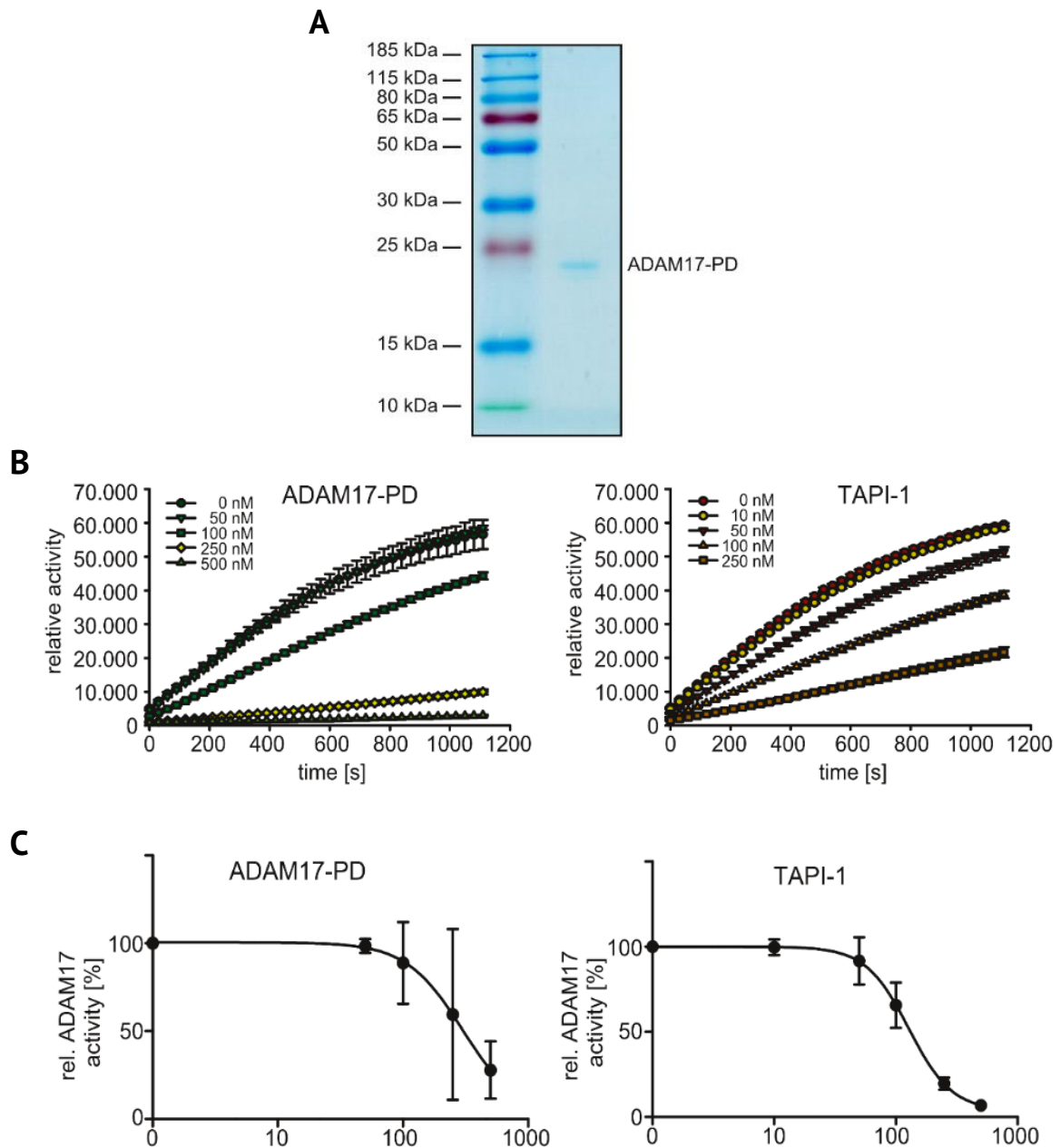


Figure 3.31: ADAM17-PD is a potent inhibitor of ADAM17 activity. **A:** Identification and purity of the ADAM17-PD analyzed with reducing SDS-PAGE and coomassie staining. 400 ng were loaded on the gel. **B:** Activity of recombinant catalytic domain of ADAM17 towards a fluorogenic TNF α -based peptide in the presence of the indicated ADAM17-PD or TAPI-1 concentrations ($n = 3$). **C:** Half maximal inhibitory concentrations (IC_{50}) of ADAM17-PD and TAPI-1. IC_{50} values were calculated using four parameter logistic curve fitting ($n = 3$).

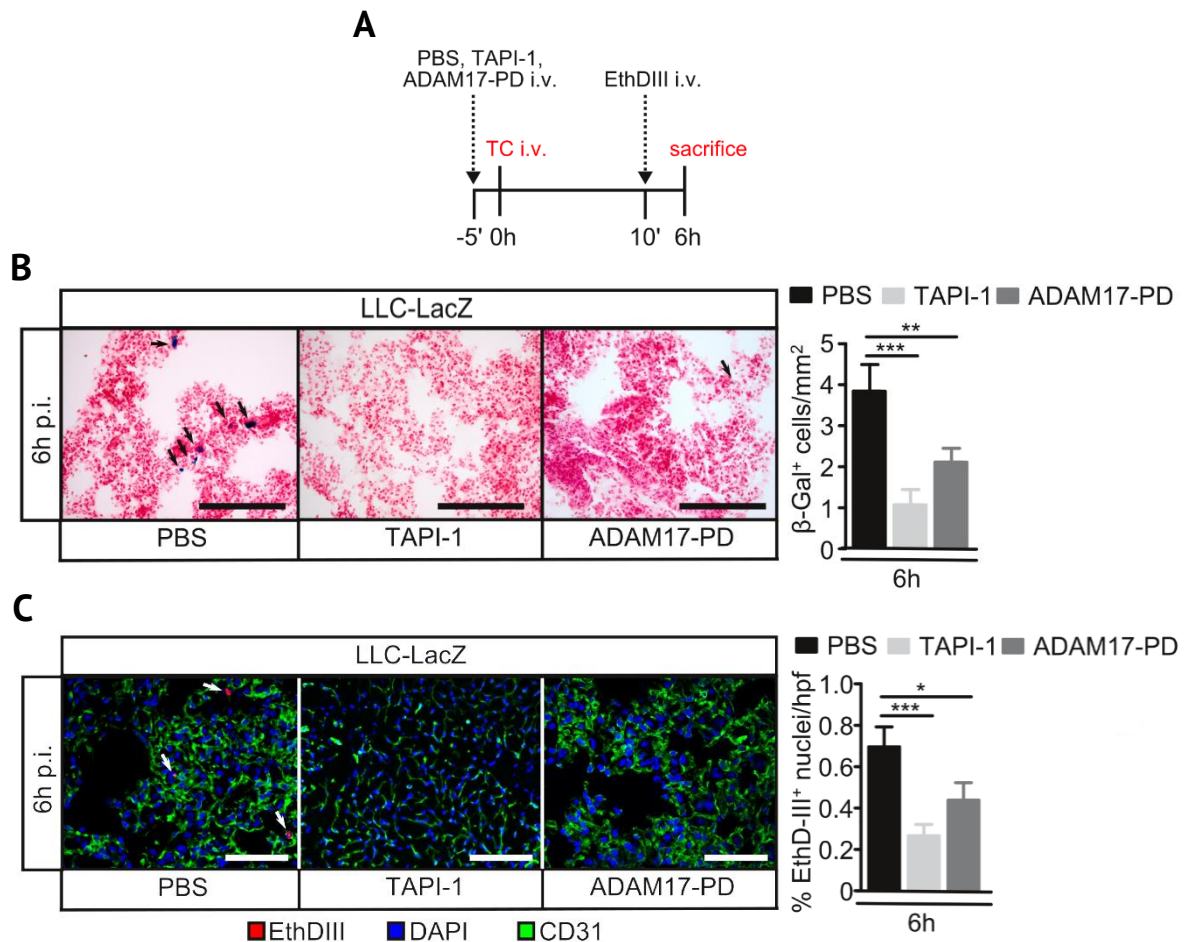


Figure 3.32: Single ADAM17-PD dose inhibits TC-induced EC necroptosis and extravasation. **A:** Timeline for the *in vivo* experiments. **B:** Representative microscopic images of β -galactosidase and nuclear fast red stained lung sections of WT mice 6 h after LLC-LacZ cell injection. 5 min prior to TC injection, PBS, ADAM17-PD or TAPI-1 was injected i.v. Scale bar indicates 100 μ m. Quantification shows mean \pm SEM (n = 4 PBS, 3 TAPI-1, 6 ADAM17-PD). Statistical significance was determined by ANOVA on ranks and Turkey's post-hoc test. p.i. = post injection. Black arrows indicate β -Gal⁺ cells. **C:** Representative images of lung tissue sections stained for CD31. WT mice were i.v. injected with LLC-LacZ cells and sacrificed 6 h later. EthDIII was injected i.v. 5 min prior to sacrifice. Scale bar indicates 100 μ m. A minimum of 5 non-overlapping images per animal were analyzed. Quantification shows mean \pm SEM (n = 4 PBS, 3 TAPI-1, 6 ADAM17-PD). Statistical significance was determined by ANOVA on ranks and Turkey's post-hoc test. p.i. = post injection. White arrows indicate EthDIII⁺ cell.

We reasoned that a single dose of ADAM17-PD is sufficient to decrease tumor formation due to impaired extravasation. Therefore, WT mice were injected with ADAM17-PD 5 min before TC injection and the mice were sacrificed 3 weeks later (Figure 3.33A,B). A single dose of ADAM17-PD prior to TC injection lead to a reduction in tumor burden by 90 %.

We here show, that i.v. injection of a specific ADAM17 inhibitor leads to reduction in metastasis which is due to impaired TC-induced EC necroptosis. Hereby a single dose of ADAM17-PD is sufficient to decrease extravasation and tumor formation significantly.

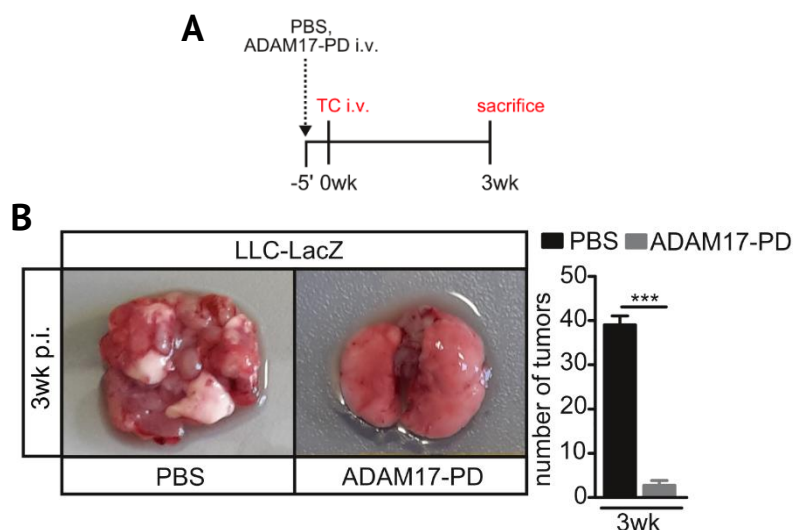


Figure 3.33: ADAM17-PD prevents tumor formation in the lung. **A:** Timeline for the *in vivo* experiment. **B:** Representative macroscopic images of lungs of WT mice injected i.v. with either PBS or ADAM17-PD 5 min prior to LLC injection. Quantification shows mean \pm SEM ($n = 3$). Statistical significance was determined by unpaired, one-tailed Student's t-Test. p.i. = post injection, wk = weeks.

These results identify ADAM17 as promising target to reduce the risk of metastasis without the need to directly interfere with the TC itself but rather manipulating extravasation efficiency of TCs.

4 Discussion

Metastatic disease is the major cause of death in cancer patients. A novel concept of therapy is highly warranted, but yet many steps in the complex metastatic cascade still remain elusive. While in the last decade cancer research predominantly focused on targeting TCs themselves, it became apparent that more advanced approaches, e.g. simultaneous targeting of the tumor microenvironment, are more beneficial for the patient.

Since several substrates of ADAM17 have been implicated in tumor development and progression, we aimed to identify ADAM17 as a regulator in metastasis.

4.1 ADAM17 activity in the microenvironment for tumor cell extravasation

TC extravasation, in particular breaching the endothelial barrier is considered as a limiting step in the metastatic process, which is thought to involve collaboration of many different cell types. Soluble factors released by ECs, immune cells and TCs themselves are just as important as direct interaction between these cell types to facilitate TC transmigration. Several substrates of ADAM proteases have been implicated in the process of metastasis and tumor growth [26]. ADAM17s' most prominent substrate TNF α e.g. was shown by Kim et al. to play a crucial role in metastasis [83]. TNF α ^{-/-} mice were partially protected from metastases formation in the lung after i.v. LLC injection. Consequently, previous work in our lab showed a strong reduction in tumor burden in hypomorphic ADAM17^{ex/ex} mice when subjected to the same metastasis model using either LLC or B16F1 cells.

Extravasation is a quite fast process as it is thought to be completed within 24 h after TCs entering the circulation [167]. We observed enhanced permeability of the endothelium of WT mice 6 h after TC injection (Figure 3.3). However, 20 h after TC injection endothelial barrier function was restored in WT mice, supporting the notion that TC-induced endothelial permeability is a transient process. Interestingly, endothelial permeability was significantly decreased in ADAM17^{ex/ex} mice 6 h after TC injection compared to WT mice, pointing to an essential role of ADAM17 in TC transendothelial migration.

Increase in endothelial permeability during TC extravasation is facilitated by many different molecular mechanisms. It was shown that macrophages release EGF to attract TCs to the endothelium and TCs in turn recruit macrophages to the endothelium by release of CCL2 [90, 107]. Macrophages subsequently release VEGF-A, which enhances endothelial permeability by activation of focal adhesion tyrosine kinase, which in turn disrupts VE-cadherin/ β -catenin

binding leading to EC junction opening [107, 168]. Additionally, these recruited macrophages were shown to release TNF α , which (most probably) indirectly stimulates EC retraction by cytoskeleton modulation [169]. While these observations suggest a role for macrophages in transendothelial migration, we showed that transmigration of human MDA-MB231 TCs through a monolayer of HUVECs or HMVECs-L *in vitro* is impaired in the absence of ADAM17 in ECs (Figure 3.2), indicating an endothelial cell-intrinsic role of ADAM17. In line with this notion, TC extravasation was reduced not only in ADAM17^{ex/ex} mice, but also in mice with EC-specific ADAM17 deficiency (Figure 3.1). In conclusion, we revealed a central role for endothelial ADAM17 in TC extravasation by enhancing endothelial barrier permeability and therefore facilitating transendothelial migration.

EC retraction as well as disruption of tight junctions are critical for TC transendothelial migration. Many ADAMs have been associated with cleavage of junction proteins [170]. We assessed shedding of two tight junction proteins 6 h after TC injection in ADAM17^{ex/ex} mice and mice with EC-specific ADAM17 deficiency, but did not detect any reduction in soluble JAM-A or VE-cadherin levels (Figure 3.8). Considering this result, it becomes evident, that other proteases might mediate tight junction opening rather than ADAM17. Therefore, modulation of endothelial barrier function by ADAM17 is not dependent on the shedding of tight junction proteins by ADAM17 itself.

Wolf and colleagues demonstrated that CCL2 directly enhances vascular permeability [106]. It was reported that LLC cells and macrophages release CCL2 in the circulation [107]. CCL2 binds to the GPCR CCR2, which via G protein $q_{11}\alpha$ induces an increase in intracellular Ca²⁺ concentration and activation of PKC β (see Chapter 1.1.4). The classical isoform PKC β is overexpressed in several cancers, which correlates with reduced survival of patients [171]. In cell culture experiments PKC β can be activated upon VEGF stimulation of bovine aortic endothelial cells [172]. Moreover, Wallace et al. showed that stromal PKC β promotes tumorigenesis in a genetic breast cancer mouse model [173]. Additionally, it was shown that stromal PKC β is indispensable for the progression of chronic lymphocytic leukemia [174]. Since it was reported that ADAM17 can be activated by PKCs [39], we assessed PKC β activation upon CCL2 binding to ECs in our metastasis model. Previous work in our lab demonstrated phosphorylation of PKC β and not PKC α upon stimulation of murine brain endothelial cells with CCL2. Moreover, CCL2 stimulation of those cells enhanced surface-bound ADAM17 activity, which could be decreased by specific inhibition of PKC β with Enzastaurin (bachelor theses of C. Borowski and L. Neukirch). We observed phosphorylation of PKC β in WT mice upon TC injection (Figure 3.6), further

indicating an activation of ADAM17 by PKC β upon CCL2-release by TCs. Consequently, PKC β ^{-/-} mice showed reduced TC numbers in the lung 6 h after TC injection and were protected from metastases formation 3 weeks after TC injection (Figure 3.7). We therefore conclude that CCL2 enhances EC permeability via a CCR2/PKC β /ADAM17 axis. However, we can not rule out that other mechanisms activate ADAM17 in ECs during TC extravasation. The study by Wolf and colleagues additionally observed phosphorylation of p38 and activation of JAK2-STAT5 pathway upon CCR2 stimulation on ECs. Since p38 is also able to activate ADAM17 by phosphorylation, this further suggests that besides PKC β there are other regulators of ADAM17 activity involved in metastasis. Taken together, we showed an essential role for PKC β and ADAM17 in ECs in TC transendothelial migration. TC- and macrophage-derived CCL2 binds to CCR2 on ECs, which via G_{q/11} α activates PKC β . Subsequently, PKC β phosphorylates ADAM17, which leads to enhanced endothelial permeability and successful TC extravasation (Figure 4.1).

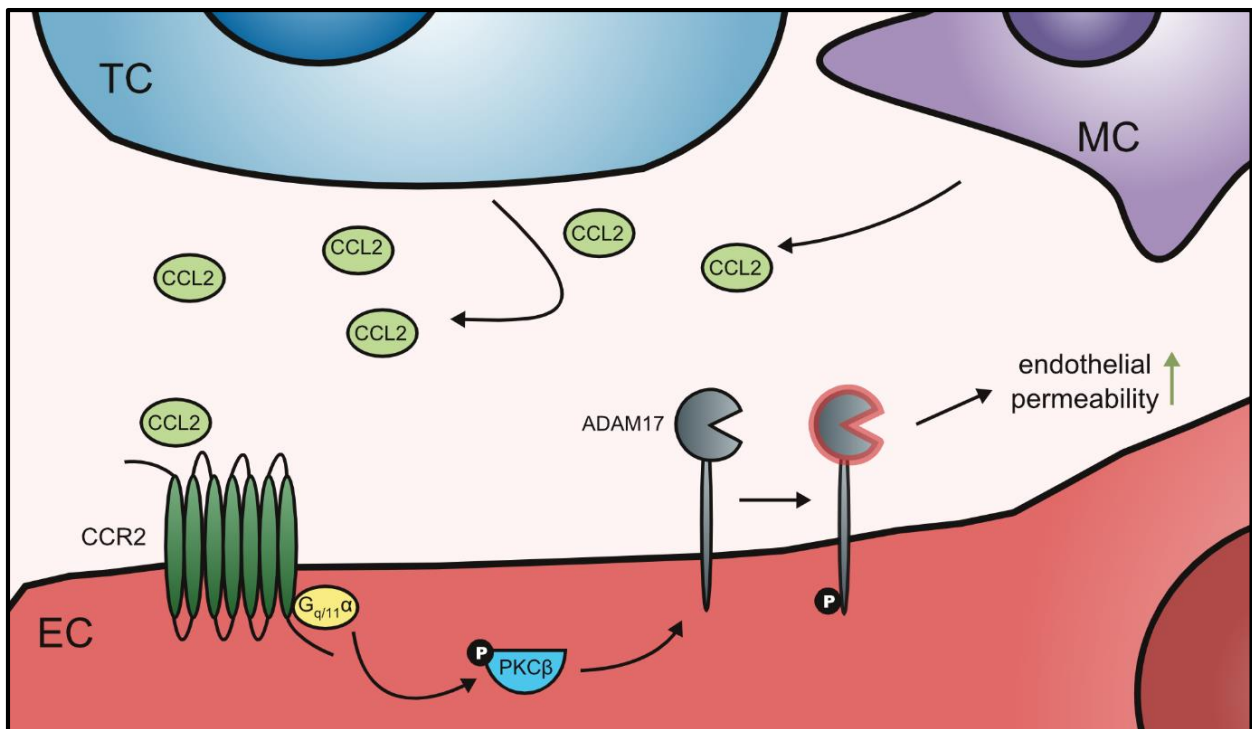


Figure 4.1: Activation of ADAM17 by PKC β on ECs in response to TC-derived CCL2. TCs and macrophages release CCL2, which binds to CCR2, a GPCR. This leads via G_{q/11} α and phospholipase C to activation of PKC β , which in turn phosphorylates and thereby activates ADAM17. Activated ADAM17 on ECs subsequently cleaves its substrates, leading to impaired extravasation of the TC. TC = Tumor cell, MC = Macrophage, EC = Endothelial cell.

4.2 Regulation of cell death by ADAM17

Cell death gained more and more attention in cancer research over the last years. However, studies mainly focused on how to restore cell death susceptibility of TCs. Recently, Strilic et al. revealed an important role of necroptosis in the microenvironment for TC extravasation. They demonstrated that TCs actively induce necroptosis in ECs, which leads to disruption of the endothelial barrier (Chapter 1.2.3) [110].

We therefore hypothesized that the loss of ADAM17 in ECs protects from TC-induced necroptosis and thereby from induction of endothelial permeability and extravasation. Indeed, we observed reduced necroptosis in ADAM17-deficient ECs in the presence of TCs *in vitro* (Figure 3.9). In accordance with the observations of Strilic et al. we also detected necroptotic ECs in WT mice 6 h after TC injection (Figure 3.11). The number of necroptotic ECs was drastically reduced in ADAM17^{ex/ex} mice and mice with EC-specific ADAM17 deficiency (Figure 3.12). These results clearly link endothelial ADAM17 to TC-induced EC necroptosis in TC extravasation.

Strilic and colleagues reported that necroptosis is induced by membrane-bound APP of TCs binding to DR6 on ECs [110]. We demonstrated that cell death induction by membrane-bound APP is dependent on ADAM17 (Figure 3.15, Figure 3.16). Moreover we identified DR6 as novel substrate for ADAM17 (Figure 3.15), indicating a general role of ADAM17 in DR6-induced necroptosis.

In our experiments, complete induction of APP-DR6 induced necroptosis was dependent on TNF-R1, since we detected reduced necroptosis in HUVECs with TNF-R1 suppression that were stimulated with membrane-bound APP (Figure 3.16). It is conceivable that upon APP-induced necroptosis TNF α is released from dying cells, which in turn amplifies cell death by stimulating TNF-R1. We investigated the importance of TNF α -TNF-R1 induced EC necroptosis *in vivo* by treatment of WT mice with Etanercept and showed that blocking of TNF α significantly reduced EC necroptosis (Figure 3.25). Consequently, TC extravasation was also impaired in the absence of TNF-R1 in mice (Figure 3.24). In conclusion, we here report TNF α -TNF-R1 induced EC necroptosis to be crucial for TC extravasation.

Since both, TNF α and TNF-R1 can be processed by ADAM17, we reasoned that TNF-R1-induced necroptosis is also dependent on ADAM17. We observed reduced EC apoptosis as well as necroptosis induced by TNF α or TNF α and zVAD, respectively in the absence of endothelial ADAM17 (Figure 3.18). We thereby confirmed that ADAM17 is a general regulator of cell death induced by APP-DR6 and TNF α -TNF-R1 in ECs.

Under physiological conditions TNF α stimulation usually leads to fast formation of complex I, NF- κ B activation and cell survival (Chapter 1.3.1). However, prolonged TNF α stimulation as well as additional stimuli may lead to assembly of cytosolic complex II and cell death via apoptosis or necroptosis (Chapter 1.3.2). We investigated TNF-R1 complex formation in the absence of ADAM17 and demonstrated that TNF-R1 complex II formation is strongly impaired in ADAM17^{ex/ex} MEFs. While we observed formation of both, complex IIa, as indicated by ubiquitinated RIPK1 and cleaved caspase-8, and complex IIb, as indicated by autophosphorylated RIPK1 and recruitment of RIPK3 in WT MEFs, TNF-R1 complex II assembly is absent in ADAM17^{ex/ex} MEFs. Since we did not observe recruitment of RIPK3 to complex IIb, we consequently did not detect any phosphorylation of MLKL in ADAM17^{ex/ex} MEFs (Figure 3.23), which is needed for execution of necroptosis [121]. These results further confirm our hypothesis that ADAM17 is necessary for TNF α -TNF-R1-induced cell death. In the absence of ADAM17 neither TNF-R1 complex IIa, nor IIb is formed which confers resistance to cell death.

Interestingly, we neither detected RIPK3 in complex II nor in whole cell lysates of ADAM17^{ex/ex} MEFs, emphasizing a regulation of *Ripk3* expression in the absence of ADAM17. Whether *Ripk3* expression is regulated in an ADAM17-dependent manner is so far unclear. It was shown that transcription of *Ripk3* can be controlled by DNA hypermethylation of its promoter [175]. In TCs expression of *Ripk3* was linked to the activation of the transcription factor Sp1 [176]. Interestingly, Benjamin and colleagues reported that activation of NF- κ B leads to Sp3-dependent suppression of Sp1 activation [177]. This suggests that NF- κ B activation decreases *Ripk3* transcription. We reasoned that in the absence of ADAM17 NF- κ B activation by enhanced TNF-R1 complex I formation is increased. Interestingly, we indeed observed constitutive phosphorylation of I κ B α in ADAM17^{ex/ex} MEFs in the absence of exogenous TNF α (Figure 3.20). Phosphorylation of I κ B α by IKK β leads to its degradation, whereby NF- κ B is released (Chapter 1.3.1). Inhibition of IKK β by TPCA-1 in HUVECs with siRNA-mediated suppression of ADAM17 sensitized the cells to TNF α -induced necroptosis (Figure 3.18), indicating constitutive activation of NF- κ B in the absence of ADAM17. These results further emphasize that in the absence of ADAM17, formation of TNF-R1 complex I, which leads to cell survival by NF- κ B activation, is enhanced. We therefore investigated composition of TNF-R1 complex I in ADAM17^{ex/ex} MEFs. Surprisingly, we neither detected receptor proximal proteins, like the adaptor protein TRADD, nor recruitment of cIAPs and HOIP, the central catalytic protein of the LUBAC complex. Consequently, RIPK1 ubiquitination, usually facilitated by the LUBAC complex, was strongly decreased in ADAM17^{ex/ex} MEFs compared to WT MEFs (Figure 3.21). In conclusion, TNF-R1

complex I formation upon stimulation with exogenous TNF α was impaired although we detected constitutive NF- κ B activation.

Since we showed that in the absence of ADAM17 neither TNF-R1 complex I nor complex II is formed, i.e. TNF-R1 signaling *per se* is impaired, we investigated whether cleavage of cell innate TNF α or TNF-R1 by ADAM17 is a prerequisite for TNF-R1 signaling.

On the one hand, Chhibber-Goel and colleagues proposed a model, in which TNF-R1 ectodomain cleavage by ADAM17, internalization and intramembrane proteolysis by γ -secretase is a prerequisite for TNF α -induced apoptosis via TNF-R1 complex I formation [162]. Therefore, we hypothesized that in the absence of ADAM17 lack of TNF-R1 cleavage impairs TNF-R1 complex IIa and b formation. The protease activity of the γ -secretase complex is facilitated by the subunits PSEN1 and 2, which is why we used PSEN1^{+/-}/2^{-/-} MEFs to prove our hypothesis. We observed that MEFs of PSEN1^{+/-}/2^{-/-} mice (Chapter 3.5) are partially protected from TNF α -induced apoptosis as well as necroptosis (Figure 3.19), which further suggests that cleavage of TNF-R1 by ADAM17 is a prerequisite for TNF-R1 internalization, γ -secretase cleavage, complex I dissociation and TNF-R1 complex II formation. We also found reduced soluble TNF-R1 levels in the absence ADAM17 *in vitro* and *in vivo* in the presence of TCs (Figure 3.17), supporting this hypothesis. However, a direct proof that ADAM17-mediated cleavage of TNF-R1 is a prerequisite for TNF α -induced cell death is still lacking. To this end, we will generate cleavage resistant mutants of TNF-R1 that were previously described elsewhere [178] and measure TNF α -induced cell death as well as investigate TNF-R1 complex formation.

On the other hand, it was shown that apart from TNF-R1, TNF-R2 signaling upon TNF α binding leads to activation of IKK β , subsequent phosphorylation of I κ B α and NF- κ B activation via the non-canonical pathway. Additionally, upon NF- κ B activation, anti-apoptotic genes are upregulated [129]. These include cIAP1/2, which stabilize TNF-R1 complex I and cFLIP, which counteracts cleavage of caspase-8 in TNF-R1 complex II [179]. It is known, that NF- κ B also upregulates TNF α expression, in a positive feedback loop [180]. TNF-R2 has a higher affinity to membrane-bound TNF α than to its soluble form. Preliminary data of our group indicate slightly increased levels of membrane-bound TNF α on the cell surface of ADAM17^{ex/ex} MEFs (data not shown). This suggests that in the absence of ADAM17 increased expression of membrane-bound TNF α activates TNF-R2 *in cis*, leading to TNF-R1-independent activation of NF- κ B. Interestingly, it was shown that stimulation of TNF-R2 by membrane-bound TNF α attenuates the cytotoxicity of soluble TNF α on two breast cancer cell lines [181, 182]. Moreover, Nicolaou and colleagues reported increased membrane-bound TNF α and TNF-R2 levels in plasma and on bone-marrow

derived macrophages of ADAM17^{ex/ex} mice in a genetic mouse model of atherosclerosis [41]. This led to constitutive TNF-R2 signaling and reduced apoptosis. Since we detected I κ B α phosphorylation even in the absence of exogenous, soluble TNF α in ADAM17^{ex/ex} MEFs, we propose that in the absence of ADAM17, binding of membrane-bound TNF α to TNF-R2 leads to cell preconditioning, which counteracts soluble TNF α -induced cell death via TNF-R1 (Figure 4.2).

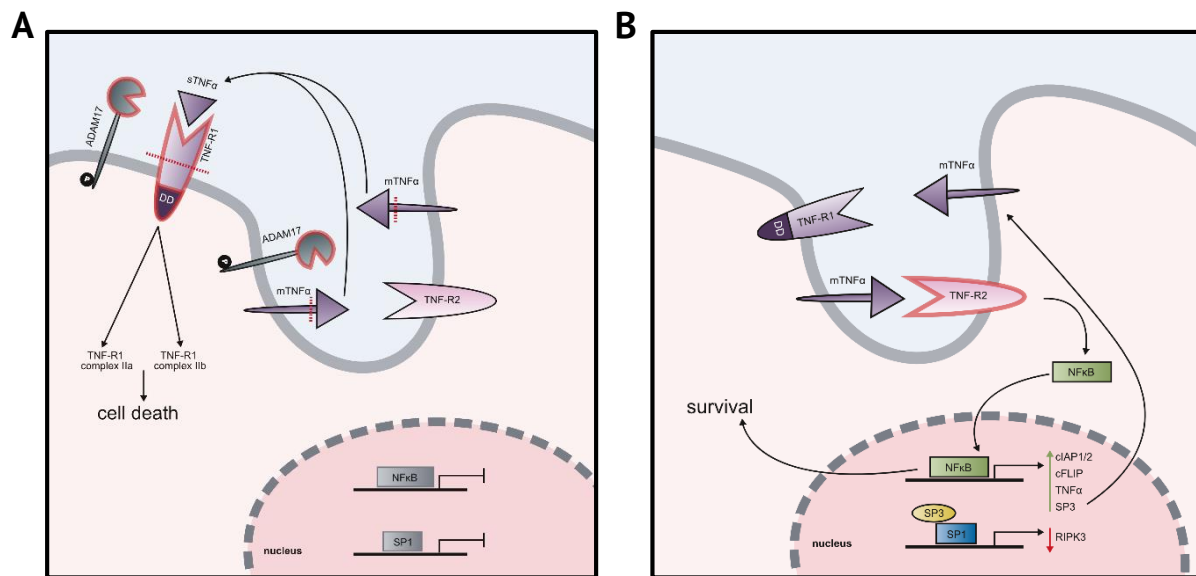


Figure 4.2: Regulation of cell death by ADAM17. A: In the presence of activated ADAM17, membrane-bound TNF α is cleaved. Soluble TNF α activates TNF-R1, leading to formation of TNF-R1 complex IIa and complex IIb. Subsequently, cell death is initiated. **B:** In the absence of ADAM17 or when its activity is inhibited, TNF α remains membrane-bound and activates TNF-R2, predominantly. TNF-R2 signaling leads to NF- κ B activation and upregulation of several anti-apoptotic genes, SP3 as well as TNF α itself. SP3 induces SP1-dependent downregulation of RIPK3. The cell survives, as TNF-R1 cytotoxic signaling is inhibited. Red halo indicates activity. Red, dashed line indicates shedding by ADAM17.

Since we suggested that PKC β activates ADAM17 upon TC-derived CCL2 activation of ECs, we reasoned that PKC β is important for TC-induced necroptosis as well. In line with our finding that PKC β activates ADAM17 in ECs during TC extravasation, we also detected reduced EC necroptosis *in vitro* and *in vivo* in the absence of PKC β (Figure 3.9, Figure 3.13), further emphasizing a role for PKC β in activating ADAM17 during TC-induced EC necroptosis.

In a recent study, Cai and colleagues suggested a role of ADAMs for the execution of necroptosis. They report activation of ADAM proteases by phosphorylated MLKL leading to substrate shedding and subsequent cell death [183]. Moreover, while PS-exposure is considered a hallmark of apoptotic cell death, leading to phagocytosis of dying cells, Gong et al. recently also observed PS-exposure of necroptotic cells [143]. Since PS-exposure to the cell surface activates ADAM17 (Chapter 1.1.4), this indicates that apoptosis as well as necroptosis enhance ADAM17 activity. Considering both publications, we cannot rule out, that ADAM17 activity is further enhanced in

the final steps of cell death, which might execute cell death or represent a feedback loop by extensive TNF α shedding.

4.3 Function of ADAM17 during tumor cell seeding

4.3.1 ADAM17 on immune cells in tumor growth

Inflammation is strongly associated with tumor development and progression. Infiltrating immune cells release cytokines, chemokines and growth factors that contribute to TC migration, survival and proliferation. We detected a time dependent increase in inflammation of lung tissue in WT mice after TC injection, but not in ADAM17^{ex/ex} mice (Figure 3.26A). In line, we observed less infiltrated myeloid cells, i.e. macrophages and granulocytes in tumor tissue of ADAM17^{ex/ex} mice 3 weeks after TC injection (Figure 3.26B). Since the release of inflammatory cytokines, like TNF α , from the surface of immune cells is mediated by ADAM17, we reasoned that ADAM17 on immune cells promotes tumor progression by shaping an inflammatory microenvironment. However, ADAM17 deficiency on myeloid cells did not protect the mice from tumor formation in the lung 3 weeks after TC injection (Figure 3.27). In conclusion, ADAM17 on macrophages and granulocytes is dispensable for TC metastasis. Whether ADAM17 on myeloid cells has an impact on inflammation in response to TC injection as well as in TC extravasation has yet to be proven. Moreover, there is controversial discussion about the specificity and efficiency of the LysM-Cre-driver that we used for targeting myeloid cells. It was shown that apart from granulocytes, monocytes and macrophages, lung alveolar cells are LysM⁺ [184]. Additionally, it remains unclear, whether both, peripheral blood and tissue resident myeloid cells are targeted. In a comparative study of different Cre-driver, Abram et al. demonstrated that while spleen, alveolar and peritoneal macrophages are targeted by LysM-Cre, peripheral blood macrophages are not [185]. Therefore, we would have to demonstrate ADAM17-depletion on peripheral blood macrophages and granulocytes in ADAM17 ^{Δ MC/ Δ MC} mice.

The adaptive immune system is as important as the innate immune system for the intensity and duration of an immune response. T cells are part of the adaptive immune system and are divided in several subsets, including T helper 1, T helper 2, T helper 17, Tregs and natural killer T cells. Differentiation of naive CD4⁺ cells is mainly dependent on cytokine composition of the microenvironment. CD4⁺ T cells have critical roles in the immune system, ranging from B cell and innate immune cell activation to suppression of immune reactions [186]. It was shown that tumor-associated CD4⁺ Tregs suppress activation of cytotoxic T cells, thereby exhibit

immunosuppressive functions [187]. Depletion of Tregs resulted in anti-tumor activity of CD8⁺ T cells. In a mouse model of breast cancer, T helper 17 cells were demonstrated to promote tumor growth by mediating angiogenesis [188]. These studies suggest a pro-tumorigenic function of CD4⁺ T cells. ADAM17 deficiency on CD4⁺ T cells was already investigated in a model of *Listeria monocytogenes* infection. While the authors detected less shedding of ADAM17 substrates, like TNF-R1, TNF-R2, TNF α and IL-6R, they did not find changes in T cell subsets. Mice with ADAM17 deficiency on CD4⁺ T cells were still able to clear primary and secondary *Listeria monocytogenes* infections [150]. ADAM17 on T cells in the context of metastasis has not been investigated yet. Here, we showed that mice with ADAM17 deficiency on CD4⁺ T cells are strongly protected from tumor formation 3 weeks after TCs injection (Figure 3.28). We therefore conclude that ADAM17 on CD4⁺ T cells promotes TC seeding. The detailed molecular mechanism behind this observation remains elusive and has to be investigated further.

4.3.2 Tumor cell proliferation mediated by ADAM17

Mice deficient for TIMP3, a physiological inhibitor of ADAM17 (Chapter 1.1.4), show increased tumor growth and angiogenesis in a subcutaneous melanoma model [189]. This proposes that ADAM17 in the microenvironment might promote TC seeding.

While we noticed that the number of LLC cell cluster in lungs of WT mice increased from 6 h to 20 h after injection, the number of TC cluster did not change in ADAM17^{ex/ex} mice (Figure 3.1). This suggests that whereas TCs in WT mice already started to proliferate 20 h after LLC cell injection, they do not in ADAM17^{ex/ex} mice. In line with these findings, we detected less proliferating cells in tumor tissue in ADAM17^{ex/ex} mice 3 weeks after LLC injection (Figure 3.29). These results suggest that microenvironmental ADAM17 not only promotes TC extravasation, but also mediates LLC cell outgrowth and proliferation. Interestingly, Lu and colleagues showed the release of soluble jagged-1 by ADAM17 from the surface of ECs, which leads to activation of Notch1 in a paracrine manner on colorectal cancer cells. Notch1 ICD functions as transcription factor and changes gene expression patterns that promote a CSC phenotype [190]. CSCs are believed to initiate and sustain tumor growth. Moreover, jagged-1-dependent activation of Notch1 is associated with metastasis, proliferation and inhibition of apoptosis of TCs [26]. Interestingly, Notch1 signaling was also described to crosstalk with other signaling pathways, like MAPK/AKT and NF- κ B pathway [191, 192]. The exact mechanism by which these pathways interact is cell and stimulus dependent.

We therefore investigated Notch activation in LLC and B16F1 cells. While we observed Notch1

activation by membrane-bound jagged-1 in LLC cells, B16F1 cells showed ligand-independent Notch1 activation, which was not further increased upon jagged-1 stimulation (Figure 3.30B,C). Consequently, we detected an increase of mRNA levels of the Notch1 target gene *Hes-1* in jagged-1 stimulated LLC cells, but no changes in mRNA levels in B16F1 cells (Figure 3.30D). Auto-activation of Notch receptors has been noticed before and is mainly triggered by trafficking of the receptor [193]. We concluded that while LLC cells are responsive to Notch1 ligands, B16F1 cells are not.

The aggressive phenotype of Notch-activated TCs is attributed to EMT. A marker for EMT is the upregulation of several proteins like Vimentin, TWIST1 and collagen VI, which are associated with a mesenchymal phenotype. Furthermore, receptor tyrosine kinase *Axl* was shown to be upregulated upon Notch1-induced EMT [194-196]. We investigated EMT in jagged-1 stimulated LLC and B16F1 cells by mRNA levels of *Vim*, *Twist1*, *Col6a1* and *Axl*. Indeed, we observed an increase in mRNA levels of these proteins in LLC cells stimulated with jagged-1. We did not detect changes in B16F1 cells, further proving that B16F1 cells exhibit constitutive Notch signaling and EMT. In conclusion, ADAM17 might participate in LLC tumor progression by liberating the Notch1 ligand jagged-1 from the cell surface of ECs. Notch1 signaling in LLC cells leads to EMT, which promotes migration, survival and progression. B16F1 cells are independent of Notch1 ligands for undergoing EMT. A direct link between ADAM17 deficiency and TC EMT *in vivo* has yet to be demonstrated.

4.4 ADAM17 as clinical target in cancer therapy

ADAM-mediated shedding has been associated with several pathologies. Especially ADAM17-mediated release of TNF α was shown to play a crucial role in inflammatory disease, like sepsis, rheumatoid arthritis and inflammatory bowel disease [26]. Therefore, specific inhibition of ADAM17 seems to be a promising treatment option. Unfortunately, due to low specificity and side effects many of the so far developed inhibitors did not reach the clinics.

Recently, Wong et al. succeeded in producing an inhibitor of ADAM17 [6]. ADAM17 is synthesized as zymogen, i.e. with an inhibitory prodomain, that blocks the catalytic domain. Usually the prodomain is cleaved off on the secretory pathway by protein convertases, like furin. In their study Wong and colleagues recombinantly produced this ADAM17-PD and showed specific inhibition of cell surface ADAM17 with an IC₅₀ of 145 nM by binding to the catalytic domain. Considering that ADAM17 deficiency in our mouse model protected from TC extravasation, we hypothesized that treatment with the ADAM17-PD would reduce metastases

formation in WT mice. Single dose i.v. injection of ADAM17-PD or TAPI-1, a broad metalloprotease inhibitor, reduced TC extravasation and TC-induced EC necroptosis by 50 % in WT mice (Figure 3.32). Moreover, ADAM17-PD inhibited tumor formation after 3 weeks by 90 % (Figure 3.33). Both results clearly resemble the impact of ADAM17 deficiency on ECs on TC extravasation and metastasis. We therefore conclude that the *in vivo* inhibition of ADAM17 by single administration of ADAM17-PD is highly protective against metastases formation in the lung. Furthermore, these experiments suggest that catalytic activity of ADAM17 is important for TC-induced EC necroptosis. Whether administration of ADAM17-PD has any side effects has to be tested in further experiments. Moreover, further characterization of bioavailability and efficiency in other metastasis models is needed.

Since we showed that ADAM17 is activated by PKC β upon TC-mediated CCL2 release, we reasoned that selective inhibition of PKC β might also reduce TC extravasation and metastasis. Treatment of WT mice with the selective PKC β inhibitor Enzastaurin reduced EC cell death by 40 %, thereby TC extravasation (Figure 3.14). Clinical studies on the treatment of solid tumors with Enzastaurin unfortunately failed, since it did not show the expected effects [197]. However, we identified Enzastaurin as promising inhibitor of TC metastasis by indirectly inhibiting ADAM17 activity. ADAM17-PD and Enzastaurin seem to be promising inhibitors of metastasis and might be used as adjuvant therapy in clinics before/while primary tumor resection, which is known to be a risk of metastasis in patients [198].

4.5 Conclusion

Our study shows for the first time an indispensable role of ADAM17 in metastasis. We demonstrate that ADAM17 enhances EC permeability and TC extravasation by mediating TC-induced necroptosis in ECs. Moreover, we identify ADAM17 as major regulator of TNF-R1 induced cell death in general. Additionally, we demonstrate activation of ADAM17 by TC-derived CCL2 via PKC β in ECs and present Enzastaurin and ADAM17-PD as potent inhibitors for TC extravasation and metastasis (Figure 4.3). We are confident that we identified ADAM17 as key player of metastasis and as promising therapeutic target.

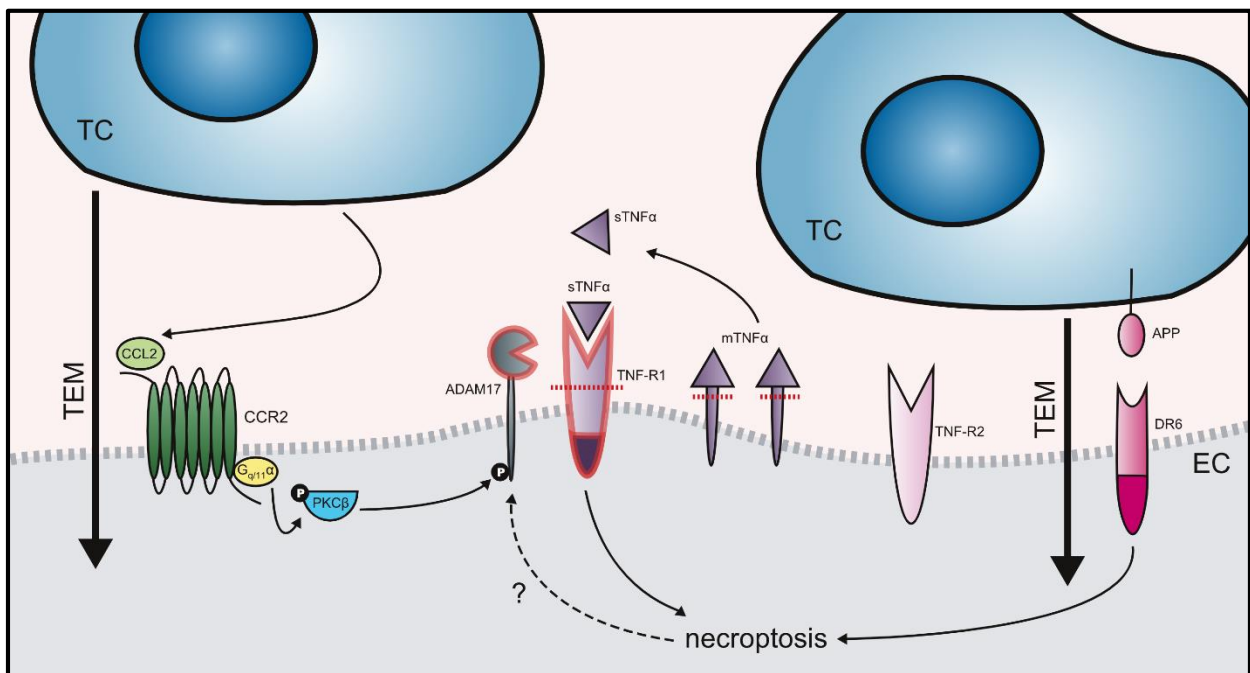


Figure 4.3: Endothelial ADAM17 in the metastatic niche. Upon binding of APP of TCs to DR6 on the EC, necroptosis is initiated, which probably activates ADAM17. Additionally, TC-derived CCL2 activates ADAM17 by CCR2-dependent phosphorylation of PKC β via Gq/11 α . ADAM17 liberates membrane-bound TNF α . Thereby shifting the balance between TNF-R1 and TNF-R2 signaling towards TNF-R1, which amplifies DR6-induced necroptosis. ADAM17-mediated cleavage of TNF-R1 is a prerequisite for cell death downstream of TNF-R1. Necroptosis of the EC leads to the release of DAMPs and enhanced permeability of the endothelial barrier, finally leading to TC transendothelial migration. Red outlines indicate activity. Red, dashed lines indicate shedding by ADAM17. EC = Endothelial cell, TC = Tumor cell, TEM = transendothelial migration.

5 References

1. **Seals, D.F. & Courtneidge, S.A.** The ADAMs family of metalloproteases: multidomain proteins with multiple functions. *Genes Dev.* 17, 7-30 (2003).
2. **Edwards, D.R., Handsley, M.M. & Pennington, C.J.** The ADAM metalloproteinases. *Mol. Aspects Med.* 29, 258-89 (2008).
3. **Milla, M.E., Leesnitzer, M.A., Moss, M.L., Clay, W.C., Carter, H.L., Miller, A.B., Su, J.L., Lambert, M.H., Willard, D.H., Sheeley, D.M., Kost, T.A., Burkhart, W., Moyer, M., Blackburn, R.K., Pahel, G.L., Mitchell, J.L., Hoffman, C.R. & Becherer, J.D.** Specific sequence elements are required for the expression of functional tumor necrosis factor-alpha-converting enzyme (TACE). *J. Biol. Chem.* 274, 30563-70 (1999).
4. **Schlomann, U., Wildeboer, D., Webster, A., Antropova, O., Zeuschner, D., Knight, C.G., Docherty, A.J., Lambert, M., Skelton, L., Jockusch, H. & Bartsch, J.W.** The metalloprotease disintegrin ADAM8. Processing by autocatalysis is required for proteolytic activity and cell adhesion. *J. Biol. Chem.* 277, 48210-9 (2002).
5. **Howard, L., Maciewicz, R.A. & Blobel, C.P.** Cloning and characterization of ADAM28: evidence for autocatalytic pro-domain removal and for cell surface localization of mature ADAM28. *Biochem. J.* 348, 21-7 (2000).
6. **Wong, E., Cohen, T., Romi, E., Levin, M., Peleg, Y., Arad, U., Yaron, A., Milla, M.E. & Sagi, I.** Harnessing the natural inhibitory domain to control TNFalpha Converting Enzyme (TACE) activity in vivo. *Sci. Rep.* 6, 35598 (2016).
7. **White, J.M.** ADAMs: modulators of cell-cell and cell-matrix interactions. *Curr. Opin. Cell Biol.* 15, 598-606 (2003).
8. **Bax, D.V., Messent, A.J., Tart, J., van Hoang, M., Kott, J., Maciewicz, R.A. & Humphries, M.J.** Integrin alpha5beta1 and ADAM-17 interact in vitro and co-localize in migrating HeLa cells. *J. Biol. Chem.* 279, 22377-86 (2004).
9. **Thodeti, C.K., Albrechtsen, R., Grauslund, M., Asmar, M., Larsson, C., Takada, Y., Mercurio, A.M., Couchman, J.R. & Wewer, U.M.** ADAM12/syndecan-4 signaling promotes beta 1 integrin-dependent cell spreading through protein kinase Calpha and RhoA. *J. Biol. Chem.* 278, 9576-84 (2003).
10. **Lorenzen, I., Lokau, J., Düsterhöft, S., Trad, A., Garbers, C., Scheller, J., Rose-John, S. & Grötzinger, J.** The membrane-proximal domain of A Disintegrin and Metalloprotease 17 (ADAM17) is responsible for recognition of the interleukin-6 receptor and interleukin-1 receptor II. *FEBS Lett.* 586, 1093-100 (2012).
11. **Düsterhöft, S., Jung, S., Hung, C.W., Tholey, A., Sonnichsen, F.D., Grötzinger, J. & Lorenzen, I.** Membrane-proximal domain of a disintegrin and metalloprotease-17 represents the putative molecular switch of its shedding activity operated by protein-disulfide isomerase. *J. Am. Chem. Soc.* 135, 5776-81 (2013).

12. **Jones, J.C., Rustagi, S. & Dempsey, P.J.** ADAM Proteases and Gastrointestinal Function. *Annu. Rev. Physiol.* 78, 243-76 (2016).
13. **Alfandari, D., Cousin, H., Gaultier, A., Smith, K., White, J.M., Darribere, T. & DeSimone, D.W.** Xenopus ADAM 13 is a metalloprotease required for cranial neural crest-cell migration. *Curr. Biol.* 11, 918-30 (2001).
14. **Zack, M.D., Malfait, A.M., Skepner, A.P., Yates, M.P., Griggs, D.W., Hall, T., Hills, R.L., Alston, J.T., Nemirovskiy, O.V., Radabaugh, M.R., Leone, J.W., Arner, E.C. & Tortorella, M.D.** ADAM-8 isolated from human osteoarthritic chondrocytes cleaves fibronectin at Ala(271). *Arthritis Rheum.* 60, 2704-13 (2009).
15. **Millichip, M.I., Dallas, D.J., Wu, E., Dale, S. & McKie, N.** The metallo-disintegrin ADAM10 (MADM) from bovine kidney has type IV collagenase activity in vitro. *Biochem. Biophys. Res. Commun.* 245, 594-8 (1998).
16. **Rose-John, S. & Heinrich, P.C.** Soluble receptors for cytokines and growth factors: generation and biological function. *Biochem. J.* 300, 281-90 (1994).
17. **Lokau, J., Nitz, R., Agthe, M., Monhasery, N., Aparicio-Siegmund, S., Schumacher, N., Wolf, J., Moller-Hackbarth, K., Waetzig, G.H., Grötzinger, J., Muller-Newen, G., Rose-John, S., Scheller, J. & Garbers, C.** Proteolytic Cleavage Governs Interleukin-11 Trans-signaling. *Cell Rep.* 14, 1761-73 (2016).
18. **Bergmann, J., Müller, M., Baumann, N., Reichert, M., Heneweer, C., Bolik, J., Lücke, K., Gruber, S., Carambia, A., Boretius, S., Leuschner, I., Becker, T., Rabe, B., Herkel, J., Wunderlich, F.T., Mittrücker, H.W., Rose-John, S. & Schmidt-Arras, D.** IL-6 trans-signaling is essential for the development of hepatocellular carcinoma in mice. *Hepatology* 65, 89-103 (2017).
19. **Kramer, H.** RIPping notch apart: a new role for endocytosis in signal transduction?. *Sci. STKE* 2000, pe1 (2000).
20. **Mumm, J.S. & Kopan, R.** Notch Signaling: From the Outside In. *Dev. Biol.* 228, 151-65 (2000).
21. **Hartmann, D., de Strooper, B., Serneels, L., Craessaerts, K., Herreman, A., Annaert, W., Umans, L., Lubke, T., Lena Illert, A., von Figura, K. & Saftig, P.** The disintegrin/metalloprotease ADAM 10 is essential for Notch signalling but not for alpha-secretase activity in fibroblasts. *Hum. Mol. Genet.* 11, 2615-24 (2002).
22. **Lammich, S., Kojro, E., Postina, R., Gilbert, S., Pfeiffer, R., Jasionowski, M., Haass, C. & Fahrenholz, F.** Constitutive and regulated alpha-secretase cleavage of Alzheimer's amyloid precursor protein by a disintegrin metalloprotease. *Proc. Natl. Acad. Sci. USA.* 96, 3922-7 (1999).
23. **Hardy, J. & Selkoe, D.J.** The amyloid hypothesis of Alzheimer's disease: progress and problems on the road to therapeutics. *Science* 297, 353-6 (2002).

24. **Black, R.A., Rauch, C.T., Kozlosky, C.J., Peschon, J.J., Slack, J.L., Wolfson, M.F., Castner, B.J., Stocking, K.L., Reddy, P., Srinivasan, S., Nelson, N., Boiani, N., Schooley, K.A., Gerhart, M., Davis, R., Fitzner, J.N., Johnson, R.S., Paxton, R.J., March, C.J. & Cerretti, D.P.** A metalloproteinase disintegrin that releases tumour-necrosis factor-alpha from cells. *Nature* 385, 729-33 (1997).
25. **Stelzer, G., Rosen, R., Plaschkes, I., Zimmerman, S., Twik, M., Fishilevich, S., Iny Stein, T., Nudel, R., Lieder, I., Mazor, Y., Kaplan, S., Dahary, D., Warshawsky, D., Guan - Golan, Y., Kohn, A., Rappaport, N., Safran, M. & Lancet, D.** The GeneCards Suite: From Gene Data Mining to Disease Genome Sequence Analysis. *Curr. Protoc. Bioinformatics* 54, 1.30.1-1.30.33 (2016).
26. **Moss, M.L. & Minond, D.** Recent Advances in ADAM17 Research: A Promising Target for Cancer and Inflammation. *Mediators Inflamm.* 2017, 9673537 (2017).
27. **Gooz, M.** ADAM-17: the enzyme that does it all. *Crit. Rev. Biochem. Mol. Biol.* 45, 146-69 (2010).
28. **Horiuchi, K., Kimura, T., Miyamoto, T., Takaiishi, H., Okada, Y., Toyama, Y. & Blobel, C.P.** Cutting edge: TNF-alpha-converting enzyme (TACE/ADAM17) inactivation in mouse myeloid cells prevents lethality from endotoxin shock. *J. Immunol.* 179, 2686-9 (2007).
29. **van Goor, H., Melenhorst, W.B., Turner, A.J. & Holgate, S.T.** Adamalysins in biology and disease. *J. Pathol.* 219, 277-86 (2009).
30. **Peschon, J.J., Slack, J.L., Reddy, P., Stocking, K.L., Sunnarborg, S.W., Lee, D.C., Russell, W.E., Castner, B.J., Johnson, R.S., Fitzner, J.N., Boyce, R.W., Nelson, N., Kozlosky, C.J., Wolfson, M.F., Rauch, C.T., Cerretti, D.P., Paxton, R.J., March, C.J. & Black, R.A.** An Essential Role for Ectodomain Shedding in Mammalian Development. *Science* 282, 1281-4 (1998).
31. **Reddy, P., Slack, J.L., Davis, R., Cerretti, D.P., Kozlosky, C.J., Blanton, R.A., Shows, D., Peschon, J.J. & Black, R.A.** Functional analysis of the domain structure of tumor necrosis factor-alpha converting enzyme. *J. Biol. Chem.* 275, 14608-14 (2000).
32. **Venturi, G.M., Tu, L., Kadono, T., Khan, A.I., Fujimoto, Y., Oshel, P., Bock, C.B., Miller, A.S., Albrecht, R.M., Kubes, P., Steeber, D.A. & Tedder, T.F.** Leukocyte migration is regulated by L-selectin endoproteolytic release. *Immunity* 19, 713-24 (2003).
33. **Farkas, L.M. & Krieglstein, K.** Heparin-binding epidermal growth factor-like growth factor (HB-EGF) regulates survival of midbrain dopaminergic neurons. *J. Neural Transm.* 109, 267-77 (2002).
34. **Geiger-Maor, A., Guedj, A., Even-Ram, S., Smith, Y., Galun, E. & Rachmilewitz, J.** Macrophages Regulate the Systemic Response to DNA Damage by a Cell Nonautonomous Mechanism. *Cancer Res.* 75, 2663-73 (2015).
35. **Miettinen, P.J., Berger, J.E., Meneses, J., Phung, Y., Pedersen, R.A., Werb, Z. & Derynck, R.** Epithelial immaturity and multiorgan failure in mice lacking epidermal growth factor receptor. *Nature* 376, 337-41 (1995).
36. **Sibilia, M. & Wagner, E.F.** Strain-dependent epithelial defects in mice lacking the EGF receptor. *Science* 269, 234-8 (1995).

37. **Threadgill, D.W., Dlugosz, A.A., Hansen, L.A., Tennenbaum, T., Lichti, U., Yee, D., LaMantia, C., Mourton, T., Herrup, K. & Harris, R.C.** Targeted disruption of mouse EGF receptor: effect of genetic background on mutant phenotype. *Science* 269, 230-4 (1995).
38. **Wilson, C.L., Gough, P.J., Chang, C.A., Chan, C.K., Frey, J.M., Liu, Y., Braun, K.R., Chin, M.T., Wight, T.N. & Raines, E.W.** Endothelial deletion of ADAM17 in mice results in defective remodeling of the semilunar valves and cardiac dysfunction in adults. *Mech. Dev.* 130, 272-89 (2013).
39. **Chalaris, A., Adam, N., Sina, C., Rosenstiel, P., Lehmann-Koch, J., Schirmacher, P., Hartmann, D., Cichy, J., Gavrilova, O., Schreiber, S., Jostock, T., Matthews, V., Häslner, R., Becker, C., Neurath, M.F., Reiß, K., Saftig, P., Scheller, J. & Rose-John, S.** Critical role of the disintegrin metalloprotease ADAM17 for intestinal inflammation and regeneration in mice. *J. Exp. Med.* 207, 1617-24 (2010).
40. **Kefaloyianni, E., Muthu, M.L., Kaeppler, J., Sun, X., Sabbisetti, V., Chalaris, A., Rose-John, S., Wong, E., Sagi, I., Waikar, S.S., Rennke, H., Humphreys, B.D., Bonventre, J.V. & Herrlich, A.** ADAM17 substrate release in proximal tubule drives kidney fibrosis. *JCI Insight* 1, 87023 (2016).
41. **Nicolaou, A., Zhao, Z., Northoff, B.H., Sass, K., Herbst, A., Kohlmaier, A., Chalaris, A., Wolfrum, C., Weber, C., Steffens, S., Rose-John, S., Teupser, D. & Holdt, L.M.** Adam17 Deficiency Promotes Atherosclerosis by Enhanced TNFR2 Signaling in Mice. *Arterioscler. Thromb. Vasc. Biol.* 37, 247-57 (2017).
42. **Schmidt, S., Schumacher, N., Schwarz, J., Tangermann, S., Kenner, L., Schlederer, M., Sibilica, M., Linder, M., Altendorf-Hofmann, A., Knosel, T., Gruber, E.S., Oberhuber, G., Bolik, J., Rehman, A., Sinha, A., Lokau, J., Arnold, P., Cabron, A.S., Zunke, F., Becker-Pauly, C., Preaudet, A., Nguyen, P., Huynh, J., Afshar-Sterle, S., Chand, A.L., Westermann, J., Dempsey, P.J., Garbers, C., Schmidt-Arras, D., Rosenstiel, P., Putoczki, T., Ernst, M. & Rose-John, S.** ADAM17 is required for EGF-R-induced intestinal tumors via IL-6 trans-signaling. *J. Exp. Med.* 215, 1205-25 (2018).
43. **Mochizuki, S. & Okada, Y.** ADAMs in cancer cell proliferation and progression. *Cancer Sci.* 98, 621-8 (2007).
44. **Sahin, U., Weskamp, G., Kelly, K., Zhou, H., Higashiyama, S., Peschon, J., Hartmann, D., Saftig, P. & Blobel, C.P.** Distinct roles for ADAM10 and ADAM17 in ectodomain shedding of six EGFR ligands. *J. Cell Biol.* 164, 769-79 (2004).
45. **Killock, D.J. & Ivetic, A.** The cytoplasmic domains of TNF α -converting enzyme (TACE/ADAM17) and L-selectin are regulated differently by p38 MAPK and PKC to promote ectodomain shedding. *Biochem. J.* 428, 293-304 (2010).
46. **Xu, P. & Derynck, R.** Direct activation of TACE-mediated ectodomain shedding by p38 MAP kinase regulates EGF receptor-dependent cell proliferation. *Mol. Cell* 37, 551-66 (2010).
47. **Miller, M.A., Meyer, A.S., Beste, M.T., Lasisi, Z., Reddy, S., Jeng, K.W., Chen, C.H., Han, J., Isaacson, K., Griffith, L.G. & Lauffenburger, D.A.** ADAM-10 and -17 regulate endometriotic cell migration via concerted ligand and receptor shedding feedback on kinase signaling. *Proc. Natl. Acad. Sci. USA.* 110, 2074-83 (2013).

48. **Soond, S.M., Everson, B., Riches, D.W. & Murphy, G.** ERK-mediated phosphorylation of Thr735 in TNF α -converting enzyme and its potential role in TACE protein trafficking. *J. Cell. Sci.* 118, 2371-80 (2005).
49. **Le Gall, S.M., Maretzky, T., Issuree, P.D., Niu, X.D., Reiss, K., Saftig, P., Khokha, R., Lundell, D. & Blobel, C.P.** ADAM17 is regulated by a rapid and reversible mechanism that controls access to its catalytic site. *J. Cell. Sci.* 123, 3913-22 (2010).
50. **Gschwind, A., Hart, S., Fischer, O.M. & Ullrich, A.** TACE cleavage of proamphiregulin regulates GPCR-induced proliferation and motility of cancer cells. *EMBO J.* 22, 2411-21 (2003).
51. **Prenzel, N., Zwick, E., Daub, H., Leserer, M., Abraham, R., Wallasch, C. & Ullrich, A.** EGF receptor transactivation by G-protein-coupled receptors requires metalloproteinase cleavage of proHB-EGF. *Nature* 402, 884-8 (1999).
52. **Inoue, A., Ishiguro, J., Kitamura, H., Arima, N., Okutani, M., Shuto, A., Higashiyama, S., Ohwada, T., Arai, H., Makide, K. & Aoki, J.** TGF α shedding assay: an accurate and versatile method for detecting GPCR activation. *Nat. Methods* 9, 1021-9 (2012).
53. **Robertshaw, H.J. & Brennan, F.M.** Release of tumour necrosis factor alpha (TNF α) by TNF α cleaving enzyme (TACE) in response to septic stimuli in vitro. *Br. J. Anaesth.* 94, 222-8 (2005).
54. **Freeman, M.** The rhomboid-like superfamily: molecular mechanisms and biological roles. *Annu. Rev. Cell Dev. Biol.* 30, 235-54 (2014).
55. **Christova, Y., Adrain, C., Bambrough, P., Ibrahim, A. & Freeman, M.** Mammalian iRhoms have distinct physiological functions including an essential role in TACE regulation. *EMBO Rep.* 14, 884-90 (2013).
56. **Maretzky, T., McIlwain, D.R., Issuree, P.D., Li, X., Malapeira, J., Amin, S., Lang, P.A., Mak, T.W. & Blobel, C.P.** iRhom2 controls the substrate selectivity of stimulated ADAM17-dependent ectodomain shedding. *Proc. Natl. Acad. Sci. USA.* 110, 11433-8 (2013).
57. **Maney, S.K., McIlwain, D.R., Polz, R., Pandyra, A.A., Sundaram, B., Wolff, D., Ohishi, K., Maretzky, T., Brooke, M.A., Evers, A., Vasudevan, A.A., Aghaeepour, N., Scheller, J., Munk, C., Haussinger, D., Mak, T.W., Nolan, G.P., Kelsell, D.P., Blobel, C.P., Lang, K.S. & Lang, P.A.** Deletions in the cytoplasmic domain of iRhom1 and iRhom2 promote shedding of the TNF receptor by the protease ADAM17. *Sci. Signal.* 8, 109 (2015).
58. **Prox, J., Willenbrock, M., Weber, S., Lehmann, T., Schmidt-Arras, D., Schwanbeck, R., Saftig, P. & Schwake, M.** Tetraspanin15 regulates cellular trafficking and activity of the ectodomain sheddase ADAM10. *Cell Mol. Life Sci.* 69, 2919-32 (2012).
59. **Gutierrez-Lopez, M.D., Gilsanz, A., Yanez-Mo, M., Ovalle, S., Lafuente, E.M., Dominguez, C., Monk, P.N., Gonzalez-Alvaro, I., Sanchez-Madrid, F. & Cabanas, C.** The sheddase activity of ADAM17/TACE is regulated by the tetraspanin CD9. *Cell Mol. Life Sci.* 68, 3275-92 (2011).

60. **Willems, S.H., Tape, C.J., Stanley, P.L., Taylor, N.A., Mills, I.G., Neal, D.E., McCafferty, J. & Murphy, G.** Thiol isomerases negatively regulate the cellular shedding activity of ADAM17. *Biochem. J.* 428, 439-50 (2010).
61. **Sommer, A., Kordowski, F., Buch, J., Maretzky, T., Evers, A., Andra, J., Düsterhöft, S., Michalek, M., Lorenzen, I., Somasundaram, P., Tholey, A., Sonnichsen, F.D., Kunzelmann, K., Heinbockel, L., Nehls, C., Gutschmann, T., Grötzinger, J., Bhakdi, S. & Reiss, K.** Phosphatidylserine exposure is required for ADAM17 sheddase function. *Nat. Commun.* 7, 11523 (2016).
62. **Amour, A., Slocombe, P.M., Webster, A., Butler, M., Knight, C.G., Smith, B.J., Stephens, P.E., Shelley, C., Hutton, M., Knauper, V., Docherty, A.J. & Murphy, G.** TNF-alpha converting enzyme (TACE) is inhibited by TIMP-3. *FEBS Lett.* 435, 39-44 (1998).
63. **Ye, J., Yuen, S.M., Murphy, G., Xie, R. & Kwok, H.F.** Anti-tumor effects of a 'human & mouse cross-reactive' anti-ADAM17 antibody in a pancreatic cancer model in vivo. *Eur. J. Pharm. Sci.* 110, 62-9 (2017).
64. **Holash, J., Davis, S., Papadopoulos, N., Croll, S.D., Ho, L., Russell, M., Boland, P., Leidich, R., Hylton, D., Burova, E., Ioffe, E., Huang, T., Radziejewski, C., Bailey, K., Fandl, J.P., Daly, T., Wiegand, S.J., Yancopoulos, G.D. & Rudge, J.S.** VEGF-Trap: A VEGF blocker with potent antitumor effects. *Proc. Natl. Acad. Sci. USA* 99, 11393-8 (2002).
65. **Miller, M.A., Sullivan, R.J. & Lauffenburger, D.A.** Molecular Pathways: Receptor Ectodomain Shedding in Treatment, Resistance, and Monitoring of Cancer. *Clin. Cancer Res.* 23, 623-9 (2017).
66. **Mohler, K.M., Torrance, D.S., Smith, C.A., Goodwin, R.G., Stremmler, K.E., Fung, V.P., Madani, H. & Widmer, M.B.** Soluble tumor necrosis factor (TNF) receptors are effective therapeutic agents in lethal endotoxemia and function simultaneously as both TNF carriers and TNF antagonists. *J. Immunol.* 151, 1548-61 (1993).
67. **Gerriets, V. & Khaddour, K.** Tumor Necrosis Factor (TNF) Inhibitors. *StatPearls* (2019).
68. **<https://www.who.int/news-room/fact-sheets/detail/cancer>.** Accessed 15/01/2019 (2018).
69. **Seyfried, T.N. & Huysentruyt, L.C.** On the origin of cancer metastasis. *Crit. Rev. Oncog.* 18, 43-73 (2013).
70. **Hanahan, D. & Weinberg, R.A.** The hallmarks of cancer. *Cell* 100, 57-70 (2000).
71. **Fynan, T.M. & Reiss, M.** Resistance to inhibition of cell growth by transforming growth factor-beta and its role in oncogenesis. *Crit. Rev. Oncog.* 4, 493-540 (1993).
72. **Joyce, J.A. & Pollard, J.W.** Microenvironmental regulation of metastasis. *Nat. Rev. Cancer* 9, 239-52 (2009).
73. **Balkwill, F.R., Capasso, M. & Hagemann, T.** The tumor microenvironment at a glance. *J. Cell. Sci.* 125, 5591-6 (2012).

74. **Pietras, K. & Ostman, A.** Hallmarks of cancer: interactions with the tumor stroma. *Exp. Cell Res.* 316, 1324-31 (2010).
75. **McAllister, S.S. & Weinberg, R.A.** The tumour-induced systemic environment as a critical regulator of cancer progression and metastasis. *Nat. Cell Biol.* 16, 717-27 (2014).
76. **Lanaya, H., Natarajan, A., Komposch, K., Li, L., Amberg, N., Chen, L., Wculek, S.K., Hammer, M., Zenz, R., Peck-Radosavljevic, M., Sieghart, W., Trauner, M., Wang, H. & Sibilias, M.** EGFR has a tumour-promoting role in liver macrophages during hepatocellular carcinoma formation. *Nat. Cell Biol.* 16, 972-7 (2014).
77. **Coniglio, S.J., Eugenin, E., Dobrenis, K., Stanley, E.R., West, B.L., Symons, M.H. & Segall, J.E.** Microglial stimulation of glioblastoma invasion involves epidermal growth factor receptor (EGFR) and colony stimulating factor 1 receptor (CSF-1R) signaling. *Mol. Med.* 18, 519-27 (2012).
78. **Lin, E.Y., Li, J.F., Gnatovskiy, L., Deng, Y., Zhu, L., Grzesik, D.A., Qian, H., Xue, X.N. & Pollard, J.W.** Macrophages regulate the angiogenic switch in a mouse model of breast cancer. *Cancer Res.* 66, 11238-46 (2006).
79. **Shweiki, D., Itin, A., Soffer, D. & Keshet, E.** Vascular endothelial growth factor induced by hypoxia may mediate hypoxia-initiated angiogenesis. *Nature* 359, 843-5 (1992).
80. **Carmeliet, P. & Jain, R.K.** Molecular mechanisms and clinical applications of angiogenesis. *Nature* 473, 298-307 (2011).
81. **LeBleu, V.S. & Kalluri, R.** A peek into cancer-associated fibroblasts: origins, functions and translational impact. *Dis. Model. Mech.* 11, 29447 (2018).
82. **Azmi, A.S., Bao, B. & Sarkar, F.H.** Exosomes in cancer development, metastasis, and drug resistance: a comprehensive review. *Cancer Metastasis Rev.* 32, 623-42 (2013).
83. **Kim, S., Takahashi, H., Lin, W.W., Descargues, P., Grivennikov, S., Kim, Y., Luo, J.L. & Karin, M.** Carcinoma-produced factors activate myeloid cells through TLR2 to stimulate metastasis. *Nature* 457, 102-6 (2009).
84. **Sceneay, J., Chow, M.T., Chen, A., Halse, H.M., Wong, C.S., Andrews, D.M., Sloan, E.K., Parker, B.S., Bowtell, D.D., Smyth, M.J. & Moller, A.** Primary tumor hypoxia recruits CD11b⁺/Ly6C^{med}/Ly6G⁺ immune suppressor cells and compromises NK cell cytotoxicity in the premetastatic niche. *Cancer Res.* 72, 3906-11 (2012).
85. **Giampieri, S., Manning, C., Hooper, S., Jones, L., Hill, C.S. & Sahai, E.** Localized and reversible TGFbeta signalling switches breast cancer cells from cohesive to single cell motility. *Nat. Cell Biol.* 11, 1287-96 (2009).
86. **Friedl, P., Locker, J., Sahai, E. & Segall, J.E.** Classifying collective cancer cell invasion. *Nat. Cell Biol.* 14, 777-83 (2012).
87. **Brabletz, T., Kalluri, R., Nieto, M.A. & Weinberg, R.A.** EMT in cancer. *Nat. Rev. Cancer* 18, 128-34 (2018).

88. **Chitty, J.L., Filipe, E.C., Lucas, M.C., Herrmann, D., Cox, T.R. & Timpson, P.** Recent advances in understanding the complexities of metastasis. *F1000Res* 7, 15064.1 (2018).
89. **Lamouille, S., Xu, J. & Derynck, R.** Molecular mechanisms of epithelial-to-mesenchymal transition. *Nat. Rev. Mol. Cell Biol.* 15, 178 (2014).
90. **Roussos, E.T., Condeelis, J.S. & Patsialou, A.** Chemotaxis in cancer. *Nat. Rev. Cancer* 11, 573-87 (2011).
91. **Quail, D.F. & Joyce, J.A.** Microenvironmental regulation of tumor progression and metastasis. *Nat. Med.* 19, 1423-37 (2013).
92. **Entenberg, D., Voiculescu, S., Guo, P., Borriello, L., Wang, Y., Karagiannis, G.S., Jones, J., Baccay, F., Oktay, M. & Condeelis, J.** A permanent window for the murine lung enables high-resolution imaging of cancer metastasis. *Nat. Methods* 15, 73-80 (2018).
93. **Chang, Y.S., di Tomaso, E., McDonald, D.M., Jones, R., Jain, R.K. & Munn, L.L.** Mosaic blood vessels in tumors: frequency of cancer cells in contact with flowing blood. *Proc. Natl. Acad. Sci. USA.* 97, 14608-13 (2000).
94. **Taddei, M.L., Giannoni, E., Fiaschi, T. & Chiarugi, P.** Anoikis: an emerging hallmark in health and diseases. *J. Pathol.* 226, 380-93 (2012).
95. **Strilic, B. & Offermanns, S.** Intravascular Survival and Extravasation of Tumor Cells. *Cancer Cell* 32, 282-93 (2017).
96. **Erpenbeck, L. & Schon, M.P.** Deadly allies: the fatal interplay between platelets and metastasizing cancer cells. *Blood* 115, 3427-36 (2010).
97. **Palumbo, J.S., Talmage, K.E., Massari, J.V., La Jeunesse, C.M., Flick, M.J., Kombrinck, K.W., Jirouskova, M. & Degen, J.L.** Platelets and fibrin(ogen) increase metastatic potential by impeding natural killer cell-mediated elimination of tumor cells. *Blood* 105, 178-85 (2005).
98. **Park, J., Wysocki, R.W., Amoozgar, Z., Maiorino, L., Fein, M.R., Jorns, J., Schott, A.F., Kinugasa-Katayama, Y., Lee, Y., Won, N.H., Nakasone, E.S., Hearn, S.A., Kuttner, V., Qiu, J., Almeida, A.S., Perurena, N., Kessenbrock, K., Goldberg, M.S. & Egeblad, M.** Cancer cells induce metastasis-supporting neutrophil extracellular DNA traps. *Sci. Transl. Med.* 8, 361 (2016).
99. **Cools-Lartigue, J., Spicer, J., McDonald, B., Gowing, S., Chow, S., Giannias, B., Bourdeau, F., Kubes, P. & Ferri, L.** Neutrophil extracellular traps sequester circulating tumor cells and promote metastasis. *J. Clin. Invest.* (2013).
100. **McCarty, O.J., Mousa, S.A., Bray, P.F. & Konstantopoulos, K.** Immobilized platelets support human colon carcinoma cell tethering, rolling, and firm adhesion under dynamic flow conditions. *Blood* 96, 1789-97 (2000).
101. **Reymond, N., d'Agua, B.B. & Ridley, A.J.** Crossing the endothelial barrier during metastasis. *Nat. Rev. Cancer* 13, 858-70 (2013).

102. **Auguste, P., Fallavollita, L., Wang, N., Burnier, J., Bikfalvi, A. & Brodt, P.** The Host Inflammatory Response Promotes Liver Metastasis by Increasing Tumor Cell Arrest and Extravasation. *The American Journal of Pathology* 170, 1781-92 (2007).
103. **Ito, S., Nakanishi, H., Ikehara, Y., Kato, T., Kasai, Y., Ito, K., Akiyama, S., Nakao, A. & Tatematsu, M.** Real-time observation of micrometastasis formation in the living mouse liver using a green fluorescent protein gene-tagged rat tongue carcinoma cell line. *Int. J. Cancer* 93, 212-7 (2001).
104. **Garcia-Roman, J. & Zentella-Dehesa, A.** Vascular permeability changes involved in tumor metastasis. *Cancer Lett.* 335, 259-69 (2013).
105. **Weis, S., Cui, J., Barnes, L. & Cheresh, D.** Endothelial barrier disruption by VEGF-mediated Src activity potentiates tumor cell extravasation and metastasis. *J. Cell Biol.* 167, 223-9 (2004).
106. **Wolf, M.J., Hoos, A., Bauer, J., Boettcher, S., Knust, M., Weber, A., Simonavicius, N., Schneider, C., Lang, M., Sturzl, M., Croner, R.S., Konrad, A., Manz, M.G., Moch, H., Aguzzi, A., van Loo, G., Pasparakis, M., Prinz, M., Borsig, L. & Heikenwalder, M.** Endothelial CCR2 signaling induced by colon carcinoma cells enables extravasation via the JAK2-Stat5 and p38MAPK pathway. *Cancer Cell* 22, 91-105 (2012).
107. **Qian, B.Z., Li, J., Zhang, H., Kitamura, T., Zhang, J., Campion, L.R., Kaiser, E.A., Snyder, L.A. & Pollard, J.W.** CCL2 recruits inflammatory monocytes to facilitate breast-tumour metastasis. *Nature* 475, 222-5 (2011).
108. **Schumacher, D., Strilic, B., Sivaraj, K.K., Wettschureck, N. & Offermanns, S.** Platelet-derived nucleotides promote tumor-cell transendothelial migration and metastasis via P2Y2 receptor. *Cancer Cell* 24, 130-7 (2013).
109. **González-Mariscal, L., Tapia, R. & Chamorro, D.** Crosstalk of tight junction components with signaling pathways. *Biochim. Biophys. Acta* 1778, 729-56 (2008).
110. **Strilic, B., Yang, L., Albarran-Juarez, J., Wachsmuth, L., Han, K., Muller, U.C., Pasparakis, M. & Offermanns, S.** Tumour-cell-induced endothelial cell necroptosis via death receptor 6 promotes metastasis. *Nature* 536, 215-8 (2016).
111. **Celia-Terrassa, T. & Kang, Y.** Metastatic niche functions and therapeutic opportunities. *Nat. Cell Biol.* 20, 868-77 (2018).
112. **Gao, D., Joshi, N., Choi, H., Ryu, S., Hahn, M., Catena, R., Sadik, H., Argani, P., Wagner, P., Vahdat, L.T., Port, J.L., Stiles, B., Sukumar, S., Altorki, N.K., Rafii, S. & Mittal, V.** Myeloid progenitor cells in the premetastatic lung promote metastases by inducing mesenchymal to epithelial transition. *Cancer Res.* 72, 1384-94 (2012).
113. **Del Pozo Martin, Y., Park, D., Ramachandran, A., Ombrato, L., Calvo, F., Chakravarty, P., Spencer-Dene, B., Derzsi, S., Hill, C.S., Sahai, E. & Malanchi, I.** Mesenchymal Cancer Cell-Stroma Crosstalk Promotes Niche Activation, Epithelial Reversion, and Metastatic Colonization. *Cell Rep.* 13, 2456-69 (2015).

114. **Weidenfeld, K. & Barkan, D.** EMT and Stemness in Tumor Dormancy and Outgrowth: Are They Intertwined Processes?. *Front. Oncol.* 8, 381 (2018).
115. **De Cock, J.M., Shibue, T., Dongre, A., Keckesova, Z., Reinhardt, F. & Weinberg, R.A.** Inflammation Triggers Zeb1-Dependent Escape from Tumor Latency. *Cancer Res.* 76, 6778-84 (2016).
116. **Junttila, M.R. & de Sauvage, F.J.** Influence of tumour micro-environment heterogeneity on therapeutic response. *Nature* 501, 346 (2013).
117. **Tait, S.W., Ichim, G. & Green, D.R.** Die another way--non-apoptotic mechanisms of cell death. *J. Cell. Sci.* 127, 2135-44 (2014).
118. **Kerr, J.F., Wyllie, A.H. & Currie, A.R.** Apoptosis: a basic biological phenomenon with wide-ranging implications in tissue kinetics. *Br. J. Cancer* 26, 239-57 (1972).
119. **Ziegler, U. & Groscurth, P.** Morphological Features of Cell Death. *Physiology* 19, 124-8 (2004).
120. **Galluzzi, L., Vitale, I., Aaronson, S.A., Abrams, J.M., Adam, D., Agostinis, P., Alnemri, E.S., Altucci, L., Amelio, I., Andrews, D.W., Annicchiarico-Petruzzelli, M., Antonov, A.V., Arama, E., Baehrecke, E.H., Barlev, N.A., Bazan, N.G., Bernassola, F., Bertrand, M.J.M., Bianchi, K., Blagosklonny, M.V., Blomgren, K., Borner, C., Boya, P., Brenner, C., Campanella, M., Candi, E., Carmona-Gutierrez, D., Cecconi, F., Chan, F.K., Chandel, N.S., Cheng, E.H., Chipuk, J.E., Cidlowski, J.A., Ciechanover, A., Cohen, G.M., Conrad, M., Cubillos-Ruiz, J.R., Czabotar, P.E., D'Angiolella, V., Dawson, T.M., Dawson, V.L., De Laurenzi, V., De Maria, R., Debatin, K.M., DeBerardinis, R.J., Deshmukh, M., Di Daniele, N., Di Virgilio, F., Dixit, V.M., Dixon, S.J., Duckett, C.S., Dynlacht, B.D., El-Deiry, W.S., Elrod, J.W., Fimia, G.M., Fulda, S., Garcia-Saez, A.J., Garg, A.D., Garrido, C., Gavathiotis, E., Golstein, P., Gottlieb, E., Green, D.R., Greene, L.A., Gronemeyer, H., Gross, A., Hajnoczky, G., Hardwick, J.M., Harris, I.S., Hengartner, M.O., Hetz, C., Ichijo, H., Jaattela, M., Joseph, B., Jost, P.J., Juin, P.P., Kaiser, W.J., Karin, M., Kaufmann, T., Kepp, O., Kimchi, A., Kitsis, R.N., Klionsky, D.J., Knight, R.A., Kumar, S., Lee, S.W., Lemasters, J.J., Levine, B., Linkermann, A., Lipton, S.A., Lockshin, R.A., Lopez-Otin, C., Lowe, S.W., Luedde, T., Lugli, E., MacFarlane, M., Madeo, F., Malewicz, M., Malorni, W., Manic, G., Marine, J.C., Martin, S.J., Martinou, J.C., Medema, J.P., Mehlen, P., Meier, P., Melino, S., Miao, E.A., Molkentin, J.D., Moll, U.M., Munoz-Pinedo, C., Nagata, S., Nunez, G., Oberst, A., Oren, M., Overholtzer, M., Pagano, M., Panaretakis, T., Pasparakis, M., Penninger, J.M., Pereira, D.M., Pervaiz, S., Peter, M.E., Piacentini, M., Pinton, P., Prehn, J.H.M., Puthalakath, H., Rabinovich, G.A., Rehm, M., Rizzuto, R., Rodrigues, C.M.P., Rubinsztein, D.C., Rudel, T., Ryan, K.M., Sayan, E., Scorrano, L., Shao, F., Shi, Y., Silke, J., Simon, H.U., Sistigu, A., Stockwell, B.R., Strasser, A., Szabadkai, G., Tait, S.W.G., Tang, D., Tavernarakis, N., Thorburn, A., Tsujimoto, Y., Turk, B., Vanden Berghe, T., Vandenabeele, P., Vander Heiden, M.G., Villunger, A., Virgin, H.W., Vousden, K.H., Vucic, D., Wagner, E.F., Walczak, H., Wallach, D., Wang, Y., Wells, J.A., Wood, W., Yuan, J., Zakeri, Z., Zhivotovsky, B., Zitvogel, L., Melino, G. & Kroemer, G.** Molecular mechanisms of cell death: recommendations of the Nomenclature Committee on Cell Death 2018. *Cell Death Differ.* 25, 486-541 (2018).
121. **Grootjans, S., Vanden Berghe, T. & Vandenabeele, P.** Initiation and execution mechanisms of necroptosis: an overview. *Cell Death Differ.* (2017).
122. **Tartaglia, L.A., Ayres, T.M., Wong, G.H. & Goeddel, D.V.** A novel domain within the 55 kd TNF receptor signals cell death. *Cell* 74, 845-53 (1993).

123. **Wilson, N.S., Dixit, V. & Ashkenazi, A.** Death receptor signal transducers: nodes of coordination in immune signaling networks. *Nat. Immunol.* 10, 348-55 (2009).
124. **Rothe, M., Sarma, V., Dixit, V.M. & Goeddel, D.V.** TRAF2-mediated activation of NF-kappa B by TNF receptor 2 and CD40. *Science* 269, 1424-7 (1995).
125. **Grell, M., Douni, E., Wajant, H., Lohden, M., Clauss, M., Maxeiner, B., Georgopoulos, S., Lesslauer, W., Kollias, G., Pfizenmaier, K. & Scheurich, P.** The transmembrane form of tumor necrosis factor is the prime activating ligand of the 80 kDa tumor necrosis factor receptor. *Cell* 83, 793-802 (1995).
126. **Grell, M., Wajant, H., Zimmermann, G. & Scheurich, P.** The type 1 receptor (CD120a) is the high-affinity receptor for soluble tumor necrosis factor. *Proc. Natl. Acad. Sci. USA.* 95, 570-5 (1998).
127. **Naude, P.J., den Boer, J.A., Luiten, P.G. & Eisel, U.L.** Tumor necrosis factor receptor cross-talk. *FEBS J.* 278, 888-98 (2011).
128. **Chan, F.K.** Three is better than one: Pre-ligand receptor assembly in the regulation of TNF receptor signaling. *Cytokine* 37, 101-7 (2007).
129. **Cabal-Hierro, L. & Lazo, P.S.** Signal transduction by tumor necrosis factor receptors. *Cell. Signal.* 24, 1297-305 (2012).
130. **Micheau, O. & Tschopp, J.** Induction of TNF receptor I-mediated apoptosis via two sequential signaling complexes. *Cell* 114, 181-90 (2003).
131. **Sun, S.C.** The non-canonical NF-kappaB pathway in immunity and inflammation. *Nat. Rev. Immunol.* 17, 545-58 (2017).
132. **Dondelinger, Y., Darding, M., Bertrand, M.J. & Walczak, H.** Poly-ubiquitination in TNFR1-mediated necroptosis. *Cell Mol. Life Sci.* 73, 2165-76 (2016).
133. **Yang, X., Chang, H.Y. & Baltimore, D.** Autoproteolytic activation of pro-caspases by oligomerization. *Mol. Cell* 1, 319-25 (1998).
134. **Salvesen, G.S. & Walsh, C.M.** Functions of caspase 8: the identified and the mysterious. *Semin. Immunol.* 26, 246-52 (2014).
135. **Moriwaki, K. & Chan, F.K.** The Inflammatory Signal Adaptor RIPK3: Functions Beyond Necroptosis. *Int. Rev. Cell. Mol. Biol.* 328, 253-75 (2017).
136. **Ofengeim, D. & Yuan, J.** Regulation of RIP1 kinase signalling at the crossroads of inflammation and cell death. *Nat. Rev. Mol. Cell Biol.* 14, 727-36 (2013).
137. **Dondelinger, Y., Jouan-Lanhouet, S., Divert, T., Theatre, E., Bertin, J., Gough, P., Giansanti, P., Heck, A.R., Dejardin, E., Vandenabeele, P. & Bertrand, M.M.** NF- κ B-Independent Role of IKK α /IKK β in Preventing RIPK1 Kinase-Dependent Apoptotic and Necroptotic Cell Death during TNF Signaling. *Mol. Cell* 60, 63-76 (2015).

138. **Jaco, I., Annibaldi, A., Lalaoui, N., Wilson, R., Tenev, T., Laurien, L., Kim, C., Jamal, K., Wicky John, S., Liccardi, G., Chau, D., Murphy, J.M., Brumatti, G., Feltham, R., Pasparakis, M., Silke, J. & Meier, P.** MK2 Phosphorylates RIPK1 to Prevent TNF-Induced Cell Death. *Mol. Cell* 66, 698-710 (2017).
139. **Lafont, E., Draber, P., Rieser, E., Reichert, M., Kupka, S., de Miguel, D., Draberova, H., von Massenhausen, A., Bhamra, A., Henderson, S., Wojdyla, K., Chalk, A., Surinova, S., Linkermann, A. & Walczak, H.** TBK1 and IKKepsilon prevent TNF-induced cell death by RIPK1 phosphorylation. *Nat. Cell Biol.* 20, 1389-99 (2018).
140. **Spit, M., Rieser, E. & Walczak, H.** Linear ubiquitination at a glance. *J. Cell. Sci.* 132, 208512 (2019).
141. **Micheau, O., Lens, S., Gaide, O., Alevizopoulos, K. & Tschopp, J.** NF-kappaB signals induce the expression of c-FLIP. *Mol. Cell. Biol.* 21, 5299-305 (2001).
142. **Stehlik, C., de Martin, R., Binder, B.R. & Lipp, J.** Cytokine induced expression of porcine inhibitor of apoptosis protein (iap) family member is regulated by NF-kappa B. *Biochem. Biophys. Res. Commun.* 243, 827-32 (1998).
143. **Gong, Y.N., Guy, C., Olauson, H., Becker, J.U., Yang, M., Fitzgerald, P., Linkermann, A. & Green, D.R.** ESCRT-III Acts Downstream of MLKL to Regulate Necroptotic Cell Death and Its Consequences. *Cell* 169, 286-300 (2017).
144. **Yoon, S., Kovalenko, A., Bogdanov, K. & Wallach, D.** MLKL, the Protein that Mediates Necroptosis, Also Regulates Endosomal Trafficking and Extracellular Vesicle Generation. *Immunity* 47, 51-65 (2017).
145. **Kasof, G.M., Lu, J.J., Liu, D., Speer, B., Mongan, K.N., Gomes, B.C. & Lorenzi, M.V.** Tumor necrosis factor-alpha induces the expression of DR6, a member of the TNF receptor family, through activation of NF-kappaB. *Oncogene* 20, 7965-75 (2001).
146. **Benschop, R., Wei, T. & Na, S.** Tumor necrosis factor receptor superfamily member 21: TNFR-related death receptor-6, DR6. *Adv. Exp. Med. Biol.* 647, 186-94 (2009).
147. **Horiuchi, K., Kimura, T., Miyamoto, T., Miyamoto, K., Akiyama, H., Takaishi, H., Morioka, H., Nakamura, T., Okada, Y., Blobel, C.P. & Toyama, Y.** Conditional inactivation of TACE by a Sox9 promoter leads to osteoporosis and increased granulopoiesis via dysregulation of IL-17 and G-CSF. *J. Immunol.* 182, 2093-101 (2009).
148. **Wang, Y., Nakayama, M., Pitulescu, M.E., Schmidt, T.S., Bochenek, M.L., Sakakibara, A., Adams, S., Davy, A., Deutsch, U., Luthi, U., Barberis, A., Benjamin, L.E., Makinen, T., Nobes, C.D. & Adams, R.H.** Ephrin-B2 controls VEGF-induced angiogenesis and lymphangiogenesis. *Nature* 465, 483-6 (2010).
149. **Clausen, B.E., Burkhardt, C., Reith, W., Renkawitz, R. & Forster, I.** Conditional gene targeting in macrophages and granulocytes using LysMcre mice. *Transgenic Res.* 8, 265-77 (1999).

150. **Link, M.A., Lücke, K., Schmid, J., Schumacher, V., Eden, T., Rose-John, S. & Mittrücker, H.W.** The role of ADAM17 in the T-cell response against bacterial pathogens. *PLoS One* 12, 184320 (2017).
151. **Newton, K., Sun, X. & Dixit, V.M.** Kinase RIP3 is dispensable for normal NF-kappa Bs, signaling by the B-cell and T-cell receptors, tumor necrosis factor receptor 1, and Toll-like receptors 2 and 4. *Mol. Cell. Biol.* 24, 1464-9 (2004).
152. **Yao, L.J., Leitges, M. & Vallon, V.** Mice lacking protein kinase C beta present modest increases in systolic blood pressure and NH₄Cl-induced metabolic acidosis. *Kidney Blood Press. Res.* 29, 36-42 (2006).
153. **Orban, P.C., Chui, D. & Marth, J.D.** Tissue- and site-specific DNA recombination in transgenic mice. *Proc. Natl. Acad. Sci. USA.* 89, 6861-5 (1992).
154. **Reichert, M., Bhamra, A., Kupka, S. & Walczak, H.** Characterization of the TNFR1-SC Using "Modified Tandem Affinity Purification" in Conjunction with Liquid Chromatography-Mass Spectrometry (LC-MS). *Methods Mol. Biol.* 1857, 161-9 (2018).
155. **Stevanovic, M.** Analysis of ADAM17 in the metastatic niche of the lung. Retrieved from MACAU, Accession number 143347, Christian-Albrechts-University Kiel (2014).
156. **Heyder, C., Gloria-Maercker, E., Hatzmann, W., Zaenker, K.S. & Dittmar, T.** Visualization of tumor cell extravasation. *Contrib. Microbiol.* 13, 200-8 (2006).
157. **Dang, M., Dubbin, K., D'Aiello, A., Hartmann, M., Lodish, H. & Herrlich, A.** Epidermal growth factor (EGF) ligand release by substrate-specific a disintegrin and metalloproteases (ADAMs) involves different protein kinase C (PKC) isoenzymes depending on the stimulus. *J. Biol. Chem.* 286, 17704-13 (2011).
158. **Koenen, R.R., Pruessmeyer, J., Soehnlein, O., Fraemohs, L., Zerneck, A., Schwarz, N., Reiss, K., Sarabi, A., Lindbom, L., Hackeng, T.M., Weber, C. & Ludwig, A.** Regulated release and functional modulation of junctional adhesion molecule A by disintegrin metalloproteinases. *Blood* 113, 4799-809 (2009).
159. **Schulz, B., Pruessmeyer, J., Maretzky, T., Ludwig, A., Blobel, C.P., Saftig, P. & Reiss, K.** ADAM10 regulates endothelial permeability and T-Cell transmigration by proteolysis of vascular endothelial cadherin. *Circ. Res.* 102, 1192-201 (2008).
160. **Graff, J.R., McNulty, A.M., Hanna, K.R., Konicek, B.W., Lynch, R.L., Bailey, S.N., Banks, C., Capen, A., Goode, R., Lewis, J.E., Sams, L., Huss, K.L., Campbell, R.M., Iversen, P.W., Neubauer, B.L., Brown, T.J., Musib, L., Geeganage, S. & Thornton, D.** The Protein Kinase C β -Selective Inhibitor, Enzastaurin (LY317615.HCl), Suppresses Signaling through the AKT Pathway, Induces Apoptosis, and Suppresses Growth of Human Colon Cancer and Glioblastoma Xenografts. *Cancer Res.* 65, 7462-9 (2005).
161. **Yuan, J., Najafov, A. & Py, B.F.** Roles of Caspases in Necrotic Cell Death. *Cell* 167, 1693-704 (2016).

162. **Chhibber-Goel, J., Coleman-Vaughan, C., Agrawal, V., Sawhney, N., Hickey, E., Powell, J.C. & McCarthy, J.V.** gamma-Secretase Activity Is Required for Regulated Intramembrane Proteolysis of Tumor Necrosis Factor (TNF) Receptor 1 and TNF-mediated Pro-apoptotic Signaling. *J. Biol. Chem.* 291, 5971-85 (2016).
163. **Bell, J.H., Herrera, A.H., Li, Y. & Walcheck, B.** Role of ADAM17 in the ectodomain shedding of TNF-alpha and its receptors by neutrophils and macrophages. *J. Leukoc. Biol.* 82, 173-6 (2007).
164. **Bauer, T., Zagorska, A., Jurkin, J., Yasmin, N., Koeffel, R., Richter, S., Gesslbauer, B., Lemke, G. & Strobl, H.** Identification of Axl as a downstream effector of TGF- 1 during Langerhans cell differentiation and epidermal homeostasis. *J. Exp. Med.* 209, 2033-47 (2012).
165. **Kluppel, M. & Wrana, J.L.** Turning it up a Notch: cross-talk between TGF beta and Notch signaling. *Bioessays* 27, 115-8 (2005).
166. **Saad, M.I., Alhayyani, S., McLeod, L., Yu, L., Alanazi, M., Deswaerte, V., Tang, K., Jarde, T., Smith, J.A., Prodanovic, Z., Tate, M.D., Balic, J.J., Watkins, D.N., Cain, J.E., Bozinovski, S., Algar, E., Kohmoto, T., Ebi, H., Ferlin, W., Garbers, C., Ruwanpura, S., Sagi, I., Rose-John, S. & Jenkins, B.J.** ADAM17 selectively activates the IL-6 trans-signaling/ERK MAPK axis in KRAS-addicted lung cancer. *EMBO Mol. Med.* 11, 9976 (2019).
167. **Chambers, A.F., Naumov, G.N., Varghese, H.J., Nadkarni, K.V., MacDonald, I.C. & Groom, A.C.** Critical steps in hematogenous metastasis: an overview. *Surg. Oncol. Clin. N. Am.* 10, 243,55, vii (2001).
168. **Chen, X.L., Nam, J.O., Jean, C., Lawson, C., Walsh, C.T., Goka, E., Lim, S.T., Tomar, A., Tancioni, I., Uryu, S., Guan, J.L., Acevedo, L.M., Weis, S.M., Cheresh, D.A. & Schlaepfer, D.D.** VEGF-induced vascular permeability is mediated by FAK. *Dev. Cell.* 22, 146-57 (2012).
169. **Wojciak-Stothard, B., Entwistle, A., Garg, R. & Ridley, A.J.** Regulation of TNF-alpha-induced reorganization of the actin cytoskeleton and cell-cell junctions by Rho, Rac, and Cdc42 in human endothelial cells. *J. Cell. Physiol.* 176, 150-65 (1998).
170. **Ponnuchamy, B. & Khalil, R.A.** Role of ADAMs in endothelial cell permeability: cadherin shedding and leukocyte rolling. *Circ. Res.* 102, 1139-42 (2008).
171. **Garg, R., Benedetti, L.G., Abera, M.B., Wang, H., Abba, M. & Kazanietz, M.G.** Protein kinase C and cancer: what we know and what we do not. *Oncogene* 33, 5225-37 (2014).
172. **Xia, P., Aiello, L.P., Ishii, H., Jiang, Z.Y., Park, D.J., Robinson, G.S., Takagi, H., Newsome, W.P., Jirousek, M.R. & King, G.L.** Characterization of vascular endothelial growth factor's effect on the activation of protein kinase C, its isoforms, and endothelial cell growth. *J. Clin. Invest.* 98, 2018-26 (1996).
173. **Wallace, J.A., Pitarresi, J.R., Sharma, N., Palettas, M., Cuitino, M.C., Sizemore, S.T., Yu, L., Sanderlin, A., Rosol, T.J., Mehta, K.D., Sizemore, G.M. & Ostrowski, M.C.** Protein kinase C Beta in the tumor microenvironment promotes mammary tumorigenesis. *Front. Oncol.* 4, 87 (2014).

174. **Lutzny, G., Kocher, T., Schmidt-Supprian, M., Rudelius, M., Klein-Hitpass, L., Finch, A.J., Durig, J., Wagner, M., Haferlach, C., Kohlmann, A., Schnittger, S., Seifert, M., Wanninger, S., Zaborsky, N., Oostendorp, R., Ruland, J., Leitges, M., Kuhnt, T., Schafer, Y., Lampl, B., Peschel, C., Egle, A. & Ringshausen, I.** Protein kinase c-beta-dependent activation of NF-kappaB in stromal cells is indispensable for the survival of chronic lymphocytic leukemia B cells in vivo. *Cancer Cell* 23, 77-92 (2013).
175. **Yang, Z., Jiang, B., Wang, Y., Ni, H., Zhang, J., Xia, J., Shi, M., Hung, L.M., Ruan, J., Mak, T.W., Li, Q. & Han, J.** 2-HG Inhibits Necroptosis by Stimulating DNMT1-Dependent Hypermethylation of the RIP3 Promoter. *Cell Rep.* 19, 1846-57 (2017).
176. **Yang, C., Li, J., Yu, L., Zhang, Z., Xu, F., Jiang, L., Zhou, X. & He, S.** Regulation of RIP3 by the transcription factor Sp1 and the epigenetic regulator UHRF1 modulates cancer cell necroptosis. *Cell. Death Dis.* 8, 3084 (2017).
177. **Benjamin, J.T., Carver, B.J., Plosa, E.J., Yamamoto, Y., Miller, J.D., Liu, J.H., van der Meer, R., Blackwell, T.S. & Prince, L.S.** NF-kappaB activation limits airway branching through inhibition of Sp1-mediated fibroblast growth factor-10 expression. *J. Immunol.* 185, 4896-903 (2010).
178. **Brakebusch, C., Varfolomeev, E.E., Batkin, M. & Wallach, D.** Structural requirements for inducible shedding of the p55 tumor necrosis factor receptor. *J. Biol. Chem.* 269, 32488-96 (1994).
179. **Wang, C.Y., Mayo, M.W., Korneluk, R.G., Goeddel, D.V. & Baldwin, A.S., Jr.** NF-kappaB antiapoptosis: induction of TRAF1 and TRAF2 and c-IAP1 and c-IAP2 to suppress caspase-8 activation. *Science* 281, 1680-3 (1998).
180. **Pahl, H.L.** Activators and target genes of Rel/NF-kappaB transcription factors. *Oncogene* 18, 6853-66 (1999).
181. **Yan, D., Qin, N., Zhang, H., Liu, T., Yu, M., Jiang, X., Feng, W., Wang, J., Yin, B., Zhang, T., Zhou, M. & Li, Z.** Expression of TNF-alpha leader sequence renders MCF-7 tumor cells resistant to the cytotoxicity of soluble TNF-alpha. *Breast Cancer Res. Treat.* 116, 91-102 (2009).
182. **Zhang, Z., Lin, G., Yan, Y., Li, X., Hu, Y., Wang, J., Yin, B., Wu, Y., Li, Z. & Yang, X.P.** Transmembrane TNF-alpha promotes chemoresistance in breast cancer cells. *Oncogene* 37, 3456-70 (2018).
183. **Cai, Z., Zhang, A., Choksi, S., Li, W., Li, T., Zhang, X.M. & Liu, Z.G.** Activation of cell-surface proteases promotes necroptosis, inflammation and cell migration. *Cell Res.* 26, 886-900 (2016).
184. **Shi, J., Hua, L., Harmer, D., Li, P. & Ren, G.** Cre Driver Mice Targeting Macrophages. *Methods Mol. Biol.* 1784, 263-75 (2018).
185. **Abram, C.L., Roberge, G.L., Hu, Y. & Lowell, C.A.** Comparative analysis of the efficiency and specificity of myeloid-Cre deleting strains using ROSA-EYFP reporter mice. *J. Immunol. Methods* 408, 89-100 (2014).
186. **Luckheeram, R.V., Zhou, R., Verma, A.D. & Xia, B.** CD4(+)T cells: differentiation and functions. *Clin. Dev. Immunol.* 2012, 925135 (2012).

187. **Tanaka, A. & Sakaguchi, S.** Regulatory T cells in cancer immunotherapy. *Cell Res.* 27, 109 (2016).
188. **Du, J.W., Xu, K.Y., Fang, L.Y. & Qi, X.L.** Interleukin-17, produced by lymphocytes, promotes tumor growth and angiogenesis in a mouse model of breast cancer. *Mol. Med. Rep.* 6, 1099-102 (2012).
189. **Cruz-Munoz, W., Kim, I. & Khokha, R.** TIMP-3 deficiency in the host, but not in the tumor, enhances tumor growth and angiogenesis. *Oncogene* 25, 650-5 (2006).
190. **Lu, J., Ye, X., Fan, F., Xia, L., Bhattacharya, R., Bellister, S., Tozzi, F., Sceusi, E., Zhou, Y., Tachibani, I., Maru, D.M., Hawke, D.H., Rak, J., Mani, S., Zweidler-McKay, P. & Ellis, L.M.** Endothelial Cells Promote the Colorectal Cancer Stem Cell Phenotype Through a Soluble Form of Jagged-1. *Cancer Cell* 23, 171-85 (2013).
191. **Li, L., Tang, P., Li, S., Qin, X., Yang, H., Wu, C. & Liu, Y.** Notch signaling pathway networks in cancer metastasis: a new target for cancer therapy. *Medical Oncology* 34, 180 (2017).
192. **Osipo, C., Golde, T.E., Osborne, B.A. & Miele, L.A.** Off the beaten pathway: the complex cross talk between Notch and NF- κ B. *Laboratory Investigation* 88, 11 (2007).
193. **Palmer, W.H. & Deng, W.M.** Ligand-Independent Mechanisms of Notch Activity. *Trends Cell Biol.* 25, 697-707 (2015).
194. **Byers, L.A., Diao, L., Wang, J., Saintigny, P., Girard, L., Peyton, M., Shen, L., Fan, Y., Giri, U., Tumula, P.K., Nilsson, M.B., Gudikote, J., Tran, H., Cardnell, R.J., Bearss, D.J., Warner, S.L., Foulks, J.M., Kanner, S.B., Gandhi, V., Krett, N., Rosen, S.T., Kim, E.S., Herbst, R.S., Blumenschein, G.R., Lee, J.J., Lippman, S.M., Ang, K.K., Mills, G.B., Hong, W.K., Weinstein, J.N., Wistuba, I.I., Coombes, K.R., Minna, J.D. & Heymach, J.V.** An epithelial-mesenchymal transition gene signature predicts resistance to EGFR and PI3K inhibitors and identifies Axl as a therapeutic target for overcoming EGFR inhibitor resistance. *Clin. Cancer Res.* 19, 279-90 (2013).
195. **Hotz, B., Arndt, M., Dullat, S., Bhargava, S., Buhr, H.J. & Hotz, H.G.** Epithelial to mesenchymal transition: expression of the regulators snail, slug, and twist in pancreatic cancer. *Clin. Cancer Res.* 13, 4769-76 (2007).
196. **Huang, Y., Li, G., Wang, K., Mu, Z., Xie, Q., Qu, H., Lv, H. & Hu, B.** Collagen Type VI Alpha 3 Chain Promotes Epithelial-Mesenchymal Transition in Bladder Cancer Cells via Transforming Growth Factor beta (TGF-beta)/Smad Pathway. *Med. Sci. Monit.* 24, 5346-54 (2018).
197. **Bourhill, T., Narendran, A. & Johnston, R.N.** Enzastaurin: A lesson in drug development. *Crit. Rev. Oncol. Hematol.* 112, 72-9 (2017).
198. **Horowitz, M., Neeman, E., Sharon, E. & Ben-Eliyahu, S.** Exploiting the critical perioperative period to improve long-term cancer outcomes. *Nat. Rev. Clin. Oncol.* 12, 213-26 (2015).

6 Appendix

6.1 Abbreviations

| | |
|-----------|---|
| °C | Degree Celsius |
| ADAM | A disintegrin and metalloprotease |
| ADAM17-PD | ADAM17 prodomain |
| ADAMTS | ADAM with thrombospondin motifs |
| APP | Amyloid precursor protein |
| APS | Ammonium persulfate |
| ATP | Adenosine triphosphate |
| bp | Basepair |
| BSA | Bovine serum albumin |
| CAF | Cancer associated fibroblast |
| CANDIS | Conserved ADAM seventeen dynamic interaction sequence |
| CCL2 | Chemokine (C-C motif) ligand 2 |
| CCR2 | C-C chemokine receptor 2 |
| CD | Cluster of differentiation |
| cDNA | Complementary deoxyribonucleic acid |
| CFSE | Carboxyfluorescein succinimidyl ester |
| clAP | Cellular inhibitor of apoptosis protein |
| CSC | Cancer stem cell |
| CTF | C-terminal fragment |
| DAMP | Damage associated molecular pattern |
| DMEM | Dulbecco's modified eagle medium |
| DMSO | Dimethylsulfoxide |
| DNA | Deoxyribonucleic acid |
| dNTP | Deoxy nucleoside triphosphate |
| DR | Death receptor |
| EC | Endothelial cell |
| EDTA | Ethylenediaminetetraacetic acid |
| EGF | Epidermal growth factor |
| EGF-R | Epidermal growth factor receptor |
| ELISA | Enzyme-linked immunoabsorbent assay |
| EMT | Epithelial-to-mesenchymal transition |
| ER | Endoplasmic reticulum |

| | |
|-----------------------|--|
| ERK | Extracellular-signal-regulated protein |
| ESCRT | Endosomal sorting complexes required for transport |
| EthDIII | Ethidiumhomodimer III |
| FADD | Fas-associated protein with death domain |
| FCS | Fetal calf serum |
| FITC | Fluorescein isothiocyanate |
| FLIP | FLICE-inhibitory protein |
| g | gram |
| GAPDH | Glyceraldehyde 3-phosphate dehydrogenase |
| Gp130 | Glycoprotein 130 |
| GPCR | G-Protein coupled receptor |
| h | hours |
| HB-EGF | Heparin-binding epidermal growth factor |
| HE | Hematoxylin and Eosin |
| HES | Hairy and enhancer of split |
| HMVEC-L | Human lung microvascular endothelial cells |
| HOIL | Heme-oxidized iron regulatory protein 2 ubiquitin ligase |
| HOIP | HOIL interacting protein |
| HRP | Horseradish peroxidase |
| HUVEC | Human umbilical vein endothelial cells |
| ICD | Intracellular domain |
| Ig | Immunoglobulin |
| IKK | Inhibitor of nuclear factor κ B kinase |
| IL-6 | Interleukin-6 |
| IL-6R | Interleukin-6 receptor |
| IP | Immunoprecipitation |
| i.p. | intraperitoneal |
| i.v. | intravenous |
| I κ B α | Inhibitor of κ B α |
| JAK | Janus kinase |
| JAM | Junction adhesion molecule |
| JNK | c-Jun N-terminal kinases |
| kDa | kilo Dalton |
| kg | kilogram |
| L | Liter |
| LLC | Lewis lung carcinoma |

| | |
|----------------|--|
| LPS | Lipopolysaccharide |
| LUBAC | Linear ubiquitination chain assembly complex |
| M | molar |
| MAPK | Mitogen-activated protein kinase |
| MEF | Mouse embryonic fibroblasts |
| MET | Mesenchymal-to-epithelial transition |
| mg | milligram |
| min | minutes |
| mL | milliliter |
| MLKL | Mixed lineage kinase domain like pseudokinase |
| mM | millimolar |
| mm | millimeter |
| MMP | Matrix metalloprotease |
| moTAP | Modified tandem affinity purification |
| MPD | Membrane proximal domain |
| NEMO | Nuclear factor κ B essential modulator |
| NF- κ B | Nuclear factor κ B |
| NIK | Nuclear factor κ B inducing kinase |
| mRNA | messenger ribonucleic acid |
| ON | Over night |
| PBS | Phosphate buffer saline |
| PCNA | Proliferating cell nuclear antigen |
| PCR | Polymerase chain reaction |
| PEI | Polyethylenimine |
| PKC | Protein kinase C |
| PS | Phosphatidylserine |
| PSEN | Presenilin |
| PVDF | Polyvinylidene fluoride |
| qRT-PCR | quantitative real-time polymerase chain reaction |
| RIP | Regulated intramembrane proteolysis |
| RIPK | Receptor-interacting serine/threonine-protein kinase |
| RNA | Ribonucleic acid |
| rpm | Revolutions per minute |
| RT | Room temperature |
| SDS-PAGE | Sodium dodecyl sulfate polyacrylamide gel |
| SEM | Standard error of mean |

| | |
|-------------|--|
| SHARPIN | SHANK associated RH domain interactor |
| siRNA | small interfering RNA |
| SN | Supernatant |
| STAT | Signal transducer and activator of transcription protein |
| TACE | TNF α converting enzyme |
| TAK | Tat associated kinase |
| TAM | Tamoxifen |
| TC | Tumor cell |
| TEMED | Tetramethylethylenediamine |
| TGF | Transforming growth factor |
| TIMP | Tissue inhibitor of metalloprotease |
| TNF | Tumor necrosis factor |
| TNF-R | Tumor necrosis factor receptor |
| TPCA-1 | 5-(p-Fluorophenyl)-2-ureido thiophene-3-carboxamide-1 |
| TRADD | TNF-R-associated death domain protein |
| TRAF | TNF-R associated factor |
| TRAIL | TNF related apoptosis inducing ligand |
| UPL | Universal probe library |
| V | Volt |
| VE-cadherin | Vascular endothelial cadherin |
| VEGF | Vascular endothelial growth factor |
| VEGF-R | Vascular endothelial growth factor receptor |
| v/v | Volume per volume |
| w/v | weight per volume |
| WT | Wild type |
| μ g | microgram |
| μ L | microliter |
| μ m | micrometer |
| μ M | micromolar |

6.2 List of Figures

| | |
|--|----|
| Figure 1.1: Classification of proteases according to their catalytic residues..... | 1 |
| Figure 1.2: Domain structure of ADAM proteases | 2 |
| Figure 1.3: ADAM-mediated shedding events | 4 |
| Figure 1.4: Generation strategy for hypomorphic ADAM17 ^{ex/ex} mice..... | 6 |
| Figure 1.5: Schematic of the metastatic cascade | 11 |
| Figure 1.6: TNF-R1 and TNF-R2 induced signaling | 17 |
| Figure 1.7: TNF-R1-induced signaling complex II | 18 |
| Figure 3.1: Impaired extravasation of TCs in the absence of ADAM17..... | 44 |
| Figure 3.2: Less TC-transmigration in the absence of ADAM17 on ECs <i>in vitro</i> | 45 |
| Figure 3.3: Endothelium in ADAM17 ^{ex/ex} mice is less permeable upon tumor cell injection..... | 46 |
| Figure 3.4: ADAM17 deficiency on ECs leads to impaired TC extravasation | 47 |
| Figure 3.5: ADAM17 deficiency on ECs strongly decreases tumor burden | 48 |
| Figure 3.6: PKC β is activated upon tumor cell injection..... | 49 |
| Figure 3.7: PKC β deficiency leads to impaired TC extravasation and reduced tumor burden in the lung..... | 50 |
| Figure 3.8: Impaired extravasation of TCs in the absence of ADAM17 can not be linked to reduced shedding of tight junction proteins..... | 52 |
| Figure 3.9: TC-induced EC death is reduced in the absence of ADAM17 <i>in vitro</i> | 52 |
| Figure 3.10: TCs induce cell death in ECs of the lung..... | 52 |
| Figure 3.11: TC-induced EC death is decreased in the absence of ADAM17 <i>in vivo</i> | 53 |
| Figure 3.12: In the absence of endothelial ADAM17 TC-induced EC death is reduced <i>in vivo</i> | 54 |
| Figure 3.13: TC-induced EC death is reduced in the absence of ADAM17-activating PKC β | 55 |
| Figure 3.14: TC-induced EC death is decreased after pre-treatment with PKC β inhibitor Enzastaurin..... | 56 |
| Figure 3.15: Cell death triggered by DR6 overexpression is impaired in the absence of ADAM17. | 57 |
| Figure 3.16: In ADAM17-deficient HUVECs APP induced necroptosis via DR6 is disabled | 58 |
| Figure 3.17: TNF-R1 shedding is impaired in the absence of ADAM17 <i>in vitro</i> and <i>in vivo</i> | 59 |
| Figure 3.18: EC necroptosis via TNF-R1 is impaired in the absence of ADAM17 | 60 |
| Figure 3.19: TNF-R1-triggered necroptosis is impeded in the absence of γ -secretase and ADAM17 | 61 |
| Figure 3.20: There is constant phosphorylation of I κ B α ADAM17 ^{ex/ex} MEFs | 62 |
| Figure 3.21: TNF-R1 complex I formation is less in the absence of ADAM17. | 63 |
| Figure 3.22: RIPK3 and caspase-8 are not recruited to TNF-R1 complex II in the absence of ADAM17 | 65 |
| Figure 3.23: Loss of ADAM17 hinders MLKL phosphorylation upon stimulation with TNF α and zVAD treatment..... | 66 |
| Figure 3.24: TC extravasation in the lung is decreased in the absence of TNF-R1 | 67 |
| Figure 3.25: TC-induced EC death is decreased in Etanercept-treated WT mice | 68 |

| | |
|---|----|
| Figure 3.26: Less associated tissue inflammation in TC injected ADAM17 ^{ex/ex} mice..... | 69 |
| Figure 3.27: The absence of ADAM17 on myeloid cells is not protective against metastasis to the lung | 70 |
| Figure 3.28: T cell-specific deletion of ADAM17 protects against tumor formation in the lung | 71 |
| Figure 3.29: LLC tumors in ADAM17 ^{ex/ex} mice display less proliferating cells compared to tumors in WT mice | 72 |
| Figure 3.30: Notch1 activation in LLCs but not B16F1 cells leads to CSC phenotype..... | 73 |
| Figure 3.31: ADAM17-PD is a potent inhibitor of ADAM17 activity | 75 |
| Figure 3.32: Single ADAM17-PD dose inhibits TC-induced EC necroptosis and extravasation..... | 76 |
| Figure 3.33: ADAM17-PD prevents tumor formation in the lung | 77 |
| Figure 4.1: Activation of ADAM17 by PKC β on ECs in response to TC-derived CCL2 | 80 |
| Figure 4.2: Regulation of cell death by ADAM17 | 84 |
| Figure 4.3: Endothelial ADAM17 in the metastatic niche..... | 89 |

6.3 List of Tables

| | |
|---|----|
| Table 2.1: Recombinant proteins..... | 24 |
| Table 2.2: Primers for genomic DNA..... | 24 |
| Table 2.3: Primers for quantitative Real-Time PCR..... | 25 |
| Table 2.4: siRNA..... | 25 |
| Table 2.5: Primary antibodies..... | 26 |
| Table 2.6: Secondary antibodies | 27 |
| Table 2.7: Cell lines | 28 |
| Table 2.8: Mice used for experiments | 29 |
| Table 2.9: ADAM17 ^{ex/ex} PCR conditions..... | 31 |
| Table 2.10: ADAM17 ^{fl/fl} PCR conditions..... | 32 |
| Table 2.11: Cre PCR conditions | 32 |
| Table 2.12: PKC β ^{-/-} PCR conditions | 33 |
| Table 2.13: ELISA Kits..... | 43 |

6.4 Curriculum Vitae

Name: Julia Bolik
Date of Birth: 25/11/1988
Place of Birth: Oberhausen
Citizenship: German

Education

2015 – 2019 PhD Student
 Institute of Biochemistry
 Christian-Albrechts-University Kiel

2014 Master Thesis
 Institute of Physiology II
 University Hospital Münster

2011 – 2014 Master program Life Science
 Westfälische Wilhelms-University Münster

2011 Bachelor Thesis
 Institute of Zoology
 Westfälische Wilhelms-University Münster

2008 – 2011 Bachelor program Life Science
 Westfälische Wilhelms-University Münster

1999 – 2008 Abitur
 Josef-Albers Gymnasium, Bottrop

1995 – 1999 Elementary School
 Rheinbabenschule, Bottrop

Presentations

Oral

IRTG Summer School on Protease & Pathophysiology, Kiel, Germany (2015)

Poster

EMBO Workshop on Cellular signaling and cancer therapy, Cavtat, Croatia (2018)

Science Signaling sponsored Best Poster Award

34. Annual Conference of the German Association of the Study of the Liver, Hamburg, Germany (2018)

Cell-VIB conference: Hallmarks of cancer, Ghent, Belgium (2016)

2nd International Symposium Protease World in Health & Disease, Kiel, Germany (2016)

DKFZ-ZMBH Alliance Forum Tumor Microenvironment, Metabolism and Metastasis, Heidelberg, Germany, (2015)

IRTG Summer School on Protease & Pathophysiology, Kiel, Germany (2015)

Publications

Bolik J., Stevanovic M., Fritsch J., Müller M., Schumacher N., Schwanbeck R., Borowski C., Neukirch L., Rieser E., Wichert R., Galun E., Bergmann J., Röder C., Schafmayer C., Egberts J.-H., Becker-Pauly C., Saftig P., Schneider-Brachert W., Leitges M., Ringshausen I., Barikbin R., Schütze S., Adam D., Krüger A., Strilic B., Sagi I., Walczak H., Rose-John S. and Schmidt-Arras D. Endothelial A Disintegrin and Metalloprotease 17 promotes metastasis *Manuscript in preparation*

Bolik J., Tirnitz-Parker J.E.E., Schmidt-Arras D. ADAM and ADAMTS proteases in hepatic disorders. *J. Ren. Hepat. Disord.* 3, 23-32 (2019)

Barikbin, R., Berkhout, L., Bolik, J., Schmidt-Arras, D., Ernst, T., Ittrich, H., Adam, G., Parplys, A., Casar, C., Krech, T., Karimi, K., Sass, G. & Tiegs, G. Early heme oxygenase 1 induction delays tumour initiation and enhances DNA damage repair in liver macrophages of Mdr2(-/-) mice. *Sci. Rep.* 8, 16238 (2018).

Fuchslocher Chico, J., Falk-Paulsen, M., Luzius, A., Saggau, C., Ruder, B., Bolik, J., Schmidt-Arras, D., Linkermann, A., Becker, C., Rosenstiel, P., Rose-John, S. & Adam, D. The enhanced susceptibility of ADAM-17 hypomorphic mice to DSS-induced colitis is not ameliorated by loss of RIPK3, revealing an unexpected function of ADAM-17 in necroptosis. *Oncotarget* 9, 12941-58 (2018).

Schmidt, S., Schumacher, N., Schwarz, J., Tangermann, S., Kenner, L., Schlederer, M., Sibia, M., Linder, M., Altendorf-Hofmann, A., Knosel, T., Gruber, E.S., Oberhuber, G., Bolik, J., Rehman, A., Sinha, A., Lokau, J., Arnold, P., Cabron, A.S., Zunke, F., Becker-Pauly, C., Preaudet, A., Nguyen, P., Huynh, J., Afshar-Sterle, S., Chand, A.L., Westermann, J., Dempsey, P.J., Garbers, C., Schmidt-Arras, D., Rosenstiel, P., Putoczki, T., Ernst, M. & Rose-John, S. ADAM17 is required for EGF-R-induced intestinal tumors via IL-6 trans-signaling. *J. Exp. Med.* 215, 1205-25 (2018).

Bergmann, J., Müller, M., Baumann, N., Reichert, M., Heneweer, C., Bolik, J., Lücke, K., Gruber, S., Carambia, A., Boretius, S., Leuschner, I., Becker, T., Rabe, B., Herkel, J., Wunderlich, F.T., Mittrücker, H.W., Rose-John, S. & Schmidt-Arras, D. IL-6 trans-signaling is essential for the development of hepatocellular carcinoma in mice. *Hepatology* 65, 89-103 (2017).

6.5 Acknowledgments

First, I would like to thank Dirk for his supervision and relentless optimism, that kept me in line. Thank you for supporting my ideas, I felt taken seriously from the first day. You encouraged me to surpass myself and had an advice for every situation. Thanks for always having an answer to my numerous questions.

I am very grateful to Stefan Rose-John for giving me the opportunity to work in his Institute. Thank you for supporting me and my project with discussions, advice and constant guidance.

Sincere thanks to Eric Beitz for co-reviewing this thesis.

I am thankful to Henning Walczak and Eva Rieser for welcoming me in their lab. Thanks for sharing valuable knowledge with us.

Many thanks go to Boris Strilic for fruitful discussions and shared knowledge, materials and methods.

I would like to sincerely thank Achim Krüger, Irit Sagi, Christoph Becker-Pauly, Paul Saftig, Nina Hedemann, Dieter Adam, Ralf Adams, Hans-Willi Mittrücker, Athena Chalaris, Björn Rabe, Roja Barikbin and Michael Leitges for providing knowledge, methods and materials to this project.

I would like to acknowledge the SFB841 for funding the project. I am also thankful to the GRK of the SFB841 and the IRTG of the SFB877 for the opportunity to improve my soft skills.

A huge thanks to all former and current members of the Institute, especially to Petra for help with administrative work and to Anne C., Anne B. and Neele for being lovely fellow sufferer.

Special thanks go to Miryam, the honorary member of the AG Schmidt-Arras. You introduced me to the whole PhD machinery and shared your lab secrets with me. Without you I would have had a rough start. Thank you very much.

Many thanks to all current and former members of the AG Schmidt-Arras. I enjoyed each cake, coffee and Mettbrötchen with you (in no particular order): Fabian, Monja, Freia, Sarah, Ilka, Louise, Pit, Anke, Christopher, Lasse, Birte, Manni, Silke, Graziella and all visiting students. Thanks for all the help and entertainment in and outside the lab.

I am grateful to my family who supported me all the way and always had my back. Thanks to you, I am who I am today.

Finally, I am deeply thankful to Robert. You believed in me even when I did not. Thank you for not getting tired.